UNIVERSITÀ DEGLI STUDI DELL'INSUBRIA

DIPARTIMENTO DI BIOTECNLOGIE

E SCIENZE DELLA VITA

Dottorato di Ricerca in Biotecnologie,

Bioscienze e Tecnologie Chirurgiche

Curriculum Chirurgico

Anatomical and functional custom made restoration techniques with Direct Metal Laser Forming technology: systematic workflow and CAD-CAM

Relatore:
Prof. A. Caprioglio

Tesi di Dottorato di:

Dr. Piero Antonio Zecca

Matricola n. 613674

XXX Ciclo di Dottorato

1 ACKNOWLEDGMENT

Questo progetto di testi è stato svolto nelle strutture della Scuola di Medicina dell'Università degli Studi dell'Insubria di Varese.

2 SOMMARIO

3 ABSTRACT ITA

3.1 INTRODUCTION

Normalmente i difetti ossei vengono riparati attraverso i processi riparativi. Nel caso di fratture severo, tumori o grandi infezioni a carico di grandi ossa, ciò è un arduo compito per la chirurgia ricostruttiva. Studi hanno rilevato che le ossa si rigenerano se il difetto è entro limiti specifici; se il difetto è oltre la misura critica è necessario il support di terapia come l'innesto di materiali allogenici o autogenici per aiutare nella rigenerazione ossea. Una delle ultime innovazioni in campo medico è lo sviluppo di tecnologie di rapid prototyping (RP) e di additive manufacturing (AM). Queste tecnologie innovative aiutano a produrre modelli fisici dai dati generate attraverso il computer aided design e stampate attraverso stampanti 3D. I modelli di prototipazione rapida (RP) sviluppano anche modelli ossei che possono essere usati per ricostruire i difetti cranici. Negli ultimi anni, la ricerca scientifica in questo settore è stata orientata verso l'uso e l'implementazione di materiali che consentirebbero un ruolo attivo dell'osso intorno alla protesi. Questi nuovi materiali permettono la crescita dell'osso sul sullaprotesi al fine di facilitare la completa integrazione nei tessuti e fornire anche gli aspetti funzionali. A questo proposito, gli studi istologici hanno dimostrato che le superfici porose degli innesti sembrano avere più interazione con le cellule ossee e le proprietà strutturali e meccaniche simili all'osso circostante. In particolare, una porosità ideale è tra i 100 ei 700 µm e maggiore è stata la porosità maggiore è stato il volume e la quantità di crescita ossea, fornendo una maggiore integrazione. Pertanto, lo scopo del presente studio è stato lo sviluppo e la sperimentazione di un flusso di lavoro affidabile per la realizzazione di innesti progettati su misura per il settore della chirurgia orale e craniofacciale che integrano le tecnologie CAD-CAM con DMLF e/o nuove tecniche dei materiali polimerici.

3.2 MATERIAL AND METHODS

Questo studio prospettico ha arruolato pazienti che richiedono un trattamento chirurgico osseo nell'area craniofacciale. Il campione del presente studio era costituito da pazienti selezionati dalle diverse strutture quali Università e/o Ospedali.

In questo studio sono stati arruolati 14 pazienti con difetti ossee cranio-facciali diversi: 8 erano uomini e 7 erano donne (età media 53 anni e SD 21 anni).

Per verificare l'affidabilità del flusso di lavoro proposto per la costruzione di innesti per la riabilitazione craniofacciale. Sono stati associati due metodi di valutazione per testare i risultati. Dei questionati sono stati dati a pazienti sottoposti a chirurgia e ai loro chirurghi per avere un'analisi soggettiva del flusso di lavoro. Per ogni paziente è stata selezionata e applicata una segmentazione per generare un modello di superficie virtuale 3D. In seguito la protesi realizzatai è stata poi sovrapposta alla progettazione protesica originale e sono

stati confrontati utilizzando Cloudcompare (versione 2.6.2). È stato valutato lo spostamento tra il file originale e il file prodotto.

3.3 RESULTS

L'analisi intra-gruppo risultante dal test ANOVA ha mostrato che non esisteva una differenza significativa tra il livello di dolore/disagio a 2 giorni e 2 settimane dopo l'intervento chirurgico, ma i pazienti hanno indicato il livello di dolore/disagio significativamente più basso a 4 settimane dopo l'intervento chirurgico rispetto a 2 giorni dopo chirurgia, anche se non significativo rispetto a 2 settimane dopo l'intervento chirurgico. Per quanto riguarda il miglioramento estetico, non sono state rilevate differenze significative da 4 settimane a 12 settimane dopo l'intervento chirurgico, ma la percezione di miglioramento estetico è stata significativamente migliorata 1 anno dopo l'intervento chirurgico rispetto a 4 settimane dopo l'intervento chirurgico. I risultati dell'analisi di correlazione Pearson tra il miglioramento estetico 1 anno dopo l'intervento chirurgico e il miglioramento estetico in base alle aspettative hanno mostrato un'alta correlazione significativa ($r = 0,89$, $P < 0,05$). L'analisi intra-gruppo risultante da ANOVA ha mostrato che non esisteva una differenza significativa nella percezione del miglioramento estetico da 4 settimane dopo l'intervento chirurgico a un anno dall'intervento chirurgico. I risultati dell'analisi della correlazione Pearson tra il miglioramento estetico 1 anno dopo l'intervento chirurgico e il miglioramento estetico in base alle aspettative hanno mostrato un'alta correlazione significativa ($r = 0.93$, $P < 0.05$). La distanza massima media del modello stampato era notevolmente inferiore a quella del modello virtuale, con una differenza media di -0,075 mm.

3.4 CONCLUSION

Secondo i risultati del presente studio, l'innesto osseo su misura realizzato con tecnica di sinterizzazione laser rappresenta una valida alternativa agli innesti ossei tradizionali con un'elevata precisione clinica e il vantaggio per evitare la morbilità del sito donatore o del paziente a causa dell'innesto animale.

4 ABSTRACT ENG

4.1 INTRODUCTION

Bone defects are usually repaired by the body's healing process itself. If severe fracture, tumor or infection occur on large bones, it poses a serious challenge to the regeneration ability of the bones. Studies have revealed that bone regenerates when the injury occurs within the specified size of the bone; if the defect exceeds critical size supportive therapies such as autografts and allografts facilitate the bone regeneration. One of the latest advancement in medical science is the rapid prototyping (RP) or additive manufacturing (AM) technologies. These innovative technologies help to produce physical models from data generated through computer-aided design and printed through three-dimensional (3D) printers. The rapid prototyping (RP) models also develop bony models which can be used to reconstruct cranial defects. During the past few years, scientific research in this area has been oriented towards the use and implementation of materials that would allow an active role of the bone surrounding the implant. These new materials would provide the growing of the bone onto and into the implant to facilitate full integration into the tissues as well as provide the functional aspects. In this regard, histological studies have shown that the porous surfaces of the grafts seem to have more interaction with bone cells and structural and mechanical properties like the surrounding bone. A range porosity between 100 and 700 µm was found to be ideal for the purposes and the greater was the porosity the greater was the volume and the amount of bone growth, providing greater integration. Therefore, the aim of the present study was the developing and testing of a reliable workflow to fabricate virtually custom-made designed grafts in the field of oral and craniofacial surgery integrating CAD-CAM technologies with DMLF and/or new polymeric materials techniques.

4.2 MATERIAL AND METHODS

This prospective study enrolled patients requiring bone graft surgical treatment in the craniofacial area. The sample of the present study consisted of patients selected from the different University and/or Hospital settings.

In this study 14 patients with different cranio-facial bone defects were enrolled: 8 were men and 7 were women (mean age 53 yr and SD 21 yr).

To test the reliability of the proposed workflow for the construction of grafts for craniofacial rehabilitation. Two evaluation methods were associated to test the results of the workflow. First surveys were given to patients undergone surgery and their surgeons to have a subjective analysis of the workflow. For each patient, a threshold segmentation was selected and applied to generate a 3D virtual surface model. This prosthesis was then superimposed on the original prosthesis design and the two were compared using

Cloudcompare (version 2.6.2). The displacement between the original file and produced file was evaluated.

4.3 RESULTS

Intragroup analysis resulting from ANOVA showed that there was not significant difference between the level of pain/discomfort at 2 days and 2 weeks after surgery, but patients indicated the level of pain/discomfort significantly lower at 4 weeks after surgery when compared to 2 days after surgery, even though not significant when compared to 2 weeks after surgery. As regard for the aesthetic improvement, no significant differences were detected from 4 weeks to 12 weeks after surgery, but aesthetic improvement perception was significantly improved 1 year after surgery when compared to 4 weeks after surgery. The results of Pearson correlation analysis between the aesthetic improvement 1 year after surgery and aesthetic improvement according to expectations showed high significant correlation ($r=0.89$, $P<0.05$). Intragroup analysis resulting from ANOVA showed that there was not significant difference in the perception of the aesthetic improvement from 4 weeks after surgery to 1 year after surgery. The results of Pearson correlation analysis between the aesthetic improvement 1 year after surgery and aesthetic improvement according to expectations showed high significant correlation ($r=0.93$, $P<0.05$). The mean maximum distance of the printed model was significantly smaller than that of the virtual model, with a mean difference of -0.075 mm.

4.4 CONCLUSION

According to the results of the present study custom made bone graft made with laser sintering technique represents a valid alternative to traditional bone grafts with high clinical accuracy and the advantage to avoid morbidity of the donor site or of the patient due to animal grafting.

5 INTRODUCTION

5.1 LITERATURE REVIEW

The present section will describe the recent literature regarding latest results in the field of oral and maxillofacial surgery. The following sections will describe the historical background of oral and maxillofacial surgery, and how the techniques have evolved to ensure functional, cosmetics and aesthetic properties of patient after surgery.

5.1.1 History of Oral and Maxillofacial Surgery:

Facial surgery comprehends several different disciplines and among the moral and maxillofacial surgery are subjected to continuous evolution. The historical background of oral and maxillofacial surgery might be traced from different procedures which are currently in scope. The first known representation of oral and maxillofacial surgery can be traced in the Egypt (2700 BC). The military surgeons in Egypt used bandages to treat mandibular fractures [1]. In this technique, bandages were soaked in honey and egg white. The research has proved autolytic debridement activity of honey which facilitates the healing of fractures. Likewise, in ancient Greece, herbal remedies were used to treat several oral diseases [2]. During the 4th century BC, Hippocrates treated dental abscesses. However, the proper forceps were not available at that time, and therefore Hippocrates suggested to extract only loose teeth [3]. Later, Hippocrates also explained the treatment of mandibular fractures. He stated that “It should be well known that, in fractures of the jaw, dressings with bandages if properly performed is of little advantage, but occasions great mischief if improperly done” [1].

In Roman Empire, Celsus (25 BC- 50 BC) lead the way of dangerous tooth extraction and successfully treated jaw fractures [4]. The fall of Roman Empire saw the rise of Arabs and the start of Islamic period of medicine. The Muslim practitioners spreaded the technique of treating various disorders such as oral fistulae, ranulas, and epuli, jaw fractures and dislocations [5]. In the Renaissance era (14 – 17 century) further evolution of oral and maxillofacial surgery occurred. The prominent practitioner Ambroise Pare (1510-1590), successfully treated broken jaws, mandibular dislocation, and tumors [6]. Among the great practitioners in oral maxillofacial surgery Mathew H. Cryer (1840-1921), Truman L. Lyon (1874-1935), Thomas L. Giler (1848-1931), and Chalmers L. Lyons (1874-1935) are worth mentioning. All of them explored the specialty of oral and maxillofacial surgery in medicine or dentistry. Its origin was medicine, but eventually, it becomes a dental specialty. Nowadays maxillofacial surgery is bridging gaps between medicine and dentistry.

Figure 1 From MS. of APOLLONIUS OF KITIUM, of Ninth Century Copied from pre-christian original, REDUCING DISLOCATED JAW.

5.1.2 Techniques to Repair Bone Defects:

Before to treat the subjects enrolled in the present sample I have conducted a narrative review of the literature to deeply understand and update the state of the art.

The present literature review followed the guidelines for the narrative review of the literature. A computerized search was conducted using Medline (to July 2017), Pubmed (to July 2017), Embase (to July 2017), and all EBM reviews (Cochrane Database of Systematic Reviews, ASP Journal Club, DARE and CCTR) (to July 2017) databases. The search algorithm which was used to get the relevant articles included: (((Maxilla*[tw] OR Maxillo*[tw]) AND (surger*[tw] OR surgi*[tw] OR "General Surgery"[Mesh] OR “History” OR “Background” [Mesh] OR "Surgery, Oral"[Mesh] OR "Oral Surgical Procedures"[Mesh] OR "Oral surgery"[tw] OR "Oral Surgical”[tw]) AND ("New Techniques"[Mesh] AND (Analyses[tw] OR Analysis[tw] OR comparison*[tw].

Inclusion and Exclusion Criteria:

Clinical human studies and clinical animal trials which were within the scope of oral maxillofacial surgery were included in the literature review. The studies were characterized in the categories such as anesthesia and pain management, Implants surgery, orthognathic/cleft/OSA, pathology, reconstruction, facial repair, Cranio maxilla facial repair, broken jaw repair.

The exclusion criteria included the following:

- In vitro studies
- Opinion papers
- Perspective letters
- Full-text articles unavailable through the author’s university library system

In case both the inclusion and exclusion criteria are not determined by the abstract, one of the reviewer access the full-text article and read it thoroughly. This identified any discrepancies with the research objective of the present literature review.

Bone defects are usually repaired by the body’s healing process itself. If severe fracture, tumor or infection occur on large bones, it poses a serious challenge to the regeneration ability of the bones. Studies have revealed that bone regenerates when the injury occurs within the specified size of the bone; if the defect exceeds critical size supportive therapies such as autografts and allografts facilitate the bone regeneration [2]. An experimental study was conducted to evaluate the biomechanical properties of open-porous titanium scaffolds in vivo. It was hypothesized that open-porous titanium scaffolds are a novel strategy to cure bone defects. These one-porous titanium scaffolds also facilitate weight bearing in the early stage, and implant failure risks might be significantly reduced. In this experimental study, two types of custom prepared Ti6AI4V open-porous

scaffolds were used in a 20 mm segmental defect in the mid-diaphysis of the metatarsus of sheep [7]. Torsional testing was performed after 12 to 24 weeks on the implanted bone and compared with the non-treated side. Biomechanical properties such as maximum torque, maximum angle, shear modulus, shear stress, torsional stiffness and fracture energy were evaluated. In addition to these, bone mineral density (BMD) was also investigated. The results revealed that both the scaffolds have similar mechanical loading capabilities after 12 weeks. Although after 24 weeks the investigated properties increased. It was also found that torsional stiffness and shear modulus and bone formation depends on scaffold material. One scaffold showed a significant increase in bone mineral density after 24 weeks while no such increase was seen in BMD of the other scaffold. This research supported the implantation of open-porous titanium scaffolds for segmental defects in the large bones which can further enhance the biomechanical stability when observed for a longer period greater than six months [7].

Moreover, a review was carried out to investigate the failure rates reported in various techniques of reconstruction of full thickness cranial defects. There is a wide range of techniques which can be used for reconstruction of calvarias defects and cranioplasty. In this review, data from 149 patients for a period of 9-years during which they underwent surgery for insertion of 151 custom made titanium cranioplasties of varying size were collected [8]. Patients' demographics, indication for cranioplasty, site, and size of the defect were obtained from clinical records. All the patients were followed up for an average of 1 year and two months. Early complications included seroma and/or hematoma were reported in 7% of the patients and in one patient continuous bleeding forced to remove the implant. One patient was reported to be dead from a hemorrhagic stroke at three days post-operation. Later on, seroma was reported in 19% of the patients but only 4% cases required implant removal [8]. The main cause identified for the failure of the implant was an infection. This review concluded that custom-made patient specific titanium cranioplasties have been tried and tested so often that they can be used for the reconstruction of all sizes of full thickness calvarial defects whether small or large.

Traumatic brain injuries are severe and often increase the intracranial pressure in the patient. Decompressive craniectomy (DC) substantially reduces intracranial pressure. There are several disadvantages associated with DC such as sinking of the skin flap and compromising the cerebral functions negatively affecting the patients. The recent research to reconstruct skull defects is aimed to overcome these disadvantages. Previous studies have highlighted the benefit of titanium mesh in the reconstruction of frontal skull defects. One of the retrospective reviews was conducted to identify the aesthetic, surgical outcomes (cranial nerves V and VII), and complications (hardware extrusions, meningitis, osteomyelitis, brain abscess and pneumocephalus) associated with the three-dimensional (3-D) titanium mesh in frontal skull reconstruction. The retrospective review was based on the records of seven adult patients (32-60 years of age) from 2011 to 2012 at a university hospital in Taiwan. An algorithm was developed according to the bifrontal skull defects and median bone ridges to facilitate computer-assisted design (CAD) of 3-D

titanium mesh implants [9]. This algorithm ensured a single operation for bifrontal skull defects. The results showed significant improvement in aesthetic, procedural and functional outcomes. However, when more time is given for healing two patients face subclinical infections. No patients showed the signs trigeminal and facial dysfunction. This study supports the implantation of 3-D titanium mesh in frontal skull reconstruction. There were few complications which can be resolved by the administration of antibiotics. The implantation of one piece 3-D titanium mesh has several advantages as compared to conventional surgeries [9]. Elderly patients and patients with bifrontal cranioplasties get maximum benefit from this strategy.

Reconstruction of bone in the head and neck to achieve good aesthetics and proper functions is quite challenging. The defects in the head and neck can be very complex and pose a serious challenge for the surgeons. The head and neck injuries can often comprise inflammation, infections, and scarring. The gold standard therapy for the repairing of such injuries is tissue grafting and vascularized flaps that help in optimal healing. However, this strategy also has several disadvantages such as limited availability, difficulty in shaping flaps, and morbidity at the donor site. The surgical techniques have evolved to improve the function and aesthetics in such injuries. In this study, advances in the oral and maxillofacial surgery are discussed. The use of custom-made implants, three-dimensional imaging, stereolithographic modeling can improve the reconstruction of bone. The robotic surgery also helps to modify current conventional reconstruction techniques without the need of mandibulotomy [10]. The most conservative method for reconstruction is tissue engineering and distraction osteogenesis which do not require autologous tissue transfer. Recent development in the facial allotransplantation has helped to replace the whole anatomical facial units and sensory recovering with reanimation. However, one drawback of this technique is life-long immunosuppression in the patients who have undergone facial allotransplants. Therefore, the use of this technique is limited to specific cases. This finding suggests that the current gold standard for reconstruction of head and neck bones is not much effective[10].

However, navigation can assist the repairing of facial fractures. The previous studies have shown the improved functional outcome in orthopedics and neurosurgery, but no such evidence is reported in oral and maxillofacial surgery. Stereolithographic models developed using mirroring templates facilitates in surgical planning simulation. These models also help to develop custom-made implants which accurately repair head and neck bone injuries. The concept of robotic surgery is relatively newer and does not change the reconstructive methods, but allows oncological procedures to be more invasive. Transoral Robotic Surgery (TORS) procedure is also helpful in inserting free flaps without performing mandibulotomy. Mandible can be reconstructed with the help tissue engineering and Transport disc distraction osteogenesis (TDDO) [10]. However, there is no evidence which supports the use of tissue engineering in the reconstruction of head and neck. The animal trials are going on in the laboratory, but no significant progress has been made in this field. Although facial allotransplantation has shown promising results,

the patients require long-term immunosuppression, and therefore this procedure is limited to only selected cases.

In the oral and maxillofacial surgery, one another advanced technology is additive manufacturing in which materials are joined by data generated from 3-dimensional model to create objects. Oral and Maxillofacial surgeons face challenges to manage the loss of craniofacial tissue due to trauma, cancer treatment, and other abnormalities. Different strategies have been employed to manage craniofacial defects properly, but only autogenous bone graft is found to be gold standard treatment in such cases. In addition to autogenous bone grafts, cell-based treatments in which adipose stem cells are used along with osteoconductive biomaterials or scaffolds also proved to be beneficial. Despite being promising, cell-based treatments require 3D scaffolds to fulfill the esthetic and functional requirements of the head including sufficient blood supply and load-bearing capacity. Now, additive manufacturing technology is used to manufacture 3D scaffolds. In one of the two existing review, current and evolving modalities are evaluated to reconstruct oral and maxillofacial bone defects. Human maxillary sinus floor elevation is used as a valid model to test the bone tissue-engineering techniques which help to get desired reconstruction after the application of 1-step surgical procedure; whereas in a 2-step surgical procedure, cells are grown ex-vivo and then seeded on scaffolds before implantation [11]. This review also highlighted that image-guided tissues-engineering technologies are used which helps to locate the surgical site and helps in the manufacturing of custom-made implants according to the specific needs of the patient. In 1-step surgical procedures, it is important to combine tissue engineering with the image guided technologies to better repair the larger oral and maxillofacial bone defects [11].

5.2 Background: State of the Art Techniques in Oral and Maxillofacial Surgery

Over the years it is necessary to use new surgical techniques and prostheses in fact is necessary a virtual pre operative surgery for planned bone resection so that implants accurately fit during the surgery. It has been seen that reconstruction of the major craniofacial defects are quite challenging and several custom-made implants have been developed to improve the reconstruction of defects. In the case of large lesions in the front-orbital region, a simple protocol is applied to perform reconstruction with PEEK (polyetheretherketone) along with resection at the same time. In the present review, it was found that navigation is required to resection the implants according to the planning accurately. Five patients needing complex reconstruction in the front-orbital region were studied, and results showed that planned resection is successful with accurate placement of the implants. Optimal orbital reconstruction permits exophthalmos correction and orbital contour symmetry. In this procedure, no major complication was reported. Hence, it can be proved that one-step technique is beneficial to reconstruct the orbit with complete symmetric cosmetic and functional results and can avoid donor site morbidity.

One another major complication in the fronto-orbital region is the presence of bony lesions which present a difficult challenge in reconstructive cranioplasty for the surgeons. The main complexities are to restore the forehead, and to let the orbital walls maintain perfect symmetry, morphology, and aesthetics. Bone grafting is the current strategy to reconstruct such cranial defects, and other techniques include the use of titanium mesh or methylmethacrylate (Jalbert and Lauwers, 2009). However, in the last decade, the reconstruction of large craniofacial defects has significantly improved, and new custom-made implants are prepared according to the requirement of each patient. Jalbert et al. used to perform optimal primary reconstruction using custom-made PEEK (polyetheretherketone) implants simultaneously with resection of large lesions in fronto-orbital region. In this study, the surgeons performed pre operative surgery with a planned bone resection so that the reconstruction was easily done in a single-step procedure. Navigation is required to accurately perform the resection according to plan. The same procedure was applied on five patients who required orbitofrontal reconstruction. The results revealed that planned resection was achieved with great precision and accurate implantation. It was also found that optimal orbital reconstruction facilitated exophthalmos correction maintaining contour symmetry. There were no complications in all five patients. Therefore, this one-step technique for reconstruction of the complex fronto-orbital region is successful. The main benefits are reduced operative time, achieving excellent cosmetic symmetry, functional aesthetics, and it avoids site morbidity.[12]

One of the experimental study was conducted to verify the modeling accuracy of various products and to create custom-made devices for bone expansion in the patients who require implantation. In this study, various two-(2D) and three-dimensional (3D) specimens and custom-made devices were generated with the help of computer aided design (CAD) and rapid prototyping (RP) method. A 3D printing machine and selective laser melting (SLM) was used to produce CAD designs using titanium (Ti) powder. The model accuracy was assessed in which the accuracy of 2D and 3D specimens, the pore structure of 2D specimens, the porosity of 3D specimens was determined. The results revealed that various parameters of 2D and 3D specimens are precise and in consonance with ISO 2768-1 [13]. Overlapped images were used to determine any error between the CAD images and scanned data. These results suggest that high modeling accuracy in various products for implantation can be achieved by using CAD/RP-SLM method [13]. Therefore, these products can have possible clinical applications.

One another study conducted to investigate the surgical outcomes in patients with craniofacial defects who have undergone surgery in which polyetheretherketone (PEEK) patient-specific prostheses designed by computer-aided programs are used for reconstruction. In this study, 13 patients were recruited who have undergone PEEK patient-specific implants (PSI). 8 out of 13 patients underwent single-step primary reconstruction in which custom-made surgical guides and custom-made prostheses were used; whereas other five underwent delayed reconstruction. In all the 13 cases, the material of implants was PEEK. During the preoperative and follow-up period, all the

patients were investigated to determine esthetics, ophthalmology and radiological evaluation. The total time is taken during operation and all the short and long-term complications were recorded. Results revealed that global position and shape of implants was satisfactory. However, in one case fitting of implant required additional adaptations. The results also showed that 11 out of 13 implants satisfactorily restored the morphological area and produced significant aesthetic results. There were no complications regarding implants in all the cases [14]. These findings suggest that PEEK computer-aided designed and manufactured implants were useful in craniofacial defects and accurately restored the three- dimensional (3D) anatomy of craniofacial region.

One another study investigated the ultrastructural composition of interfacial tissues with special emphasis on the implant surface structure and open-pore area of the bone. It has been seen that load-bearing orthopedic applications, metal implants proved to be beneficial because of its interconnected pore structure which helps in bone ingrowth and reduce the stiffness ultimately eliminate stress-shielding effects. In this study, 3D printed sold, and macro porous Ti6AI4V implants were assessed in adults' sheep femora after six months of healing. Raman spectroscopy and electron microscopy were used correlatively to study the ultrastructural composition of bone-implant interface. The results revealed that mineral crystallinity and the mineral-to-matrix ratio at the interface was like that of native bone. However, it was also found that interfacial tissue has lower Ca/P ratios, lower carbonate content, higher proline phenylalanine and tyrosine level which shows that these tissues are relatively less mature. The process of bone healing was found to be advance at porous implant surface as compared to solid implant surface depending on the phenylalanine and tyrosine levels like that of native bone. It was found that mechanosensing infrastructure in bone, the osteocyte lacuna canalicular network have a higher percentage of canaliculi approximately 40% high; whereas the osteocyte ratio per mineralized surface was found to be 36-71% higher at the interface between the bone and implant after an extended healing period [15].

It has been argued that osseointegration research the success of implant surface is usually evaluated by quantification of newly formed bone instead of its composition, structure, and maturation. Shah et al. explains a novel strategy to assess the ultrastructure and composition of bone which has interconnected open-pore structure. Raman spectroscopy is a valuable procedure to determine the molecular composition at various implant sites after long-term healing. Therefore, it was possible to determine the composition of interfacial tissue after prolonged healing. There is a great capacity to sense mechanical loading at the upper 1/3rd regions which have higher N.Ot/B.Ar near the porous implant [15].

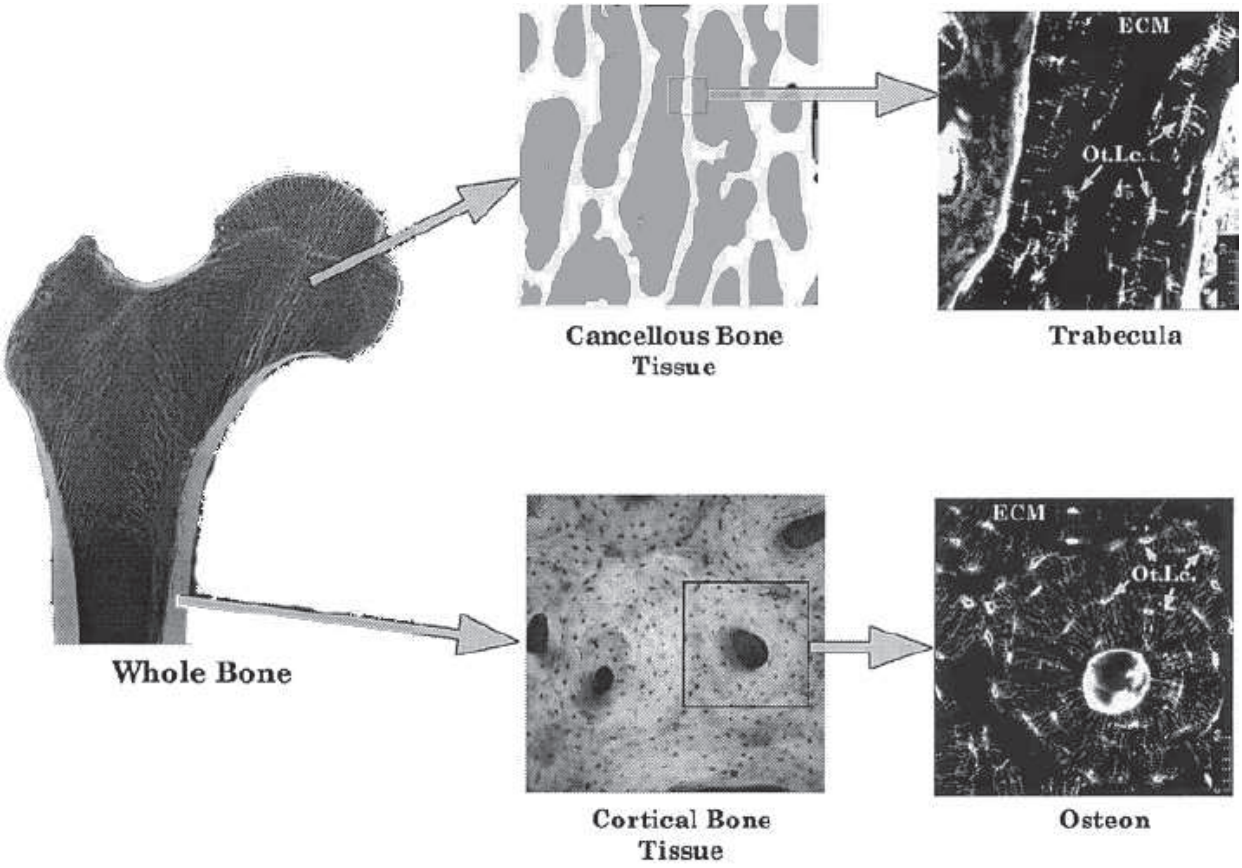

Figure 2The organization of bone at the tissue and cellular levels.

Studies have shown that reconstructive surgery and facial allotransplantation have advanced in the recent times, but in Craniomaxillofacial defects, prosthetic rehabilitation is the only specific approved treatment available[16, 17]. However, the use of endosseous implants in prosthetic craniofacial reconstructions showed a significantly reliable method. Standardized plate-like titanium implants are available for low bone areas. Congruent fitting of these implants at the recipient site require manual adaptation which often causes drawbacks such as prolong surgery, technical complexity, and poor functional outcome. Therefore a custom-made patient-specific implant was developed by data generated from Digital Imaging and Communications in Medicine (DICOM [18]). Toso et al. used a prefabricated patient specific implant was introduced in a 64-year-old man with a partial nasal defect. The earlier plate-like implant failed in this patient due to Osler disease. Therefore, a patient-specific implant was fabricated from computer-aided design and computer-aided manufacturing (CAD/CAM) technology. This technique helped to ensure ideal geometry of implant according to the patient need and accurate placement. The results revealed that patient-specific implant was planted successfully without consuming much time. The functional and aesthetic outcome was also excellent after 6-months. These findings proved that application of prefabricated patient-specific implants is ideal for holding craniofacial prostheses and should be used in specific cases [18].

One of the study conducted to investigate a new engineering strategy to develop cranial implants with possible future applications in medical implant fabrications. It is evident

that the reconstruction of the defect of the hard-cranial tissue injuries are the consequences of trauma or iatrogenic etiology which serves to protect the underlying brain and warrants sufficient reconstruction of the defect. The recent literature has mainly focused on the fabrication of patient-specific titanium cranial implants. The techniques to fabricate patient-specific titanium implants (PSI) are of two types: one is direct technique, and other is indirect technique [19]. However, with the improvements in the medical imaging and computer modeling, computer-aided prefabricated patient-specific implants have gained significant popularity. Despite the popularity of direct method patient-specific implants, the indirect method has specific advantages over direct method. Optical three-dimensional techniques provide details of the fabricated patient-specific implants [19]. Therefore, this new technique was found to be more suitable for (PSI).

One another study supported the idea of customized titanium mesh repairing cranial defects. The main objective of this study was to use reverse engineering techniques and develop a customized titanium meshes which improve the communication between doctors and patients on implants designs. Studies have shown that titanium cranioplasty is widely accepted and used the technique for cranial defects repair. The study used the computed tomography scan data of patients who have cranial defects and generated three-dimensional virtual models. This titanium meshes were used in cranioplasty surgery of 8 patients. The postoperative results were observed through computed tomography scanning and were analyzed by rainbow difference tomography. The analysis showed that all the patients were satisfied with the titanium meshes. This shows the significant importance of new method which allows surgeons, engineers, and patients to work in collaboration and modify implants according to the requirement. This method also facilitates communication and comprehensive evaluation of the designed implants with better outcomes [20].

Calvarial defects are complicated, and their reconstruction should ensure biomechanical stability, protect the cerebral nerves and restore the cranial contour. The materials used to cover calvarial defects include xenografts, autografts, and allografts. In addition to these synthetic alternatives, autologous bones are also used. Surgeons usually prefer autologous bones to synthetic materials. However, autologous bones are not always feasible to fill the defect size, and issues such as unacceptable donor-site morbidity occur. The most advanced 3D printings enable the fabrication of titanium implants according to the requirement of the patients and ensures perfect reconstruction of calvarial defects. One of the reports aimed to highlight the experience of bone reconstruction in three large calvarial defects with custom design fabricated titanium implants. In this study, three calvarial defects were reconstructed with the help of custom made 3D porous titanium implants from 2013 to 2014. These calvarial defects occurred due to traumatic hematoma or meningioma in the fronto-temporal-parietal, parietooccipital, and parieto-temporal areas. 3D computed tomography (CT) generated data was used to prepare customized implants. 3D Design software and electron beam melting machine were also used to perfectly design custom titanium implant specific to patient needs. All the

prepared custom implants were compared and evaluated with the 3D-printed skull models for each patient. After the confirmation, these implants were laid and fixed with 8 mm screws [21]. The results revealed that these custom-made 3D implants filled the calvarial defect precisely without occupying any extra space. No complications were reported in the operative site. Postoperative CT scans were performed to examine the position of implants. It was concluded that synthetic material implants are most appropriate in the reconstruction of large calvarial defects. These custom-made implants provide strength, durability, and precision. Therefore, a custom-made 3D titanium implant was considered the optimal material for calvarial reconstruction [21].

In oral and maxillofacial surgery elastic modulus of the metallic orthopedic implant is usually 6-12 times larger than that of cortical bone which yields shielding stress, and bone atrophies can cause fracture at the interface of reconstructing. It was proposed that creating pores into the implants will significantly reduce the elastic modulus. Three-dimensional printing (3DP) can create dual porosity in the implants. It can produce micro pores and macro pores using computer-aided designs. The main objective of this study was to fine-tune three-dimensional printing (3DP) to reduce elastic modulus of 3DP titanium implant like that of bone so that shielding stress is removed. Mercury porosimetry and surface profilometry were used to test the physical parameters such as density, porosity and surface roughness of implants. Titanium was selected due to its excellent biocompatibility, corrosion resistance, low elastic modulus, high strength, and durability. The secondary objective of the study calculated the 3DP titanium-bulk modulus ratio and predesigned porosity. The physical and mechanical properties of the titanium implant were customized by a binder (polyvinyl alcohol) and heating the titanium samples to form coherent mass without melting. The porosity and compressive modulus of fabricated titanium samples were found to be 32.2-53.4% and 0.86-2.48GPa respectively [22]. These parameters lie within the range of bone elastic modulus. The porosity of 3DP titanium samples and the porosity of the bone is plotted on a graph which revealed that pore size and wall thickness could be customized to form the desired porosity.

One of the latest advancement in medical science is the rapid prototyping (RP) or additive manufacturing (AM) technologies. These innovative technologies help to produce physical models from data generated through computer-aided design and printed through three-dimensional (3D) printers. The rapid prototyping (RP) models also develop bony models which can be used to reconstruct cranial defects. A retrospective study was conducted at Helsinki University Central Hospital from 2009-2010 to investigate the use of RP generated models in oral and maxillofacial surgery. The study emphasized on the indications of RP models use and their CT examinations to obtain required data. Two different methods multislice CT (MSCT) and cone beam CT (CBCT) were also evaluated to study the RP models. In the study, a total of 114 RP models were designed for 102 patients [23]. The mean age of all the patients was reported to be 50.4 years at the time of RP model production. The main indicators for modeling are reported to be malignant lesions (29%), secondary reconstruction (25%), prosthodontic treatment (22%),

orthognathic surgery (13), benign lesions (8%), and TMJ disorders (4%). 92 cases were examined through MSCT and 22 cases examined through CBCT. It was found that 75% of the models were conventional hard tissue models. Only 2 RP models out of 114 models were found to be soft tissue models [23]. The main findings of the study were the benefit of RP models in treatment planning and production of custom made implants. These models help in better treatment planning and enhance the intraoperative efficiency.

Surgeons find it difficult to reconstruct mandible after a maxillofacial surgery. The best choice of reconstruction available right now is microvascular free-flap reconstruction which uses bone. However, recent research has led to the discovery of CAD-CAM technique for mandibular reconstruction. This new technique also helps in the better planning of reconstructive surgery maintain the aesthetic and prosthetic outcome of the patient. The aim of this paper is to evaluate the effectiveness of CAD-CAM technique in a patient who has mandibular defects. In 18 neoplasms cases, mandible and fibular were cut using CAD-CAM technique of reconstruction with the aid of vascularized bone free-flap and surgical guides. The surgery was planned to design and create customized surgical devices. The cases were followed up after 12 months. Out of 18 cases, only one died, and all others are alive without any complication. The survival rate of the reconstructive microvascular flap was recorded 100% [24]. There were no major or minor microvascular problems. Likewise, no donor site complications were recorded. These findings suggest that CAD-CAM technique is particularly useful in the reconstruction of the mandible with both bi-dimensional and tri-dimensional defects. The protocols used in the CAD-CAM technique proved more benefits than harms to the patients. So, this could be the way forward for mandible reconstruction. Mandibular defects are critical and have several complications in head and neck reconstructs. For a long time, alloplastic implants were used for mandibular reconstruction in patients with discontinuous mandibular defects. However, several complications were associated with alloplastic implants including hardware extrusion and plate fracture which often occur in secondary salvage reconstructions. The recent research is focused on restoring the functions and aesthetics of 40-mm canine mandibular discontinuity defect with the help of custom-made titanium bone graft and autologous iliac bone grafts. In this study, researchers have designed customized bone grafting plate with the support of Reverse Engineering-Computer Aided Design-Rapid Prototyping technology. The experiment was performed on the right mandibular body of 9 hybrid dogs. The defect was reconstructed with the help of a customized plate and autologous cancellous iliac blocks. The bone metabolism and reconstitution of the graft was evaluated with the help of sequential radionuclide bone imaging. Furthermore, biomechanical testing, three-dimensional micro computed tomographic scanning, and histological examination was also performed on the specimens. The results showed that mandibles were reconstructed in perfect symmetry with the help of customized grafting plate and bone continuity of the mandibles [25]. The follow up of 12 weeks revealed that cancellous iliac graft was changed to hard bone block possessing strength like native mandibles. There was a fibrous tissue in between remodeled bone graft and a titanium plate. These findings suggest that prototyped

grafting plate can successfully restore mandibular discontinuity defects and yield perfect aesthetics and functional reconstructions [25].

Studies have revealed that poor cosmetic results are obtained by reconstructing the cranial bone defects with the help of natural materials [26, 27]. However, other studies show that implants produced from computer aided designing and manufacturing techniques have significantly better cosmetic results. The recent research at the Neurosurgery and Maxillofacial Surgery Department of Limoges University Hospital Center have introduced a relatively new concept to use hydroxyapatite (HA) in the custom0made ceramic implants for the reconstruction of craniofacial bone defects of more than 25cm^2. The aim of the present study was to highlight the mechanical and osteoconductive properties of custom-made HA implants in large craniofacial bone defects. The custom-made HA implants were prepared in three-dimensional shapes with the use of stereo lithography techniques so that implants can fill the patient's skull without any molding. Eight patients were treated with these HA implants from 2005-2008 with 12 months of postoperative follow-up. The results revealed that surgical procedure was comparatively simple and no major complications such as infection were reported in the patients. Satisfactory cosmetic results were obtained, and both the patients and surgeons were satisfied with the results. These findings suggest that using ceramic HA custom made implants large craniofacial bone defects can be reconstructed in adults and children above eight years old without any serious complications [28].

6 OBJECTIVES

In orthopedic and prosthetic cranio-maxillo-facial reconstructive surgery the need to replace portions of anatomic bony tissue following the loss of the afore mentioned portions for any injury or surgical resection attributable to another pathological cause is often required. In these patients, both morphological and functional aspects might be evaluated leading to the evolution of the techniques used in the same industrial manufacturing.

Historically the materials used in such cases for the grafts of the missing portions were made with the use of screws and acrylic bone cement, resulting in a rigid component that has different mechanical characteristics if compared to the surrounding bone, with the constant risk of failure of the graft.

During the past few years, scientific research in this area has been oriented towards the use and implementation of materials that would allow an active role of the bone surrounding the implant. These new materials would provide the growing of the bone onto and into the implant to facilitate full integration into the tissues as well as provide the functional aspects. In this regard, histological studies have shown that the porous surfaces of the grafts seem to have more interaction with bone cells and structural and mechanical properties like the surrounding bone. A range porosity between 100 and 700 µm was found to be ideal for the purposes and the greater was the porosity the greater was the volume and the amount of bone growth, providing greater integration.

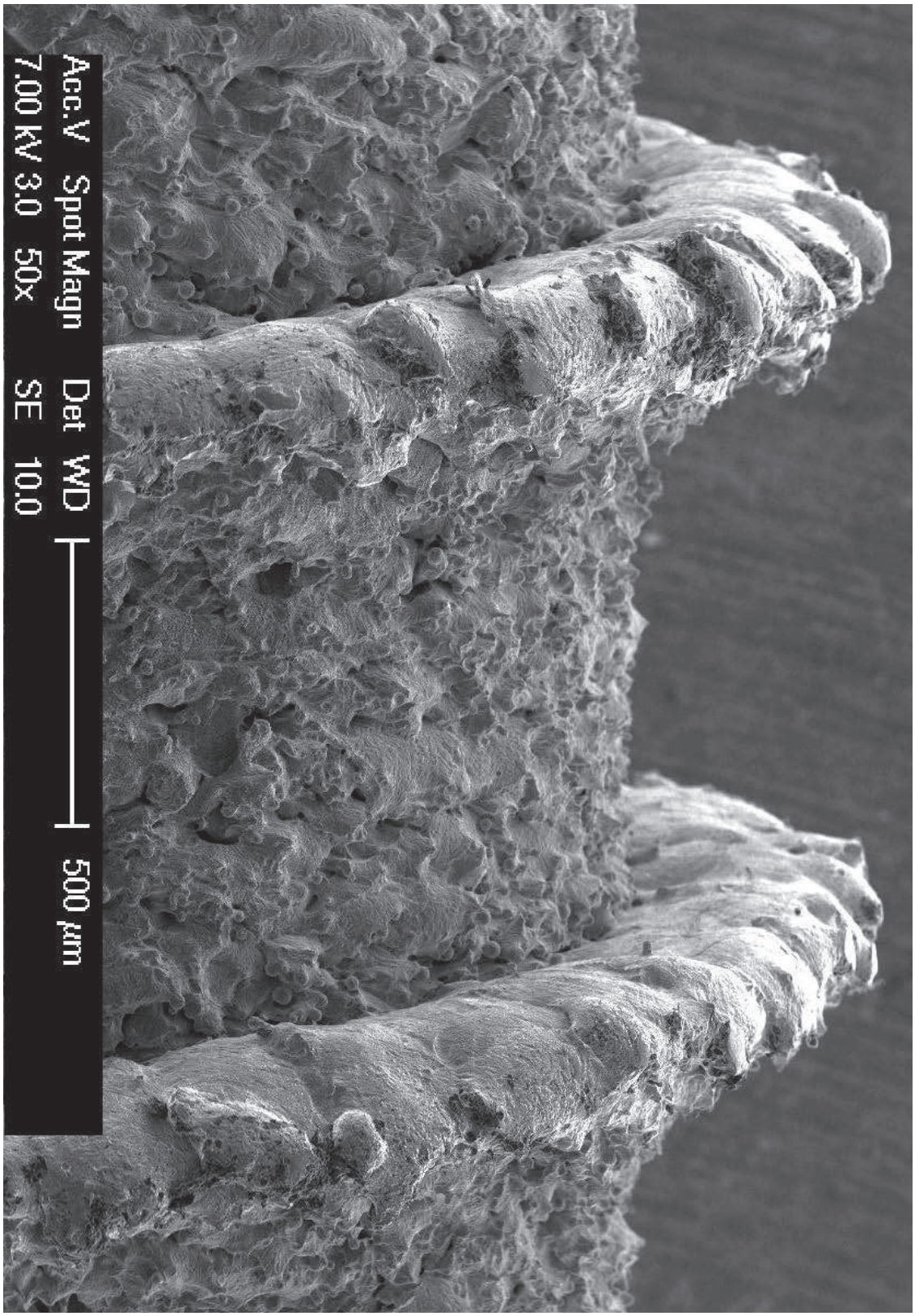

Figure 3 example of titanium laser sintered surface

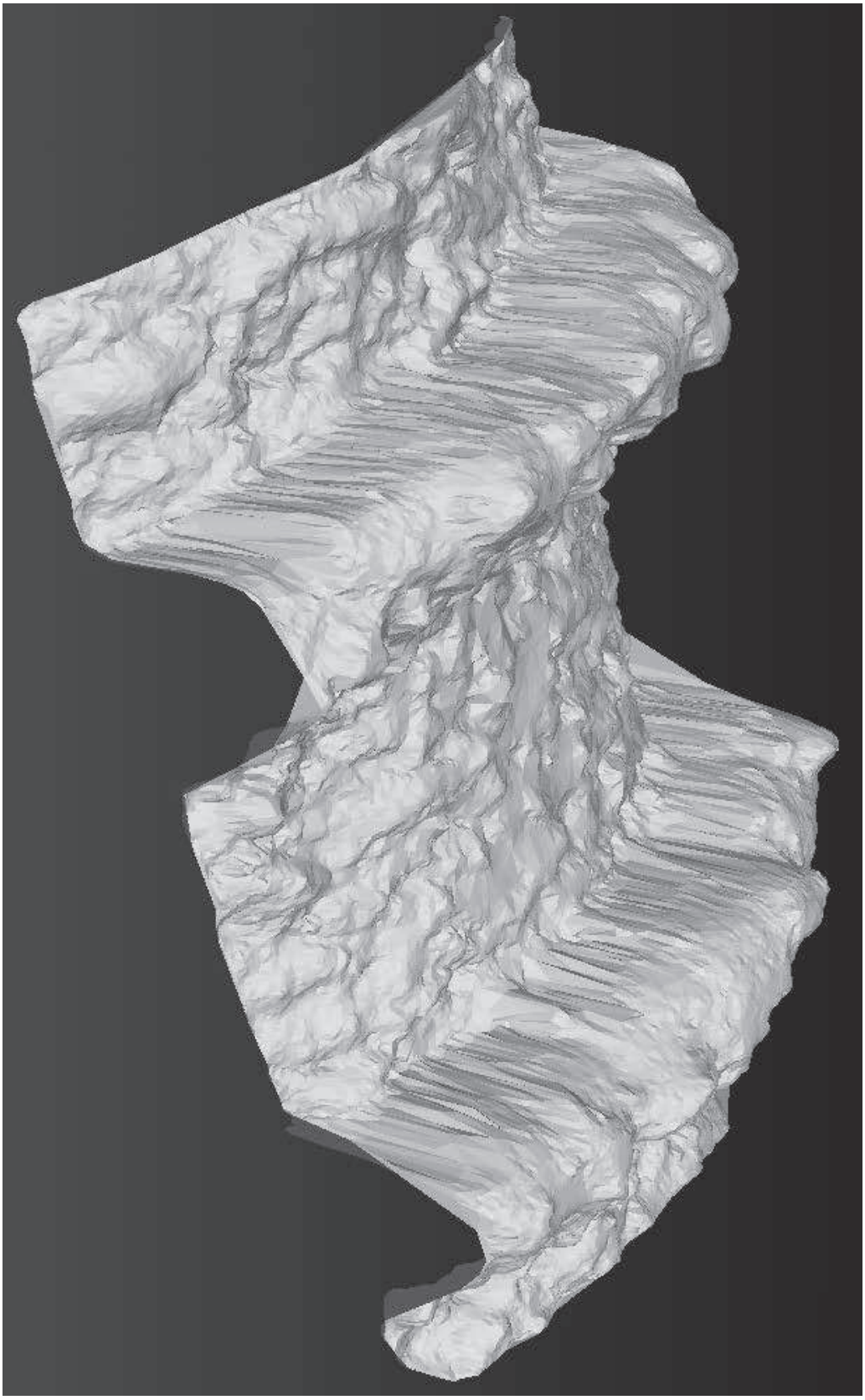

Figure 4 3d recostruction of laser sintered titanium surface

The main problem regarding the morphological structure of the implant is linked to the mechanical alterations that the graft undergoes to present a suitable surface for the integration. In fact, it would be weakened excessively in some cases due to the presence of numerous pores and conventional construction methods of these systems do not seem to have satisfied the needs.

Then alternatives were proposed; among these techniques Rapid Prototyping seemed to arouse considerable interest nowadays.

Among the different systems the Direct Metal Laser Forming (DMLF) technology allowed the building of structures presenting controlled porosity through a process of melting where a laser beam, led by the computer, can join very small cells of metals then creating the designed 3D object layer by layer. This method has the capability to directly build 3D metallic components from metal powder with minimal or no post-processing requirements and to control the porosity of the object to obtain more porosity near the surface and to reduce it when approaching the core. The described structure would allow for a better adjustment of the graft with the bone concerning the mechanical properties and loads and forces distribution. Moreover, the porosity provides for the integration of the graft within the surrounding bone due to the mechanical connections provided by the bone in-growth.

DMLF technologies can fabricate complex shapes of a custom-designed component using precursor powders to build these shapes through computer-controlled, self-assembly by melting powder layers using a laser beam. Until recently, DMLF technologies were not able to build custom-designed components from biocompatible metal or alloy powders such as stainless steel, Ti, Ti-6Al-4V and other Ti-alloys, and cobalt-chromium (Co-Cr) alloys (29% Cr, 6% Mo, balance Co by weight). Ti and its alloys exhibit the most suitable characteristics for biomedical applications because of their high biocompatibility, specific strength, and corrosion resistance (Niinomi, 2001).

Indeed, the majority of hip and knee implants over the past decade have been performed using Ti-6Al-4V.

The novelty of this technology lies in the fact that orthopedic structures can be produced with predefined physical and mechanical properties, so that their strength and bone in-growth characteristics can be optimized for specific locations within the body. Most of these millions of joint replacements, bone plates, etc. are generic, mass-produced components which do not work well with patients having an abnormal or unusual anatomy. In these situations, custom-designed implant components are preferred or required. This is also particularly true for cranioplasty especially where the missing piece of bone is large, requiring an implant component to be fabricated to follow the overall skull curvature. A further challenge in implant component fabrication is the necessity to produce complex shapes, including thin-walled sections, where cutting operations can

take a long time owing to significant material removal; up to 80% of bar stock from which knee implants are fabricated is converted to metal chips or scrap material.

Among the advantages of DMLF techniques the possibilities rely in projecting and realizing the implant by virtual technologies and workflows. Recently the spreading of low dose computed tomography (CT) protocols and cone beam CT (CBCT) allowed the lowering of radiation dose for cranio-facial imaging and diagnosis. These 3D imaging techniques might be easily integrated with CAD-CAM technologies then allowing to fabricate virtually custom-made designed graft according to clinical needs. Moreover, regarding the cranio-maxillo-facial region, the presence of bilateral and symmetrical structures allows to carefully replay the missing portions by copying them from the contralateral existing part form the CT images and 3D renderings.

The limits of the presented methods are related to the need of further studies which might confirm the interesting results of the existing case reports.

Therefore, the aim of the present study was the developing and testing of a reliable workflow to fabricate virtually custom-made designed grafts in the field of oral and craniofacial surgery integrating CAD-CAM technologies with DMLF and/or new polymeric materials techniques.

7 MATERIAL AND METHODS

7.1 RESEARCH PARTICIPANTS

This prospective study enrolled patients requiring bone graft surgical treatment in the craniofacial area. The sample of the present study consisted of patients selected from the different University and/or Hospital settings. As a routine procedure, a signed informed 8consent was obtained from patients, before starting treatment, for use of the diagnostic records for scientific purposes. The protocol was reviewed and approved by the Ethics Committee of the University of Insubria (n' 826, 10/08/2013) and the procedures performed comply with the World Medical Organization's Declaration of Helsinki.

Delivering integrated care is a strategic direction for the health to improve health outcomes and reduce costs deriving from inappropriate and fragmented care

Complex facial reconstruction is a challenging procedure as it requires uptake and healing of both hard and soft tissue components. Several factors influence wound healing, and systemic disease, as reflected by this study, is one of the most important determinants. Although systemic problems such as diabetes, long term steroid therapy and tobacco use have been established as risk factors for poor soft tissue healing, the role of these factors in facial fractures, which are usually a combination of bony and soft tissue injury, has not been established.[29] The selection criteria that we used in this study are as follows. (Tabella 2Table 1)

Inclusion	**Exclusion**
Patients with bone loss but enough soft tissue for the flap to cover the scaffold	Patients with local pathology that caused the bone loss (cancer, trauma) in progress
Patients with motivation for the physiotherapy after surgery	Patients where general health status did not allow the surgery
Patient that	Presence of systemic disease comprising diabetes, steroid use, and tobacco
CT not affected of metal scattering near the reconstructive site	Growing patients
patients who have no other reconstructive therapy options	hypersensitivity or allergies to metals

Table 1Inclusion/Exclusion criteria

7.2 RESEARCH CONTEXT

The present research project is a prospective study with the aim to perform short and long-term evaluation of custom made bone grafts in di Ti-6Al-4V fabricated with DMLF techniques integrated with CAD-CAM technologies employed in cranio-maxillo-facial

rehabilitation. Moreover, a reliable and reproducible workflow for the graft manufacturing would be described and validated.

7.3 TOOLS

7.3.1 Acquisition Data

Every patient enrolled in the present study underwent precise workflow of exams comprising CBCT/TC scans (different settings) of the skull to quantify and precisely visualize and measure the defect and soft tissue face scan. After the production of the digital model (cranio-facial prosthesis) and the post processing each titanium model was scanned by a 3D handheld scanner (EinScan-Pro, Shining 3D, China, 0.05 mm accuracy) to evaluate the accuracy though a superimposition method.

7.3.1.1 Acquisition of the Volume CBCT-TC

For years the accuracy of TC fan beam or Spiral Computer Tomography (SPC) was higher than CBCT resolution. The SCT homographs considered in this study are at the gold standard of their performance and allow an average accuracy of 3.05 pixels/mm, which is sufficient for the planning. In a Kaoru Kobayashi study [30] on the different precision between SCT and CBCT it has been shown that the vertical measurement error is between 0 and 1.11 mm on images produced by SCT, between 0.01 and 0.65 mm on images from CBCT (in all equipment tested only one value exceeded 1 mm). In general, the bibliography shows that the margin of error of conventional tomography is between 0.5 and 2 mm, but the measurement error should necessarily be less than 1 mm for planning. CBCT equipment has a much higher precision, averaging 8.6267 pixels/mm, more than double than an STC resolution.

Figure 5 CBCT working process

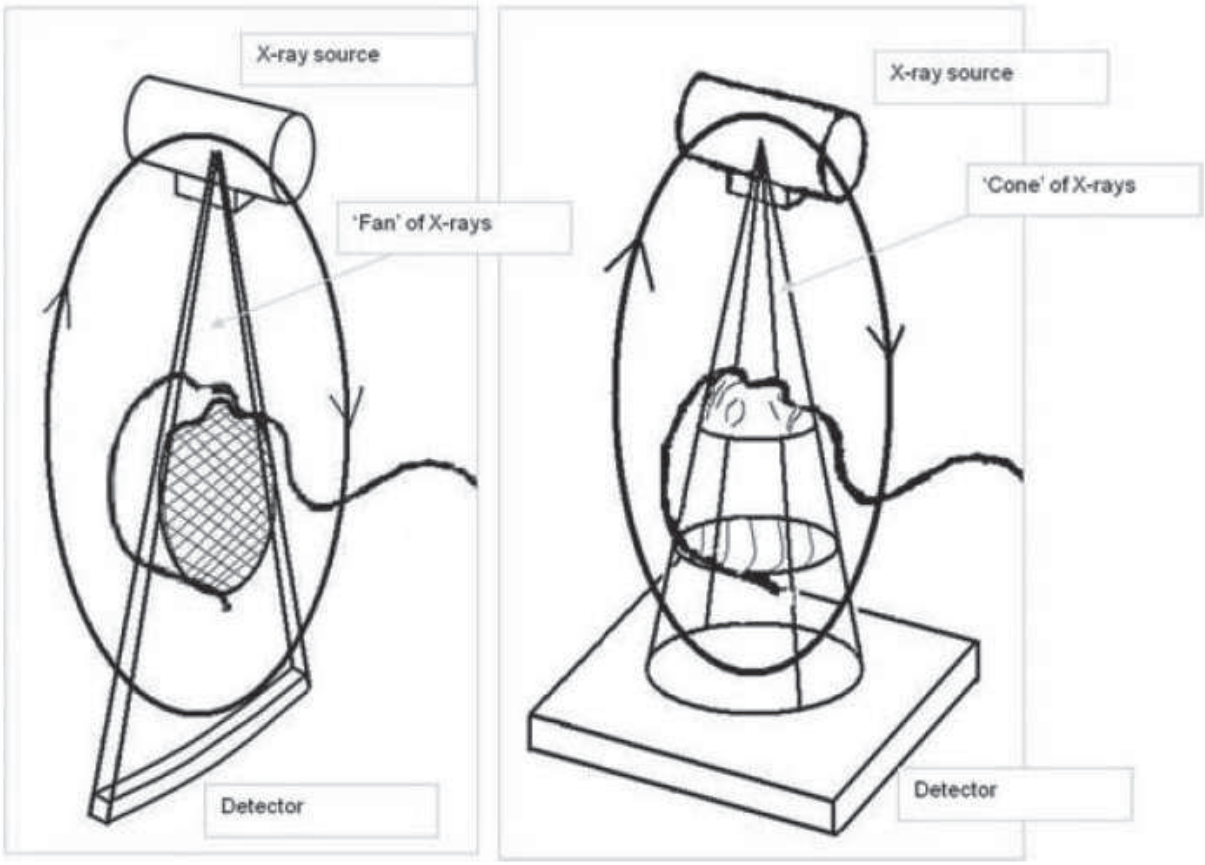

Figure 6. Differences between FanBeam and Cone Beam

Moreover, only a few devices can produce images with a real 16-bit gray depth (equal to 65,536 gray tones); others generate 12-bit images (equivalent to 4,096 tons of gray), that is, a smaller amount of information. These grayscale depths can be fully appreciated only through Dicom certified monitors; in fact, traditional computer monitors, the gray has an 8-bit resolution of 256 gray levels. Only the value of white and black is exactly calibrated, while the entire grayscale is not linear, but follows an exponential trend with expansion and compression. It is therefore possible that some gray neighbors are not practically distinguishable between them. It should also be noted that the variation in brightness and contrast is generally not linear with the viewing angle. Using standard monitors does not make it possible to view all the information present but only 50 percent of the gray tones present in the case of 16-bit images. Therefore, all the work done in this search has been carried out on a DICOM Certified Monitor. In addition, CBCT has advantages both in dosimetry and image quality, which could become the standard in three-dimensional radiology in the maxillofacial sphere. For this study, it was not possible to standardize the equipment used since the cases came from different hospitals around the world, the spatial resolution ranged from 0.5 to 1.5 mm.

7.3.1.2 Soft-tissue analysis

For each patient, a 3D facial scan was also performed to assist in the design of the graft so that a soft tissue reconstruction would be as true as possible. For this purpose, we used where possible a Primesense (Primesense Carmine 1.09, Subsidiary of Apple Inc., Israel, 2005) low-cost scanner adapted for this purpose. The subject-to-scanner distance was set at 80 cm and scan time was 30 s on average. The scanner depth sensor data were 640 × 480 pixels. Data were recorded on a desktop workstation with a 2.6GHz i7 Intel processor (Dell, Wicklow, Ireland). Light conditions were set for reliable data capture. The subjects were seated with the lips relaxed and with the head in natural head position (NHP) (self-balance "mirror" position) as described by previous authors. If a subject moved between scans, the procedure was repeated and the data of the first scan were eliminated from the study. The data were acquired by dedicated Skanect software (developed by the ManCTL Company, 2011, Madrid).

Figure 7 Example of a 3D scanned face

If it was not possible to acquire through a 3d scanner we can use 3D facial reconstructions obtained from CT or CBCT.

From our previous study it has been shown that soft tissue analysis proposal based on 3D facial scans showed good reliability and reproducibility even though further studies are needed to confirm the findings of the research. Such scanning is not only needed to have soft tissue but also to perform cephalometric measurements to restore the correct size and position of the bones to be reconstructed.

Figure 8Primesense scanner, low cost scanner

Figure 9Einscan-pro, high quality 3D scanner

7.3.2 Segmentation

Image segmentation is an essential procedure to analyze the image structure as other processing steps heavily depend on its results, and a wide variety of segmentation techniques have been reported in the last two decades. Some of its applications related to many fields, such as medical imaging, document analysis, object recognition, and SAR segmentation and quality inspection of materials [6]. Image thresholding based on gray level histogram information is an important technique for image segmentation. Most

techniques can be roughly categorized into two groups: global thresholding and local thresholding. The former means the process of a whole image with only one threshold, while the latter means that one separates an image into several sub images and then handles each sub image with a selected threshold.[31]

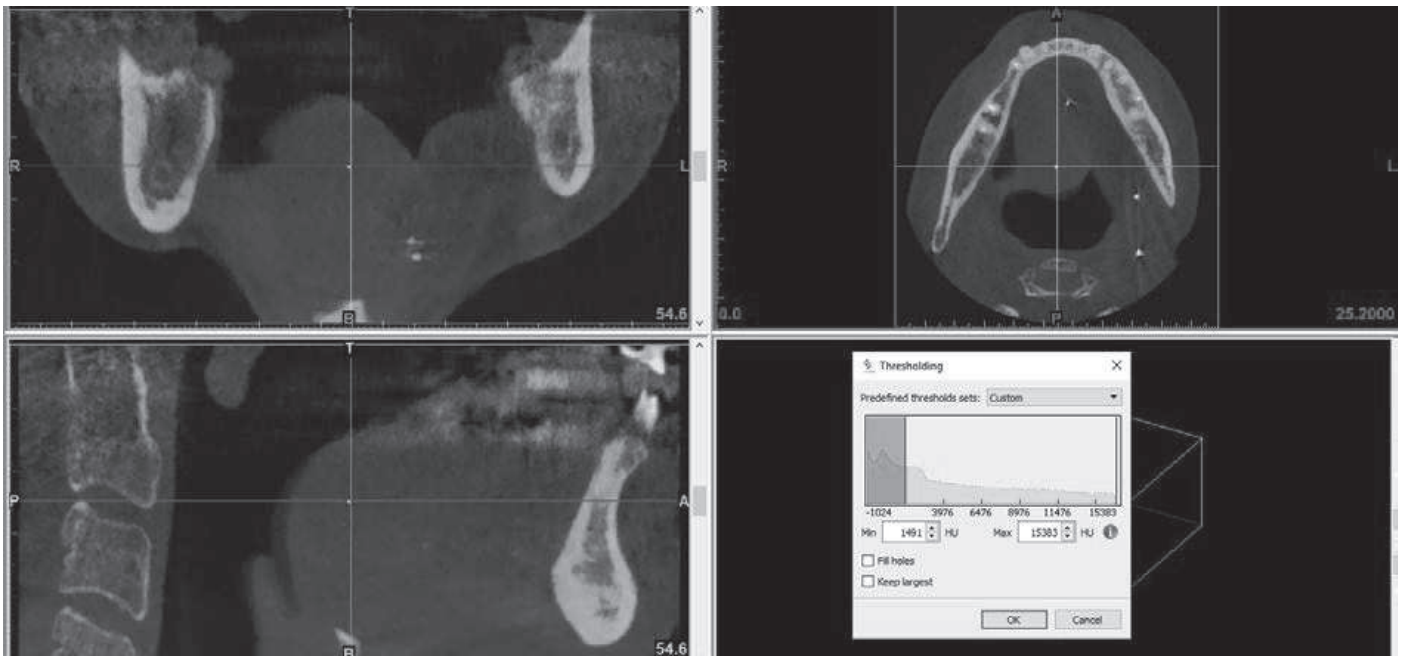

Figure 10 Simple thresholding technique

It is intuitively apparent that the accuracy of the 3D segmentation procedure is related to the voxel size during acquisition with 0.25 mm voxel size an appropriate compromise between diagnostic accuracy and patient radiation dose.[32]

The investigation of in vivo volumetric determination utilizing CBCT images has been shown to yield slight differences from actual physical volumes within − 4% to +7% [21]. However, there is a lack of a clearly defined gold-standard 3D segmentation protocol in the literature.[33]

	Newtom GIANO©		Sirona GALILEOS©	
	MIN	MAX	MIN	MAX
Threshold 1	99	15383	228.94	1262
Threshold 2	115.38	15383	248.94	1262
Threshold 3	131.77	15383	268.94	1262
Threshold 4	***148.15***	***15383***	***288.82***	***1262***
Threshold 5	164.53	15383	308.94	1262
Threshold 6	180.91	15383	328.94	1262
Threshold 7	197.30	15383	348.94	1262

Tabella 1 different volume with different thresholding level and different machines.

Segmentation process allows to delineate and define structures separating them with the final purpose to obtain 3D virtual models and clear visualization of each component. Spreading of CBCT in dentistry led clinicians and researchers to learn, improve and better understand these image processing techniques. The segmentation could be manual or automatic. Manual segmentation requires the operator to delineate structures slice by slice, while automatic or semi-automatic segmentation uses different density values (grey level units) of tissue to delineate their boundaries. Nevertheless, automatic segmentation is not always and completely user-bias free. Thresholding based segmentation uses density values to detect objects from a background. The segmentation object can be defined based on one lower threshold and it will contain all pixels in the images with a value higher than or equal to the threshold value.

The accuracy and reliability of the thresholding based segmentation could vary on the thresholding value which could be manipulate by the user in most of DICOM viewers and software's.

A study was performed by the authors to test reliability and reproducibility of choosing thresholding value during thresholding based segmentation process of teeth compared to the standard dimension of virtual dental casts.

The method validation was carried out using extraoral typodont which underwent to cbct scan with two different machines of the same type (CBCT A1 and CBCT A2. Scan protocol: 90 KV, 10 mA, 18 s) and one of different type (CBCT B. Scan protocol: 85 KV, 7 mA, 4 s).

The image data consisted of 537 slices, with a slice thickness of 1.5 mm, a resolution of 2200 x 1700 pixels for upper and lower arches, respectively. Then digital scan using an intraoral scanner (3Shape TRIOS®, 3Shape A/S, Copenhagen K, Denmark) of the typodont were performed to obtain a reference 3d model.

DICOM files were loaded to a computer with a i7 processor, running Windows 7 Professional (Microsoft, Redmond, Wash) operating system. The software used to perform segmentation of cbct scans was 3D Slicer (Open source software, version 4.3.1 64bit).

One expert user was asked to indicate the most accurate thresholding value to perform teeth segmentation in his perception. The 3D Slicer software allows to indicate thresholding value by scrolling a bar with immediate feedback of segmentation computed on image slices. Then 3 higher and 3 lower thresholding were defined by starting from the expert thresholding value with a step defined by the software. Then surface rendered 3d models were built correspondent to every thresholding value. All the segmentation derived 3d models were registered with a best fit alignment technique to the scan obtained by the intraoral scanner used as reference using Cloud Compare software (Open source software, version 2.6.0). The segmentation error was calculated by color displacement maps on 3d superimposition for the evaluation of the discrepancy between the different thresholding values and the reference 3d model. The SPSS software, version 13.0 (SPSS® Inc., Chicago, Illinois, USA) was used to perform the statistical analyses. Parametrical methods were used after having tested the existence of the assumptions though the Shapiro-Wilk test and Levene test for the normality of the distributions and equality of the variances among the three sets of superimpositions, respectively. The data were analyzed for maximum outer displacements and maximum inner displacement form the reference 3d model. Analysis of variance (ANOVA) test was used to determine if there were statistically significant differences among the three sets of superimpositions. Bonferroni correction was applied for statistically significant differences after post – hoc analysis. Alpha was set at 0.05.

So, we found that segmentation techniques based on the thresholding are not reliable and reproducible. Several software might be used to perform segmentation of the structures, as briefly described in the following paragraph.

7.3.2.1 ITK SNAP

ITK-SNAP has emerged as a useful tool in biomedical imaging research. This medical image processing application, which is available as open source, has a variety of manual and semiautomatic tools that aid in extracting 3D images of different anatomical regions in different modalities. This application focuses mainly on segmentation and features that do not involve segmentation have been minimized. Therefore, it is user efficient and easy to use. Using the ITK algorithm, various anatomical parts can be identified and outlined

using snake based segmentation. The anatomical structures can be reconstituted from the inside so that the contour of the bone surface is maintained. The various parameters of the algorithm can be altered to process images either manually or semi-automatically.

Segmentation is achieved by subdividing each region based on the voxels. The methods used for segmentation include the Intensity Range method and Image Edge method. In the intensity range method, voxels are grouped based on their intensity (using grayscale analysis given in the software). The structure formed is limited to the operator's chosen intensity range. The image edge method analyzes the gradient between adjacent voxels. When the gradient value is high, values close to 0 form an edge. Each structure thus formed by a subgroup of voxels is assigned a color code so that regions can be identified in the 3D image. It is also possible to use tools such as paintbrush and polygon tools for finer finishing of each slice. All images are stored in DICOM format.

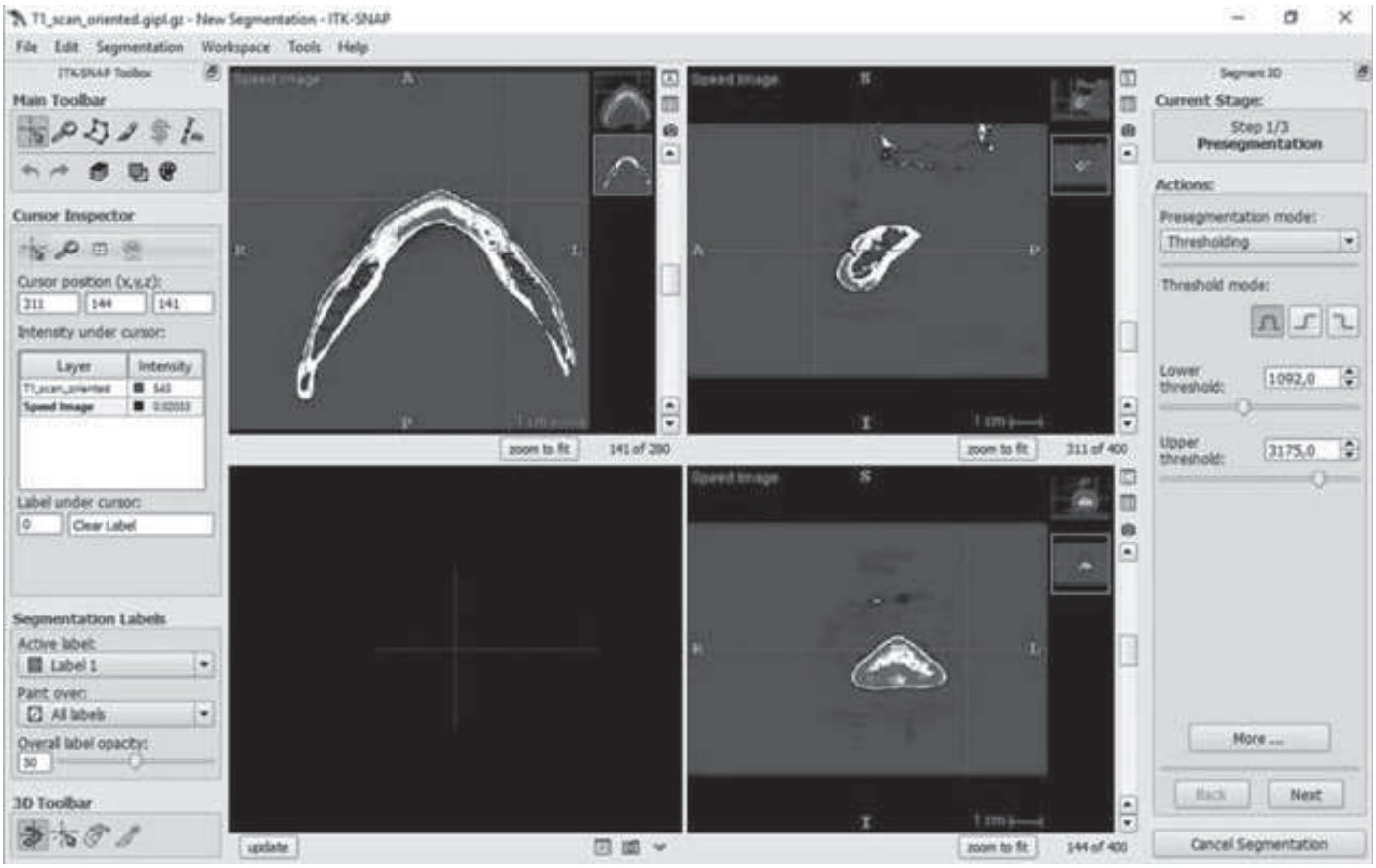

Figure 11Presegmentation with intensity technique

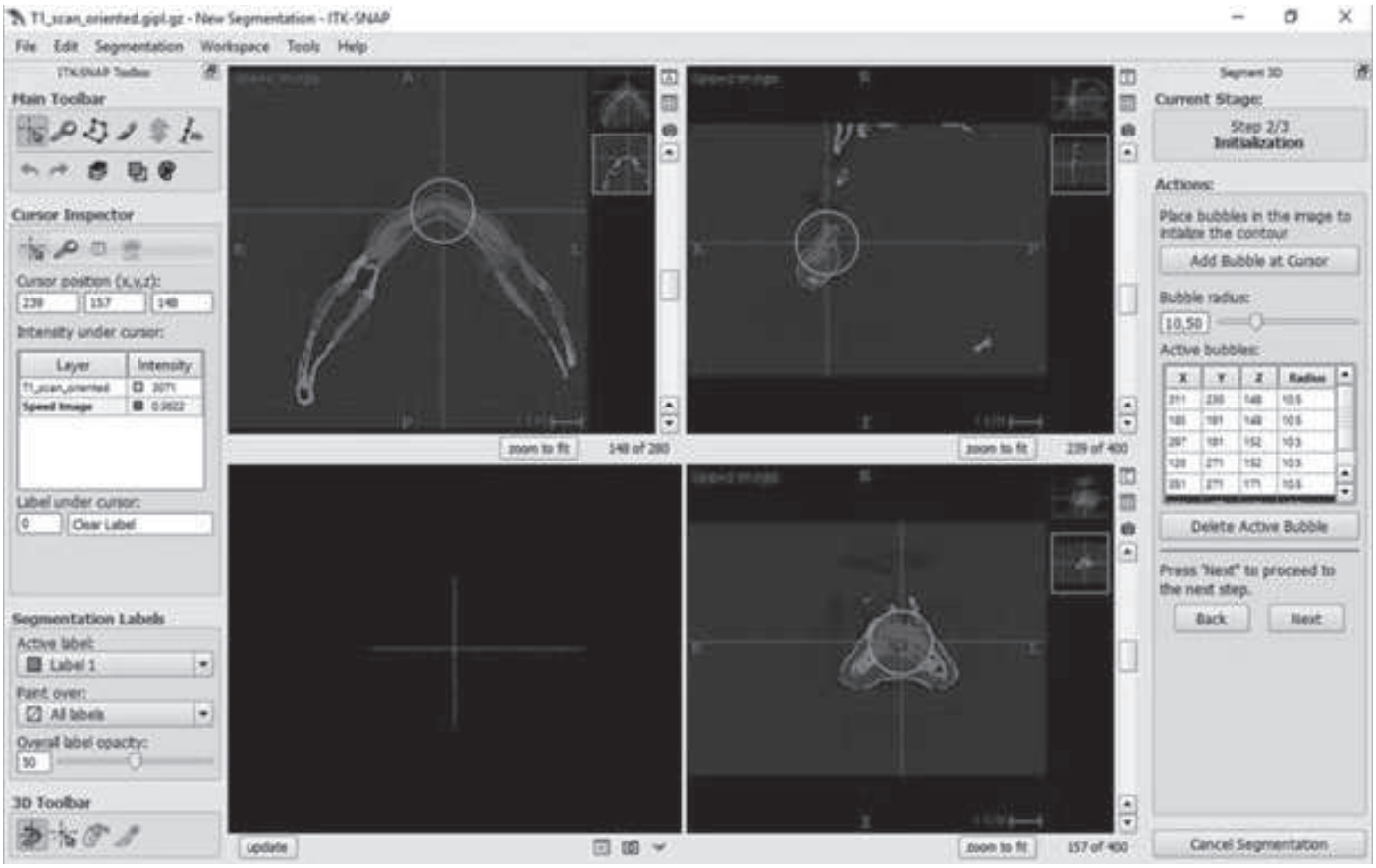

Figure 12adding "bubbles" to perform the semgentation

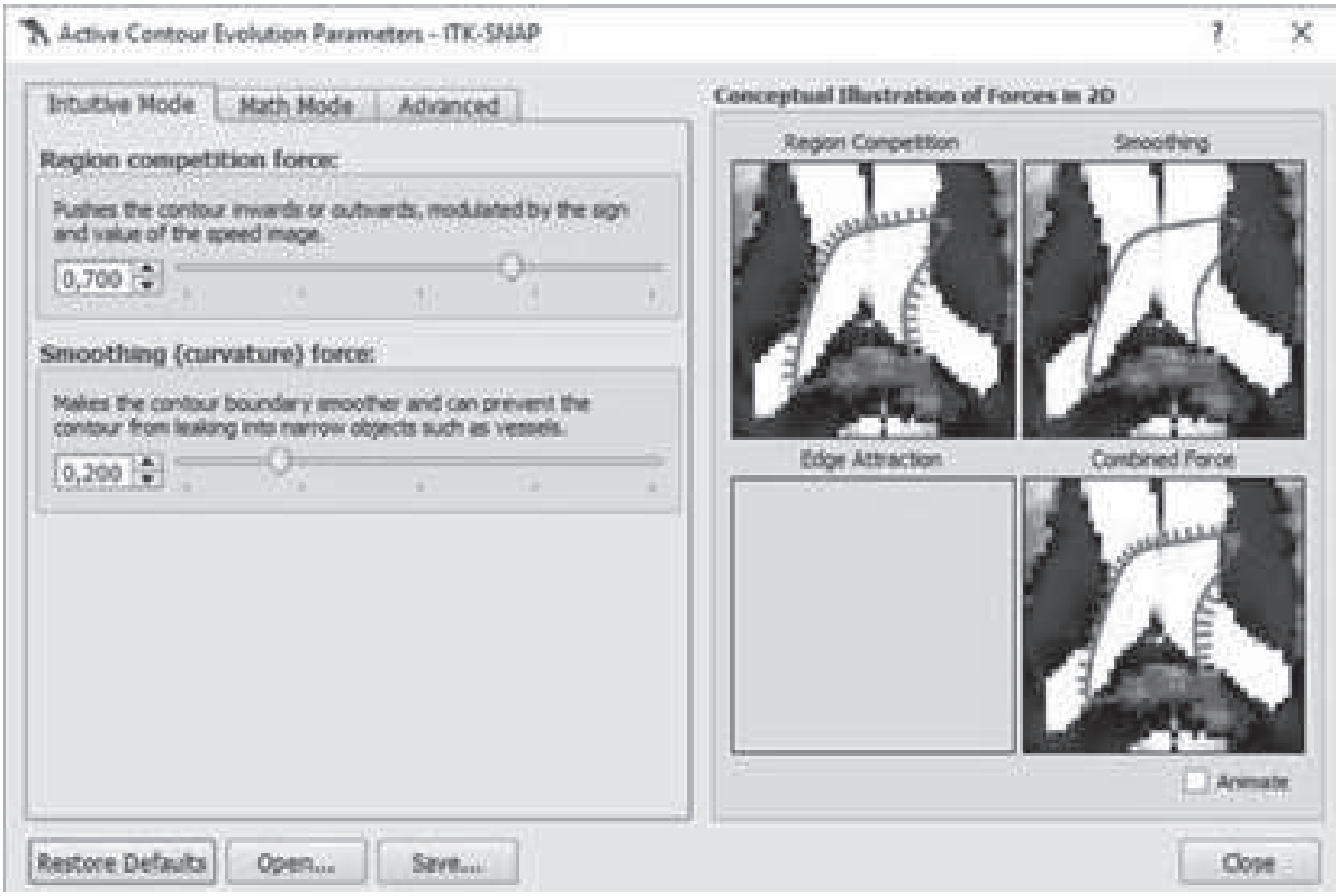

Figure 13 Bubble parameters, each value change the growing effets of the bubbles

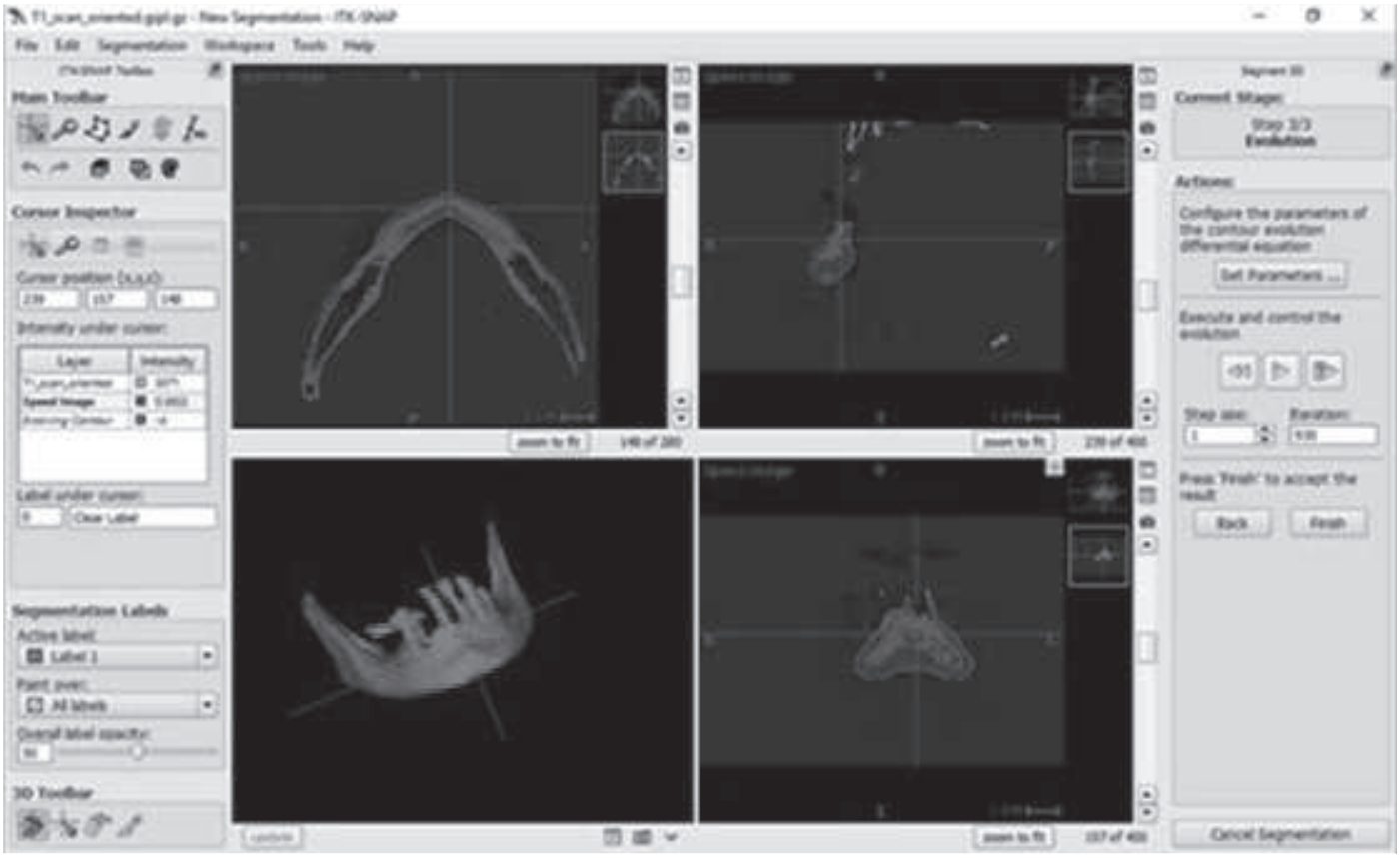

Figure 14 Segmented model

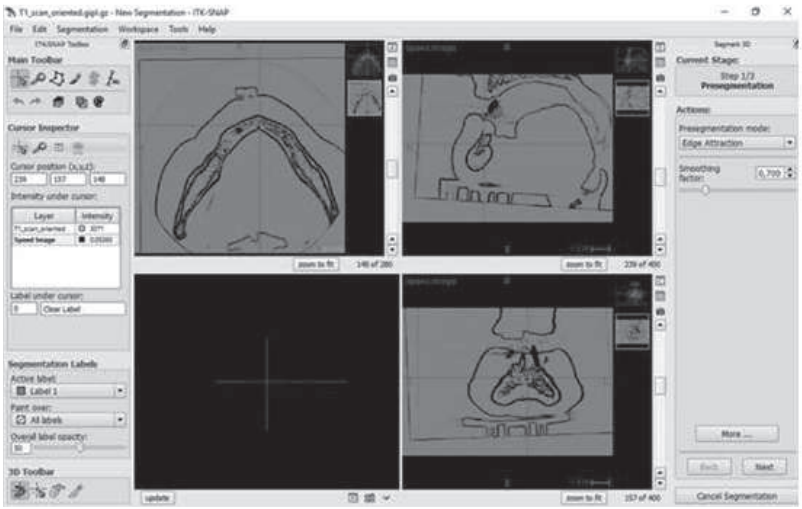

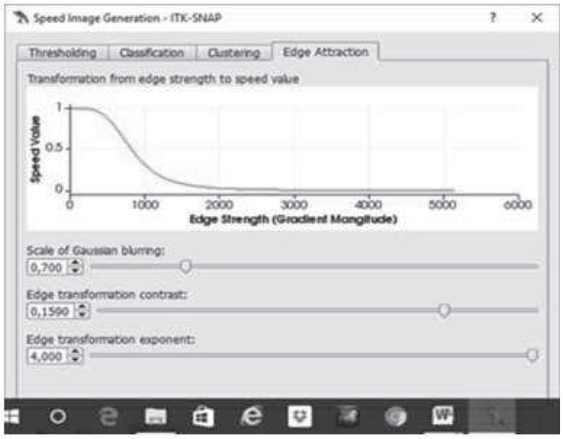

Figure 15 Other pre-segmentation technique, with EdgeAttraction techinque

7.3.3 3D Modelling

In reconstructing any defect, not only the pathology but also the surrounding anatomical areas must be printed for proper three-dimensional orientation. Other techniques that create connections but maintain the relative distance can also be used.

A certain minimum number of layers is required to be reconstructed in any defect to achieve adequate thickness for a strong model. This number varies for each material; for instance, it is only 1 mm for materials like polyamide, transparent resin and ABS plastic. However, for multicolored materials the thickness must be at least 2mm. This must be followed to avoid breakage or tearing of the final 3D model.

If the reconstructed model is expected to have hollowing, such as in case of sinus cavity or tumor, drainage holes must be accommodated in the design. These drainage holes, which must be at least 5mm in diameter, allow the residual material to come out, thereby preventing pressure buildup and breakage of the model. (Figure 6, Figure 7)

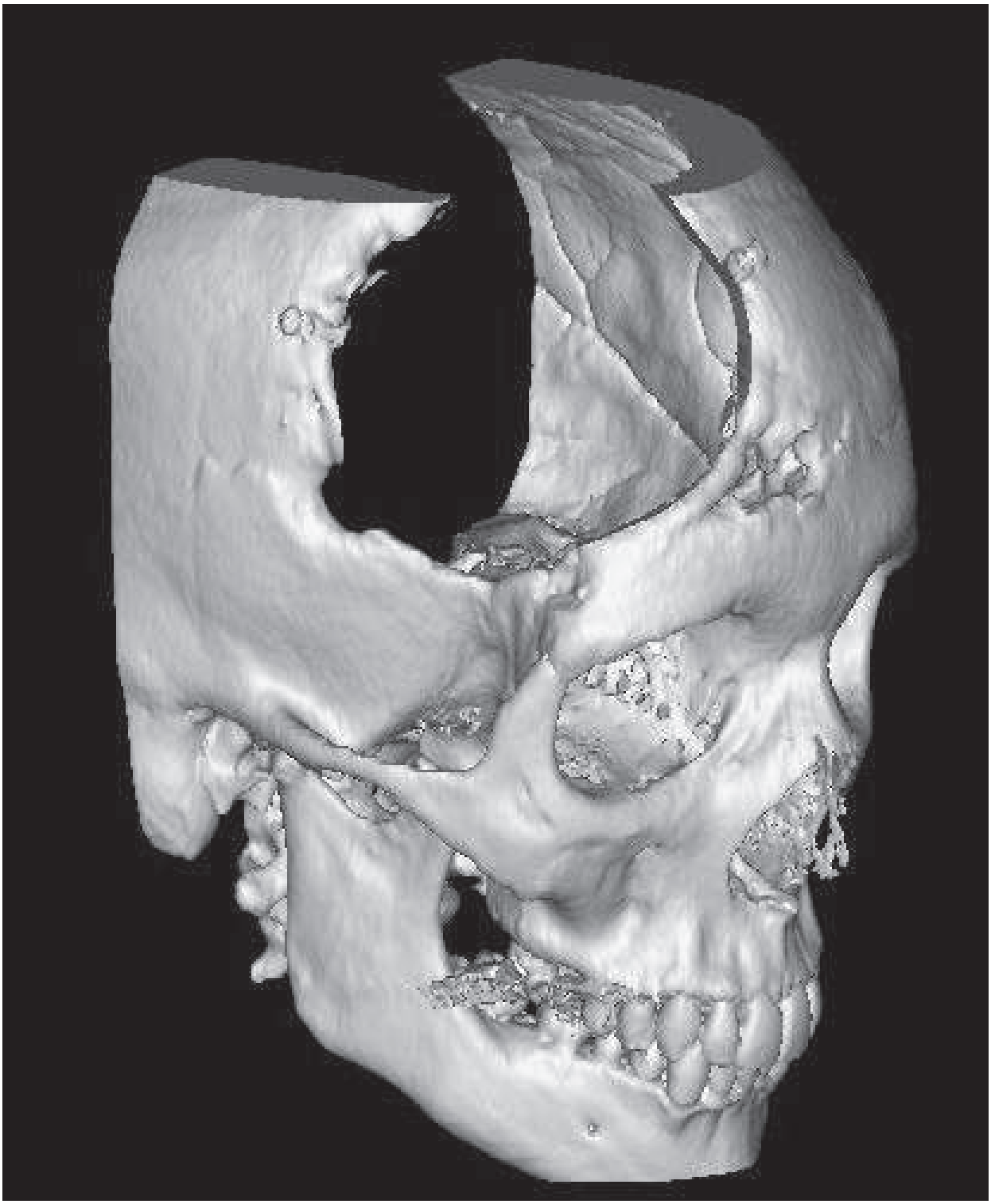

Figure 16 example of a bone defect. 3D model reconstructed from a CT

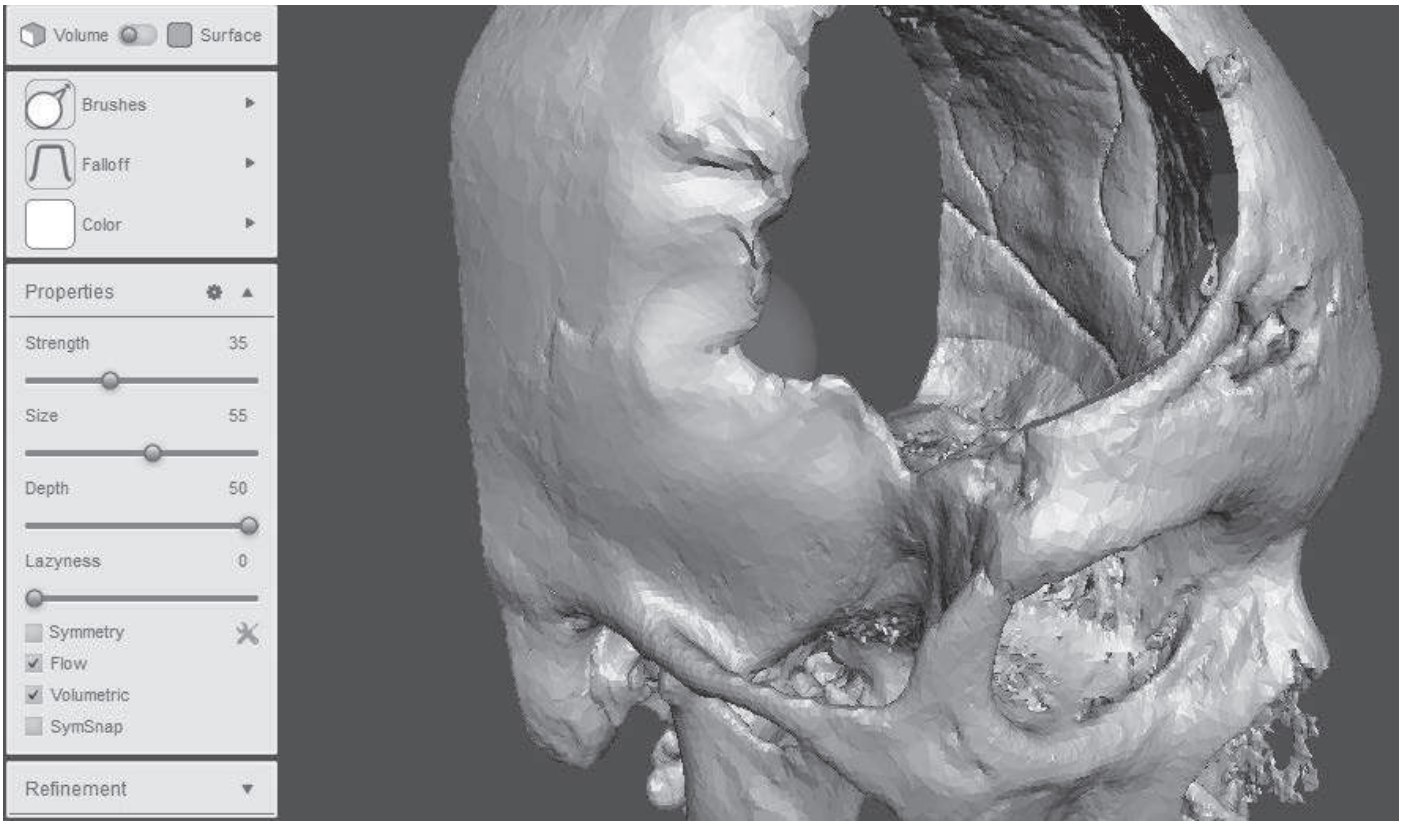

Figure 17 recostruction with manual tecnique. In this case with Meshmixer software (Autodesk)

Figure 18 modelling with mirror tecnique. 3D model generated with 3DSlicer software.

7.3.3.1 Voronoi Geometry

To avoid the problem of stress shielding we have decided to use the voronoi geometries and hereafter a narrative review of the literature of this technique.

The research question was to investigate the role of Voronoi geometry in bone reconstruction. A computerized search was conducted using Medline (to July 2017), Pubmed (to July 2017), Embase (to July 2017), and all EBM reviews (Cochrane Database of Systematic Reviews, ASP Journal Club, DARE and CCTR) (to July 2017) databases.

The search algorithm use was: ((Voronoi*[tw] OR Voron* [tw] AND (geometry*[tw] OR 3D*[tw] AND (surger*[tw] OR surgi*[tw] OR "General Surgery"[Mesh] OR "Surgical Procedures, Operative"[Mesh] OR "surgery"[Subheading])) OR "Bone Reconstruction" [Mesh] OR "CTscan" [tw]) AND (Techniques[tw] OR (3D Modelling)[tw] OR (3D Cell Modeling)[tw]).

Inclusion and Exclusion Criteria

The inclusion criteria included the following:

- Clinical human studies
- 3D Modeling
- Studies pertained to oral and maxillofacial surgery
- Voronoi Geometry
- Implant studies

The exclusion criteria included the following:

- Non-human studies
- In-vitro studies
- Opinion papers
- Perspective letters
- Meta-Analysis
- Thesis or Dissertations

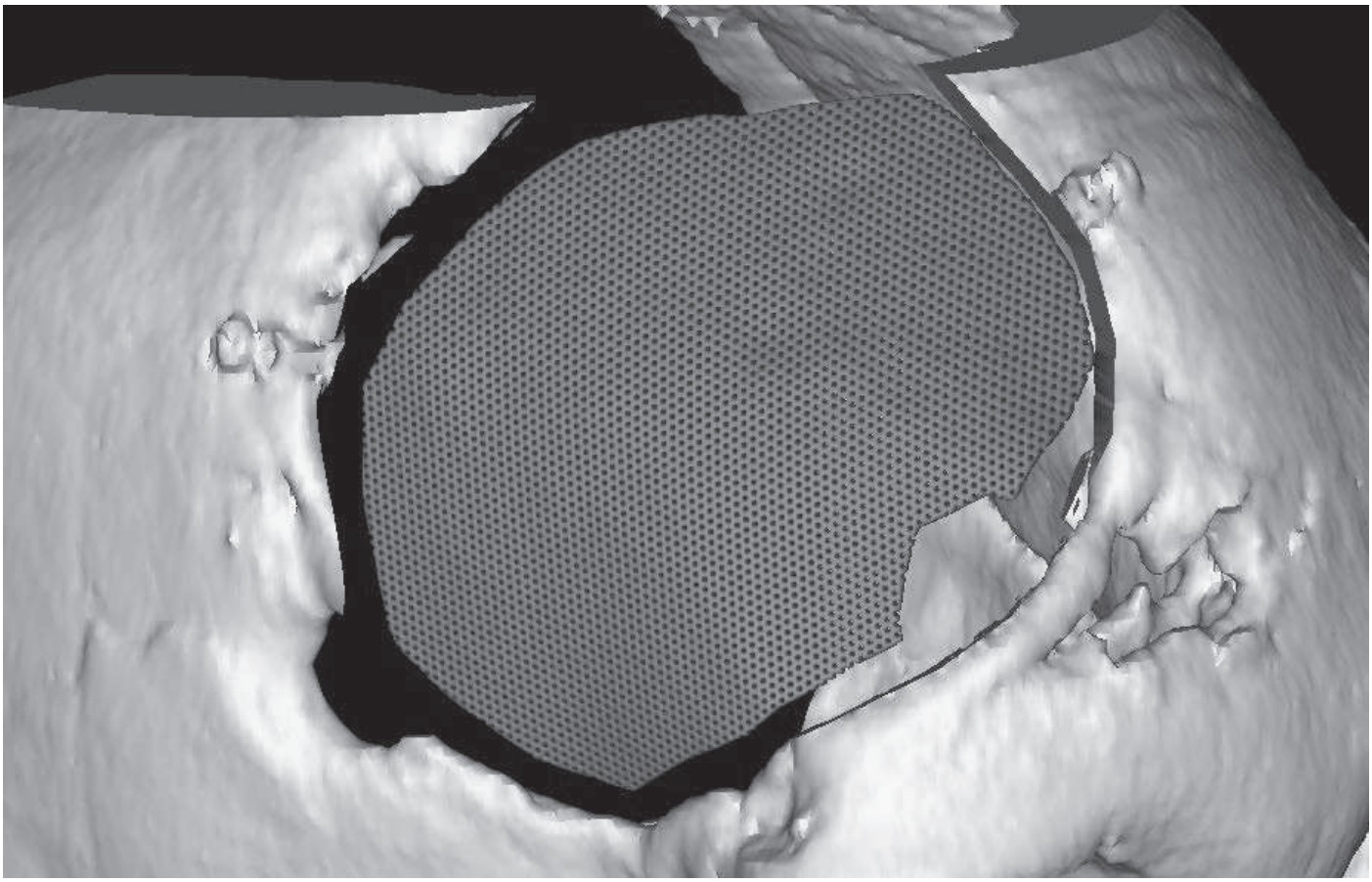

Figure 19 different suface characterization: simple holes

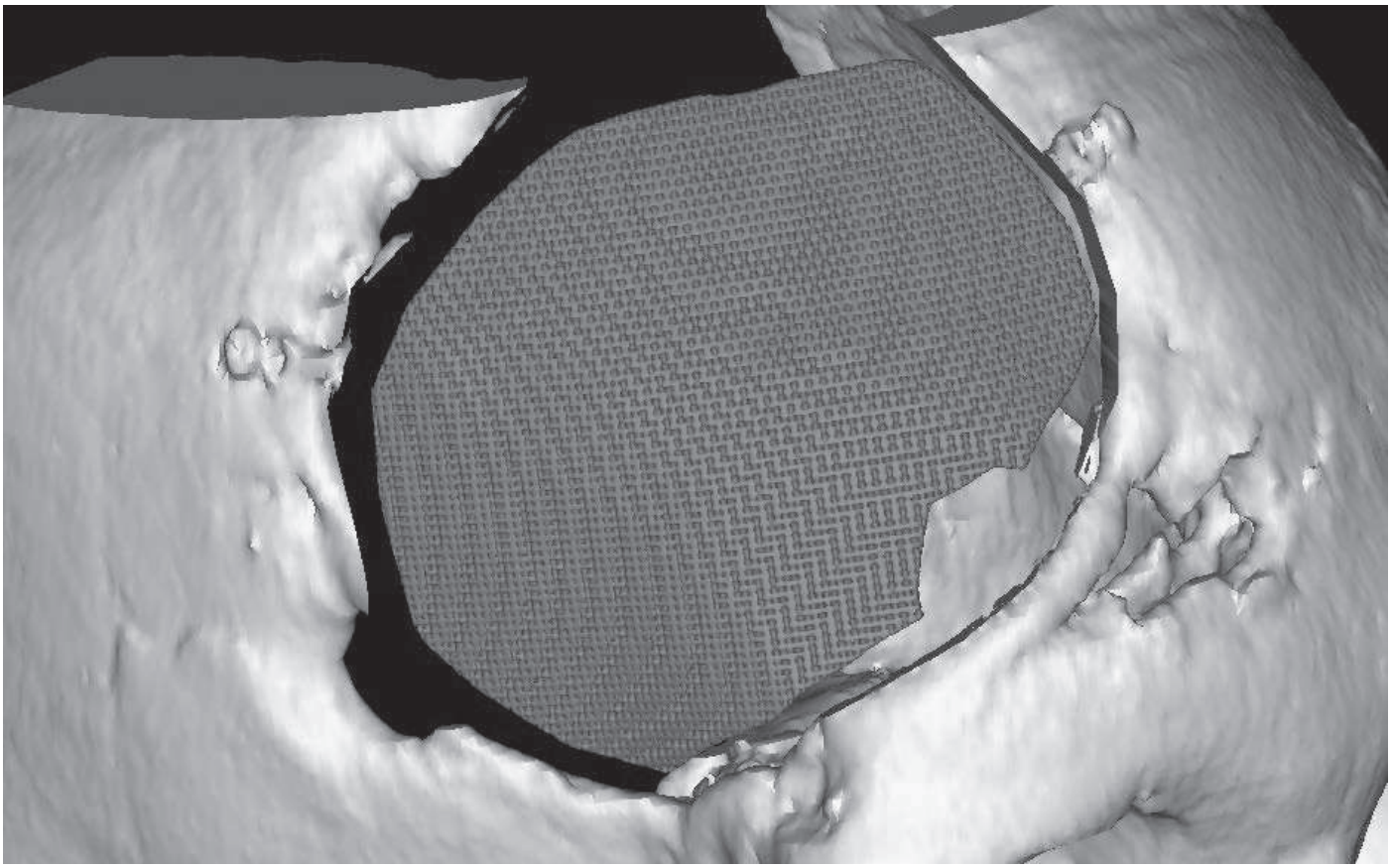

Figure 20 different suface characterization: lattice surface

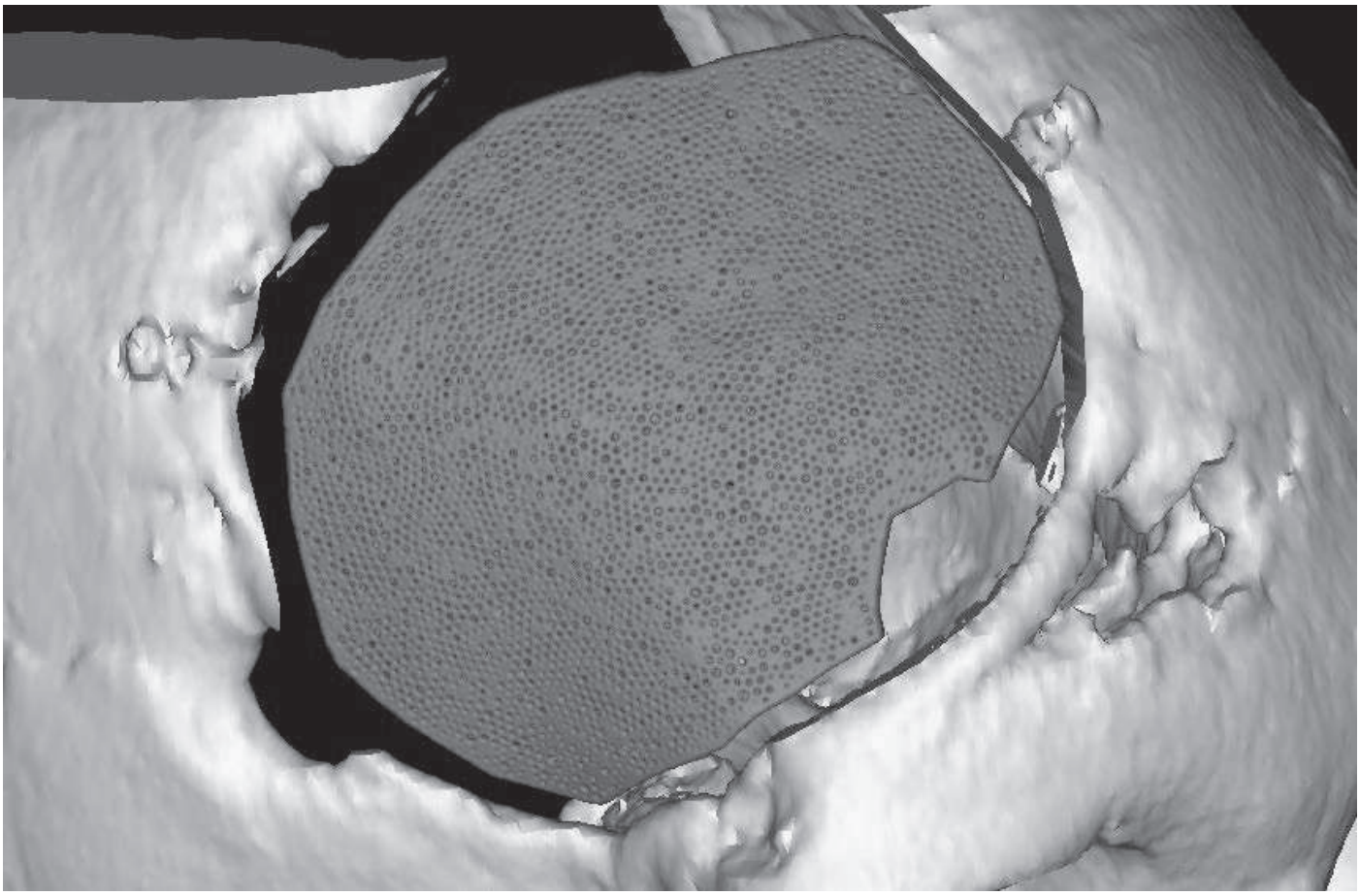

Figure 21 different suface characterization: one suface voronoi

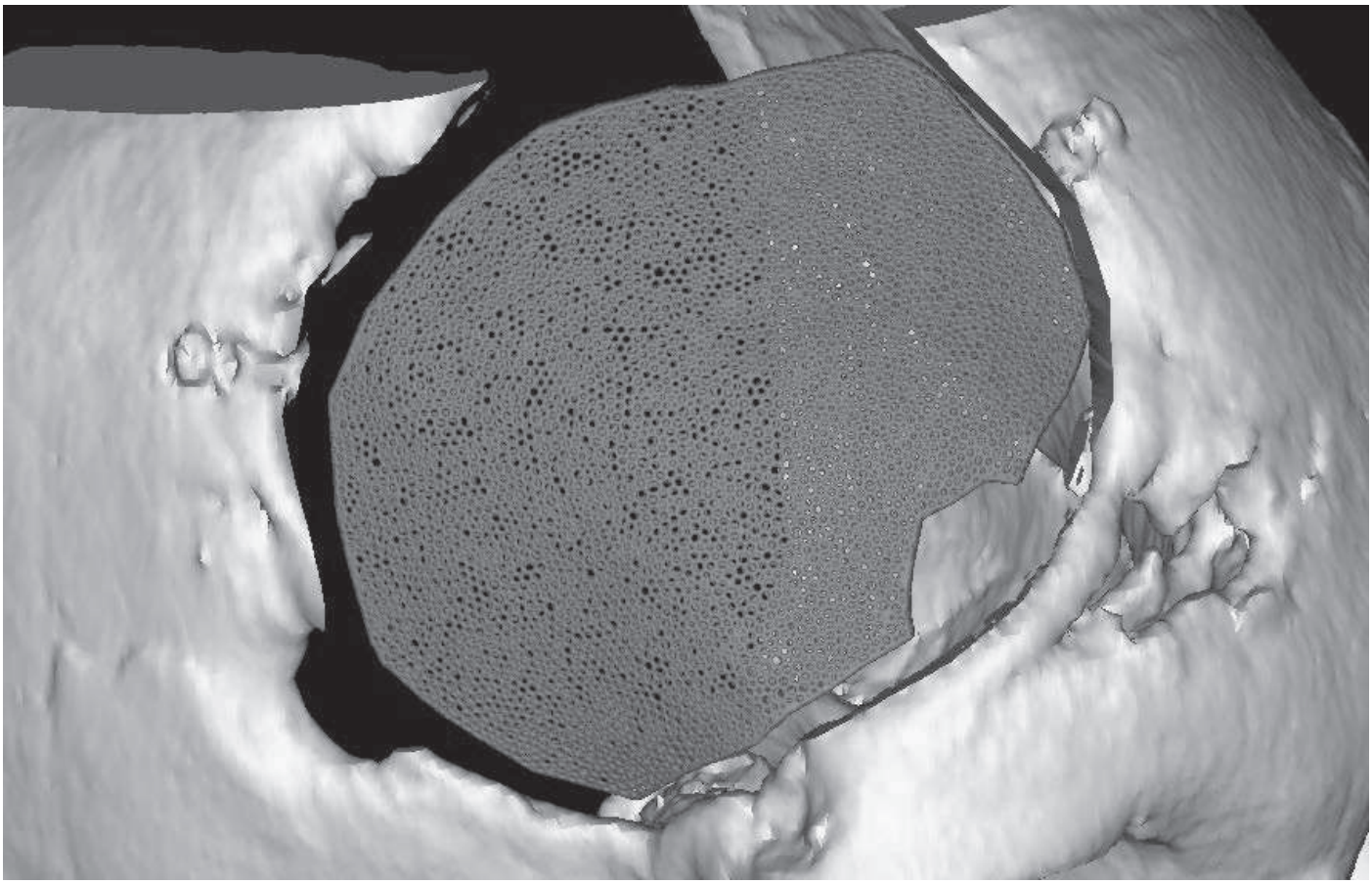

Figure 22 different suface characterization: two suface voronoi

A study was conducted for fracture risk prediction during osteoporosis by using 3D bone micro architecture modeling. The microstructure of normal human bone and osteoporotic bone was analyzed by developing a novel 3D computational bone framework. A Bayesian model is also used to analyze bone fracture risk on life style characteristics. Many fundamental questions are answered by a graphical model such as some life styles are dangerous or not? What are the most wanted factors for bone fracture and deterioration? As a result, people stop smoking to protect their bone health. Measurements in biological, geometrical and mechanical domains demonstrated our model by showing the properties of bone microstructure. This study predicts that the success of matching fractal dimension is the essential and start-up step for mechanic assessment research on our 3D bone network and mechanistic appreciative of bone microarchitecture and identifying topological network features related to crack proliferation characteristics and fracture risk. The extensive empirical study on fracture risk and model of 3D bone micro-architecture increase concept of bone disease risk from interplay of human BMD valuation with the presence of different major factors [34].

Another study was conducted by Aidong Zhang to develop a spatial model for testing the bone mineral density and micro architecture for quantitative assessments. A special network model was investigated. Voronoi tessellation was used which showed the bone mineral lattice and bone mineral foci was distributed according to a normal distribution.

X-ray imaging model was also developed and used. One of the exclusive aspects of this model was that structures like loosely organized, densely mineralized and spongy trabecular bone, compact cortical bone appears and transition seamlessly because of this modeling strategy. No need for an artificially enforced edge between the cortical and trabecular bone in this model. Primary determinants of trabecular-cortical structural are the basic steps of density distribution between Voronoi centers and pruning steps. The normal and diseased bone of 20 to 80 years old patient is compared by simulations which show the effectiveness of the model, especially for osteoporosis. For modeling imaging data in clinical trials and pharmacodynamic stimulations of bone, the native spatial model may be helpful [35].

Another study was conducted which analyses the bone cell network from synchrotron radiation micro-CT images. This study was Voronoi based. In this study, a new method is used to compute features on canaliculus from 3D SR micro-CT images and assessed their distribution around every lacuna. Women, tibial samples are taken by three SR micro-CT images technique, and descriptive statistics are applied. The imaging procedure is well described in section 2. Pre-processing of 3D images which include the computation of morphometric parameters and the segmentation of the LCN is outlined in section 3. This study found that the average Lc.CaTess.S was around 15 µm2 in the three women cortical bone samples. The value of each sample was increasing from 14.2 µm2 to 16.9 µm2, demonstrating a lower density of the canaliculi connected to the lacunar surface in the young sample (F1: 46 y.o.) than the elder one (F3: 87 y.o.). The higher standard deviation of Lc.CaTess.S, 7.5 in F3 (87 y.o.) compared to 4.2 in F1 (46 y.o.), might also indicate more heterogeneity in the canaliculi location in the elder bone sample [36].

Another study was conducted which used the Voronoi tessellation method by designing novel bone like 3D porous scaffolds. To obtain 3D virtual isotropic porous interconnected models, the Voronoi method has \been processed. 3D trabecular bone-like structures were designed using the novel CAD software GrasshopperTM v.0.9.0076 and other different software was used. It is observed that for a fixed value of NNP a survey of different porous structures can be obtained in such a way that when BV/TV increases, BS/TV, and Tb.Th also increases but Tb.Sp and Tb.N decrease. It is also observed that by adjusting the NNP, an appropriate Voronoi scaffold model can be designed to adjust the properties of its equivalent Implicit Surface model. For example, a Voronoi scaffold model with 10 NNP gives nearly the same results than both, Cylinder Grid and Schwarz Primitive models [37].

A study conducted by A. M. Makiyama gives us the analysis of crack growth in 3D Voronoi Structure. A model was used which quantifies the role of crack growth to the fatigue reaction of a low density, random, open-cell Voronoi structures like osteoporotic trabecular bone. This model gave the good representation of decrease in secant modulus at the low-stress range. To assess the effect of normalized stress range, initial crack size, density and cell geometry on fatigue life a parametric study is performed. The initial crack length and density are more sensitive in fatigue life. Comparison between the data of crack model growth and trabecular bone of fatigue life are given in this study. A Larger

difference in trabecular bone data shows that it is impossible to distinguish between crack growth and dominated creep fatigue [38].

A study conducted by Jakub Michonski which is utilizing analysis of back surface topography data to support documentation of diminishes x-ray exposures and severity of the deformity. Conversion (3DMADMAC) system environment and -D measurement with algorithms of directional merging was utilized and calculated for -D measurement with algorithms of directional merging. The data obtained from the measurement is in the form of raw point clouds. A cloud of points represents an unordered set of points, where each point is characterized by its Cartesian coordinates, color (RGB or gray scale, depending on the type of detector), the normal vector of the surface and quality factor corresponding to the uncertainty of coordinates' determination . Weights calculated on Voronoi diagram not only decrease the probability near the boundaries of the cell but also the influence of locations of landmarks. It confuses the optimization process when feature takes extreme values for points near the border. Positions obtained with the developed algorithms are validated concerning precision of manual landmark signal by experts. Preliminary confirmation proved that the landmarks were localized suitably, with accuracy depending mostly on the character of a given structure. It was concluded that recognition should mainly take into account the shape of the back surface, putting as little stress on the statistical estimate as possible [39].

Another study was conducted which generated the Voronoi diagram for some unbiased samples in the geodesic metric, and these samples are selected from original points. This study generates the triangle meshes for scattered data consist of redundant points. By Voronoi diagram, the mesh model of seeds is constructed. Poisson disk sampling is taken to select seeds and helps to produce the Voronoi diagram. The strategy of this study is to run around the problems that the geodesic distances are sensitive to neighboring points rather than basis on Voronoi diagram. In the first experiment, the number of points used about 3 million and uniform and adaptive reconstructions are then carried out. The second experiment is on dragon which contains 2 million original points, and the numbers of seeds are 4,800, 8,500, 18,000 and 64,000 obtained by adjusting disk's radius [40]. After then, their accuracies are estimated by comparing them with the original dense mesh model. Adaptive renovations can be achieved by a little changing the uniform policy in selecting seeds. Actions of this method are examined, and accuracy assessments are done. Experimental results show the proposed method is reliable and effective.

Another study was conducted by Jun Wu, Niels Aage in which they present a method to produce bone-like porous structures as lightweight infill for preservative manufacturing. This method builds upon and spreads the general, voxel-wise topology optimization scheme. Bone-like infills are tested under different robustness criteria. Natural materials look to suggest that physical robustness comes with ordered complexity in shape and topology. The local capacity constraint aids this purpose by inspiring a structural organization of microstructures to support agreed outside forces. The very distinctive approach to ensure forcefulness to uncertain loads in topology optimization is to optimize concerning multiple or worst-case loading situations. While colorant manufacturing

enables the production of complex shapes, it still takes a few constraints, e.g., regarding feature size, overhang surfaces, and enclosed voids. Preferably such constraints shall be combined into the optimization procedure [41].

Another study was conducted in which the CFE for complicated domains presented in this study have been implemented except for the case of spatially varying elasticity parameters. Validation of the methods used here for the elasticity case is work in progress. First experiments indicate that the threshold according to works well. This method determines the segmented volume by counting voxels with a gray value above or below a fixed value. It seems to be unnecessary to use the CFE segmentation instead, which makes finding the threshold more than two orders of magnitude more expensive regarding CPU time. A CFE multi grid solver using V2 cycles for scalar isotropic discontinuous coefficients has been implemented with the adoption of the coarsening weights so that the coarsened basis functions form a partition of unity [42]. We observe that the multi grid preconditioning is not effective and that performing the coarsening described above (not surprisingly) takes longer than standard coarsening. In the cases considered here, the multi grid method is effective and not significantly slower than the standard multi grid, but still outperformed by the SSOR- pre-conditioned CG solver [42].

Another study was conducted to improve the geometrical parameters of open-porous titanium frameworks to match the elastic properties of human cortical bone concerning an acceptable pore size. An optimization approach is used to numerically investigated three different scaffold designs i.e. pyramidal, cubic and diagonal. For the creation of lattice structures of the scaffold, beam elements were utilized. Strut diameter was 0.2 to 1.5 and pore size was 0 to 3.0 mm.in the first sep geometrical parameters were changing to obtain a modulus of 15 GPa (Young's modulus of cortical bone) and a pore size of 800 µm was meant to enable cell ingrowth. Additionally, the mechanical performance of the enhanced structures under bending and torsion was examined. Consequences for bending modulus were between 9.0 and 14.5 GPa. In compare, shear modulus was lowest for cubic and pyramidal design of approximately 1 GPa. Here, the diagonal design had shown a modulus of nearly 20 GPa [43]. The results for the parameter variation of the cubic structure are like our previously published work. Here the different strut geometry, i.e. circular and rectangular was taken into account for numerical investigations of open-porous titanium scaffolds that have been compared to results from experimental testing [43].

Another study was conducted to introduce a methodology to segment the LCN from 3D synchrotron radiation nano-CT images. Segmentation of such structures is challenging due to several factors such as limited contrast and signal-to- noise ratio, partial volume effects and a huge number of data that needs to be processed, which restrains user interaction. They show a large number and good continuity of the segmented canaliculi. Nevertheless, according to a detailed visual inspection of 50 slices randomly selected from the available samples, some imperfections were found: 39 out of 50 slices were classified as good, but nine as moderate and two as poor [44]. The moderate and poor grading was assigned to the slices, in which surplus pathways have been extracted. Since

fluids circulating in the LCN are sensed by the osteocytes, the complete information about the lacunae and their surroundings is needed to understand the biomechanical behavior of the LCN [44].

Another study was conducted which compares the effects of density reductions from uniform thinning of struts. Young's modulus was used. The effects of strut removal on Young's moduli of regular and Voronoi two and three-dimensional structures are compared. The regular two and three structures are arrays of hexagons and tetrakaidecahedron. Three-dimensional structures are less sensitive due to higher connectivity. Results showed that changes in bone density due to resorption of trabecular have a much more dramatic effect on mechanical properties than those due to uniform thinning of the trabeculae.

One of the studies was conducted to integrate information on risk factors and bone mineral density. A novel 3D computational bone framework was developed, and parameters are predictable from imaging data obtained with dual energy x-ray imaging and absorptiometry methods. Many cellular and biochemical interactions are evaluated from pharmacodynamics cellular based homeostasis and understood the metabolic bone reaction. Bone material was distributed, and Voronoi Tessellation and Stochastic Edge Pruning were applied. This study gave result in the form of a spatial component of such a modeling framework and the mechanism of osteoporosis and how bones micro architecture [35].

One of the studies was conducted to characterize Voronoi-based biomimetic bone scaffold morphologically. It was produced by interactive generative design process and through the additive manufacturing system. The characterization was performed according to the indices in trabecular bone structures. The biomimetic cubic bone scaffold was initially designed with controlled porosity (P% = 80%) having a mean pore size of (Dp = 0.800 mm) and it was manufactured with Ti6Al4V using EOSINT M270 laser sintering system. Scanning Electron Microscopy evaluated the surface morphology of scaffold with the aid of special Energy Dispersive X-ray Spectrometry. A high-resolution micro-CT SkyScan 1172 was used to examine the internal morphology of bone scaffold. The tools such as ImageJ with BoneJ which is specially designed to take the images of bone analysis was used to the morphometric assessment of bone scaffold. It measures the indices to characterize the bone scaffold according to the trabecular bone structure. Despite low porosity (P% = 73%) and small mean pores size (Dp = 0.695mm) of Ti6Al4V scaffold, it was fabricated with interconnected porous architecture and intact trabecular skeleton [45]. The results revealed that the main indices of the trabecular bone structure are similar to that of actual bone when characterized morphologically. This method of fabrication allows to produce biomimetic bone scaffolds of the desired porosity and mean pore size. These biomimetic scaffolds also facilitate the reproduction actual bone architecture of trabecular bone, and therefore these are the most suitable scaffolds for Bone Tissue Engineering according to the patient-specific requirements [45].

In bone tissue engineering, it is imperative to accurately design and produce the lost tissue to maintain structural and functional aesthetics of the bone. Synthetically produced scaffolds form the structural template and when the cells regenerate scaffolds bear the load of surrounding tissues [46, 47]. One of the study was aimed to design a method that helps in the production of biomimetic scaffolds for bone tissues by Voronoi lattice. It has been that 3D scaffolds successfully sustain the regeneration of new tissues at the site of damage in the human body. To demonstrate the clinical application of 3D scaffolds several experimental studies are conducted which focus on the design, the material, and the manufacturing process so that a fully biocompatible lattice is designed. At present, most of the regular 3D shapes are based on unit cells geometry with repetition of unit cells. The introduction of general design method yielded a very efficient generation of biomimetic porous lattices according to the patient anatomy. These are very fast and intuitive. In addition to these, the pore size and porosity were exceptionally accurate. Moreover, the CAD approach to design scaffolds also provides benefits as it produced a watertight mesh of porous scaffolds which are used for various bone grafts in surgery. These findings support the preparation of scaffolds from interactive generative design approach which is based on Voronoi diagrams. These diagrams can be simply modified according to the surgical needs to maintain percentage porosity and pores size. The method of biomimetic lattices are used in bone tissues cases and follow the Generative Design approach of Voronoi diagrams [48].

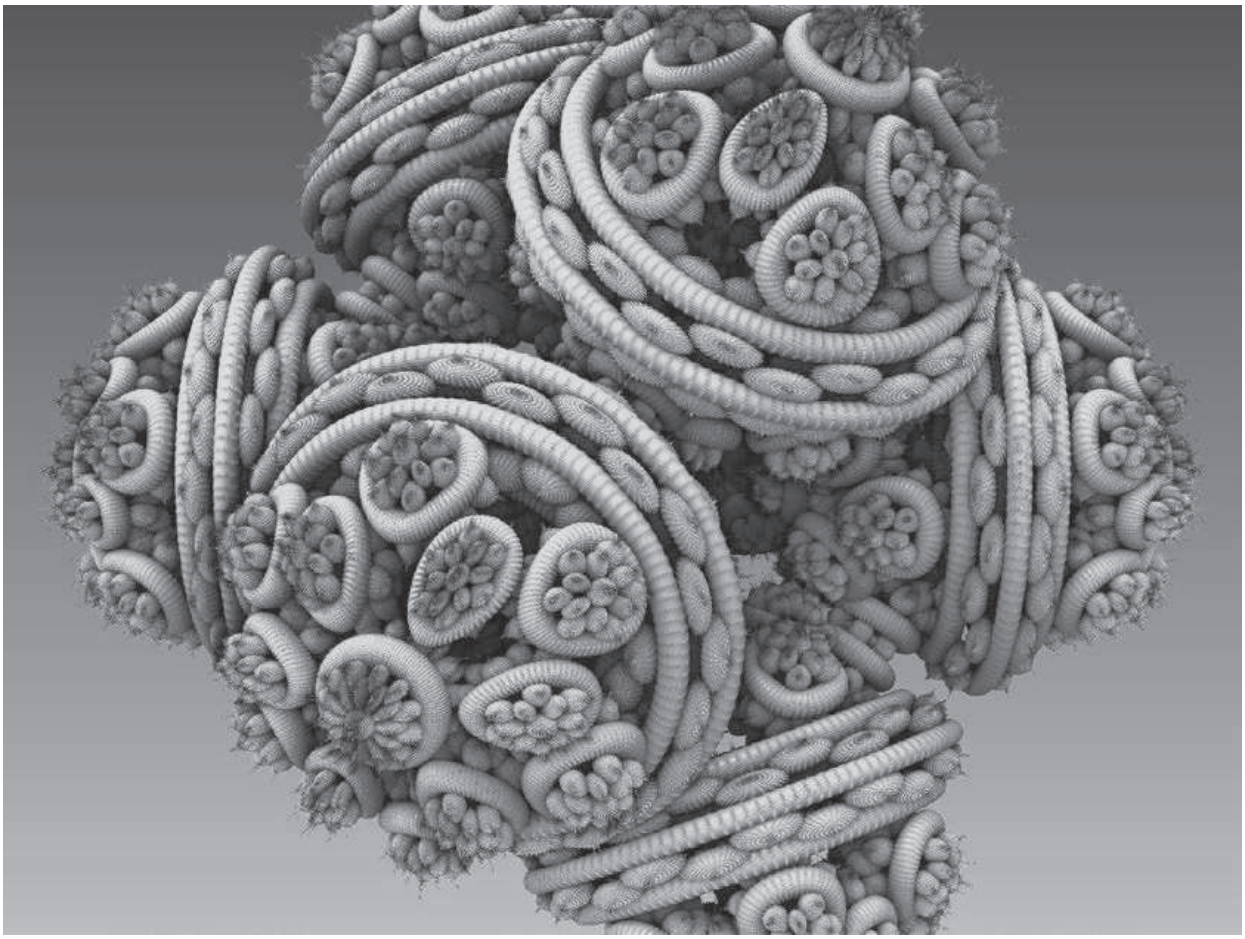

Figure 23. 3D fractal Voronoi object

One another study conducted to investigate a new method "Adaptive Quadratic Voronoi Tessellation" (AQVT) which handles the sparsity and non-uniformity problems reported in cell shapes designs. The cell grows in multilayer patterns, and similarly, tissues also grow in a multi-cellular fashion which highlights the need for a 3D reconstruction technique to estimate 3D shapes and sizes of cells with precision using Confocal Microscopy (CLSM) image slices. The present method to quantification is CLSM imagining which require more than one image slices per cell. Likewise, in *Live Cell Imaging* for active tissues require small resolution to avoid any damage to the cell from exposure to high-resolution laser radiations. The present study has proposed a new method of anisotropic Voronoi Tessellation which helps to capture the images of growing cells in all its axes. Its parameters can be easily estimated from confocal image slices of each cell and its tessellation can provide accurate 3D cell shapes. The proposed method is tested, and the results revealed that AQVT based reconstruction could accurately predict the 3D shapes of the majority of SAM cells [49].

It is believed that the incidence of fracture cases per year is nearly 15 million and therefore bone is one of the most commonly transplanted tissues. Reconstructive options for bone defects include autografts, allografts and alloplastic material. Auto and allografts are prone to pain, infection and immune rejection which led to the need for improving

alloplastic scaffolds. The optimal bone scaffold should be like normal bone regarding mechanical, biological and microstructural properties to allow sufficient diffusion of nutrients and bone cells. It should also be biodegradable.[37] However, most scaffolds lack mechanical strength and vascularity.

Using the Meshnoturb command of the Rhinoceros 3D software, the three-dimensional models were converted into closed polysurfaces with a mean value of about 20,000 surfaces. These were then exported as Initial Graphics Exchange Specification files to Comsol Multiphysics v.4.2.a software. The workstation used for accurate mechanical computing wad Hewlett Packard workstation (Intel core i5, 96 GB). This utilized 350,000 tetrahedral mesh elements and required a maximum of 10 minutes for meshing and a minimum of 5 minutes for analysis. Printing was done using Poly-L-lactide and the properties evaluated for this material included Young's modulus (Es = 3.3 GPa), Poisson's ratio (m = 0.3) and density (q = 1.3 g/cm3). The model was subjected to compression experiments which included displacement of the top surface (maximum engineering strain, emax= 1%), fixation of the bottom surface and symmetry of the remaining surfaces. Other parameters evaluated included the true reaction stress at the bottom surface, von Mises stress, displacement field and strain energy density. The Young's modulus of porous material (Ep) was also calculated as the ratio between true reaction stress at the bottom surface and axial engineering strain.

The current study used the Voronoi tessellation method, which is a mathematical software that can be linked to both the model designing software as well as the additive manufacturing technology. This, therefore, allows the fabrication of implants that can mimic all properties of bone and favor optimum cell penetration, osteoconduction and nutrient diffusion. The Voronoi scaffolds have porosities in them like the trabecular pattern of bone. The number and thickness of trabeculae can be controlled during the design process of this scaffold. In vivo and In vitro behavior of these scaffolds is still an unexplored area and future research can focus on the behavior of these scaffolds.

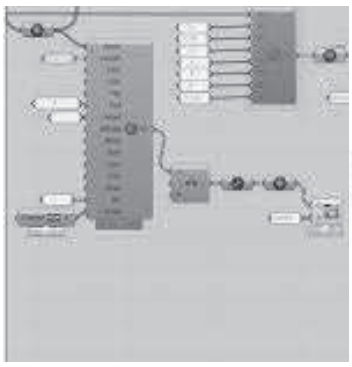

7.3.4 CAM production

7.3.4.1 Laser-Sintering Titanium

The implant model was created using selective laser melting. A high-powered ytterbium fiber laser, which uses a wavelength of 1060 to 1100 nm, is used to melt metallic powders into a predetermined shape based on CAD data [7, 12]. First, a layer of powder is deposited over the building platform, which then acts as a base for selective deposition of layers of powder. Each cross section of the model is scanned by the laser, which then selectively deposits the powder accordingly and melts it to fuse it. This process continues until the entire model is scanned and reproduced. The build chamber and component is cleaned after completion and the excess powder is filtered out and reused.

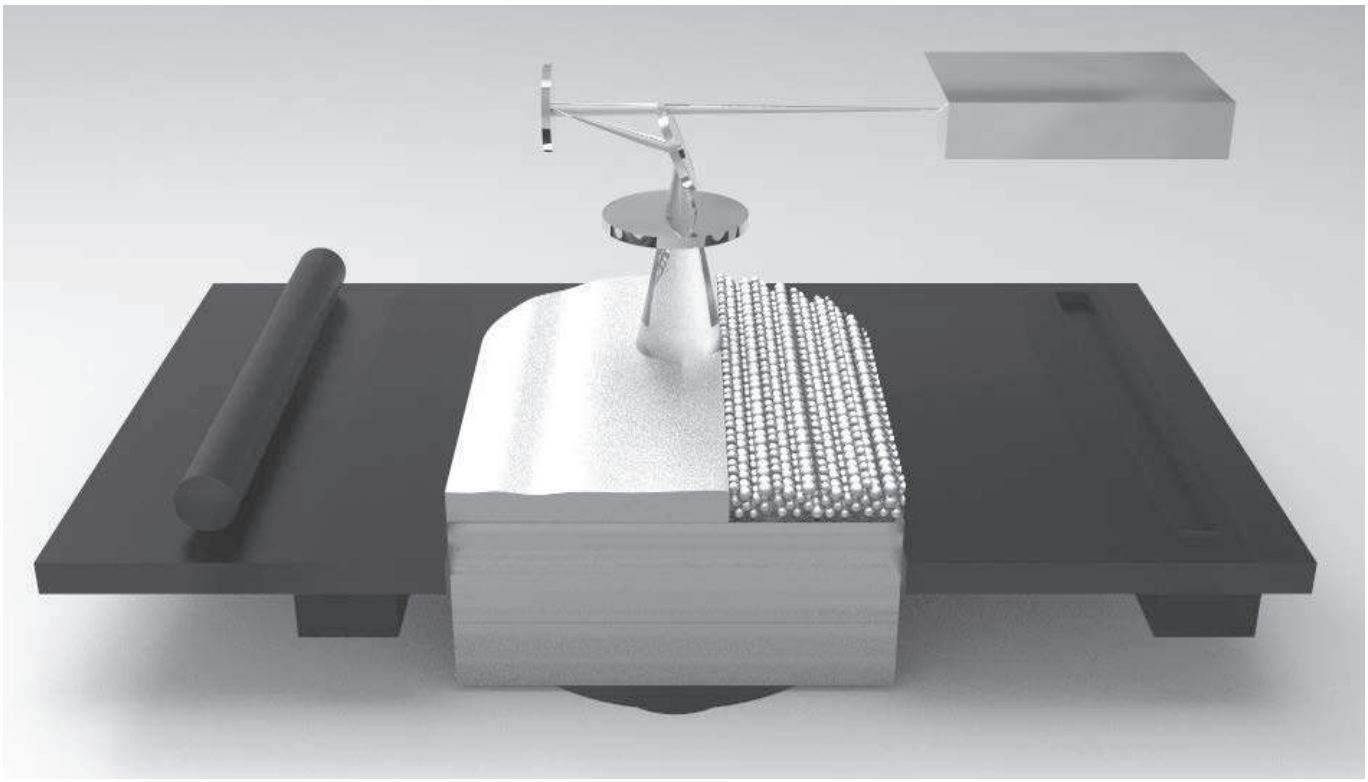

Figure 24 SLS melting process

Initially, the chamber is evacuated completely. Then, in order to maintain an atmosphere with low oxygen content, it is filled with inert gas such as argon. The content building is carried out in this tightly controlled atmosphere, thereby preventing contamination of the material, especially by expelled debris, and avoiding exposure to nitrogen and oxygen.

The SLM technique presents several advantages. It can reproduce parts of high geometrical complexity. It does not require expensive molds as it can be directly printed from a CAD model. The production steps are minimized resulting in low labor and tooling costs. It is highly flexible and changes in design can be quickly made. It generates very little waste and can utilize hard materials which are otherwise difficult to process due to their high melting point.

However, this technique does also have certain drawbacks:

- The deposition rate and build volume are relatively low.
- It's hard to control the presence of defects such as pores, which can lead to lack of fusion.
- More importantly, it is difficult to reproduce part quality and its
- testing has not been standardized.

Because the interaction times are short and heat input is extremely localized, there can be large thermal gradients and buildup of thermal stresses. This leads to segregation and

development of non-equilibrium phases; for instance, martensite can be formed with Ti6Al4V alloys. It can also lead to increased surface roughness and porosities.

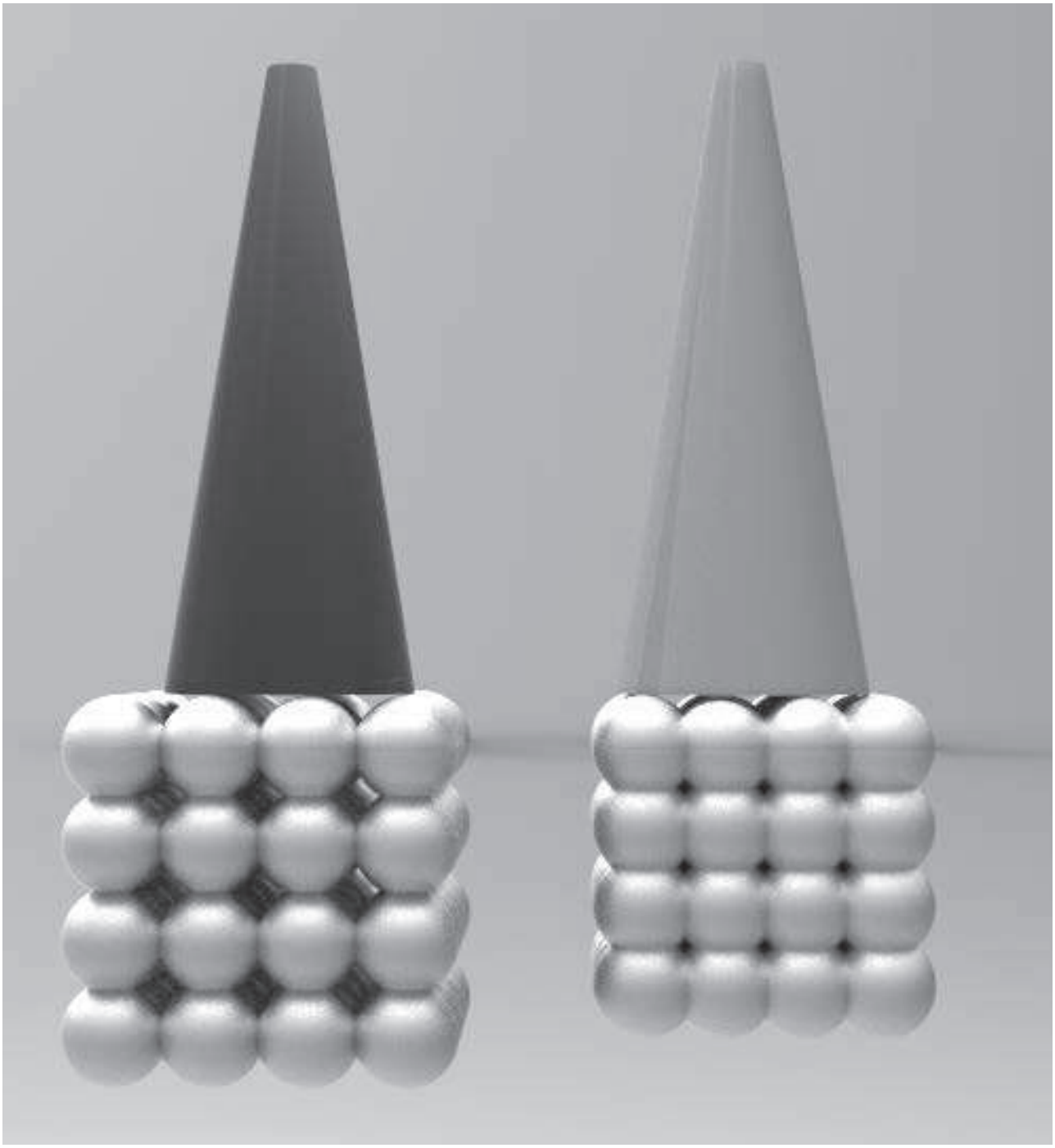

Figure 25. the difference between DMLS (Direct Metal Laser Sintering) on the left and DMLM (Direct Metal Laser Melting) are:
- use of a more powerful laser for DMLM

- in DMLS the molecules are only partially melted and therefore have less productive stress but the final product is less resistant

- in the DMLM, on the other hand, there is a complete fusion of the metal particles, creating a greater stress to the metal during production, but creating projections with the same characteristics as the solid metal.

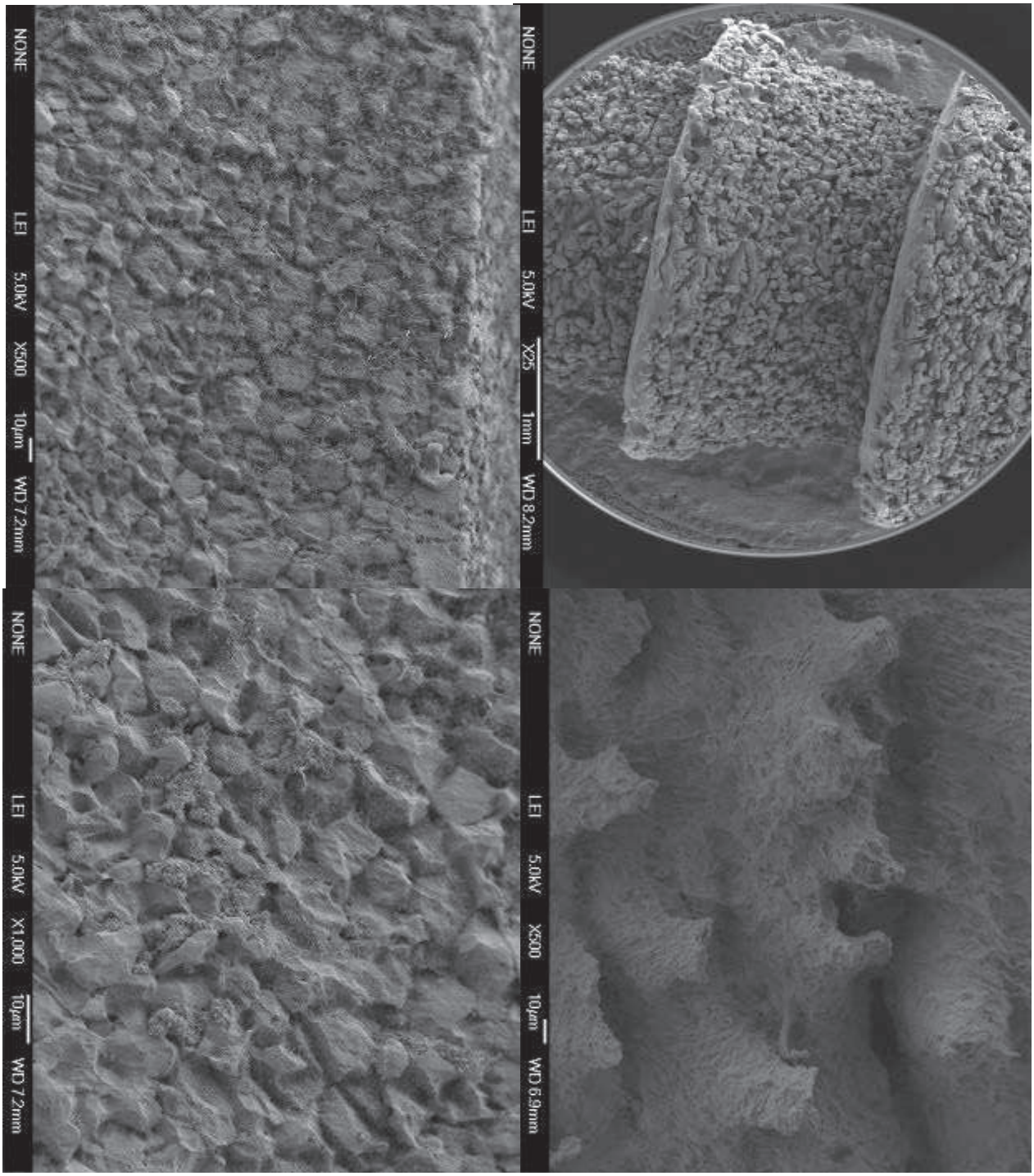

Figure 26 surface roughness of the sintered titanium

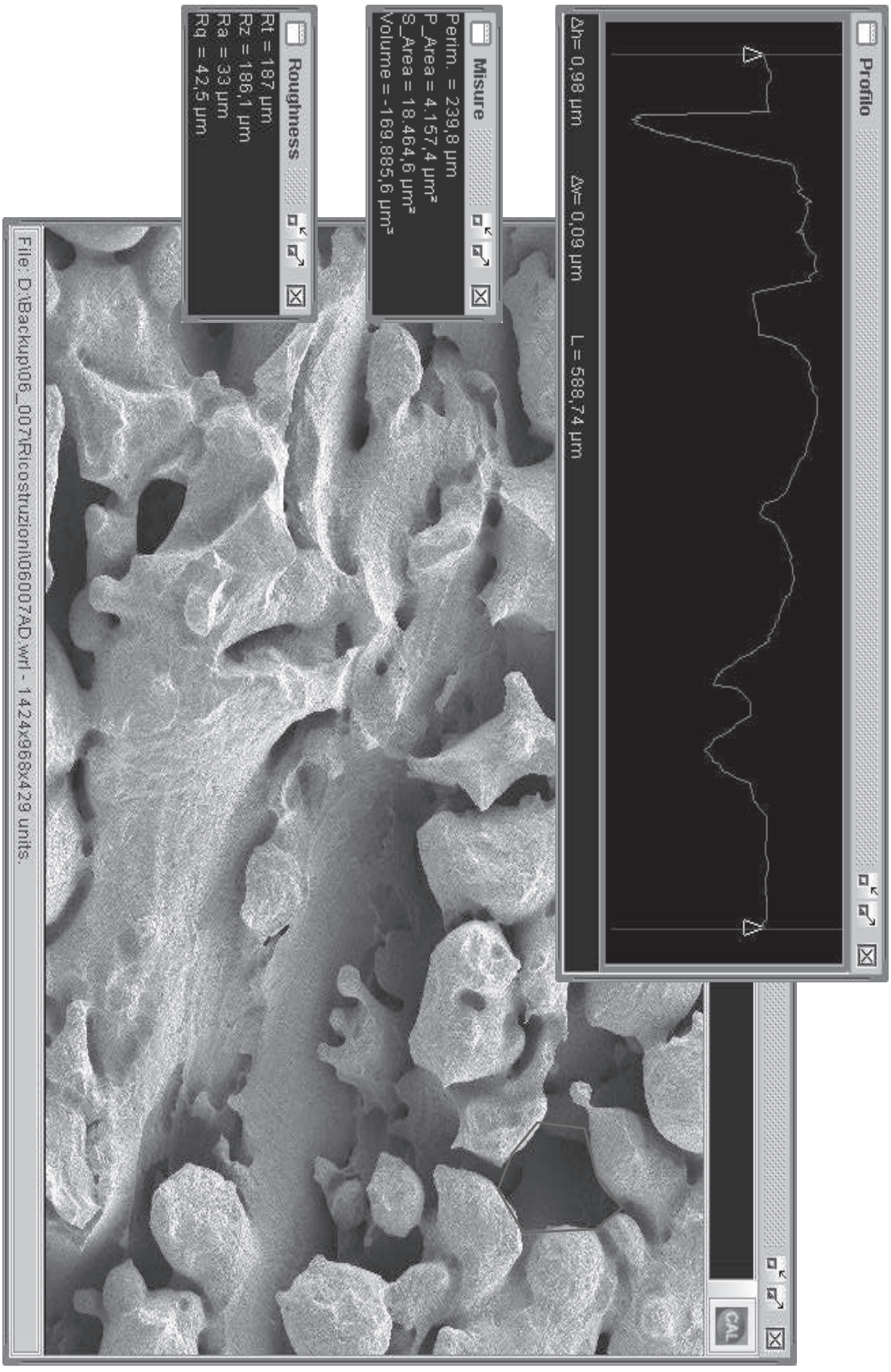

Figure 27 surface roughness analisys

Material data sheet

EOS Titanium Ti64 for EOSINT M 270 Systems (Titanium Version)

A number of different materials are available for use with EOSINT M systems, offering a broad range of e-Manufacturing applications. EOS Titanium Ti64 is a titanium alloy powder which has been optimized especially for EOSINT M 270 systems (Titanium Version). Other materials are also available for EOSINT M systems, and further materials are continuously being developed - please refer to the relevant material data sheets for details.

This document provides a brief description of the principle applications, and a table of technical data. For details of the system requirements please refer to the relevant information quote.

1 Description, application

EOS Titanium Ti64 is a pre-alloyed Ti6Al4V alloy in fine powder form. This well-known light alloy is characterized by having excellent mechanical properties and corrosion resistance combined with low specific weight and biocompatibility.

This material is ideal for many high-performance engineering applications, for example in aerospace and motor racing, and also for the production of biomedical implants. Parts built in EOS Titanium Ti64 fulfil the requirements of ASTM F1472 regarding maximum concentration of impurities.

Standard processing parameters use full melting of the entire geometry. Parts built from EOS Titanium Ti64 can be machined, spark-eroded, welded, micro shot-peened, polished and coated if required. Unexposed powder can be reused.

Applications:

- direct manufacture of functional prototypes, small series products, individualised products or spare parts
- parts requiring a combination of high mechanical properties and low specific weight, e.g. structural and engine components for aerospace and motor racing applications, etc.
- biomedical implants

EOS GmbH - Electro Optical Systems
Robert-Stirling-Ring 1
D-82152 Krailling / München
Telephone: +49 (0)89 / 893 36-0
Telefax: +49 (0)89 / 893 36-285
Internet: www.eos.info

2 Technical data

General process and geometric data

Minimum recommended layer thickness	30 µm 1.2 mil
Min. wall thickness [1]	0.3 - 0.4 mm 8 - 20 mil
Surface roughness (as built)	Ra 9 - 12 µm, Rz 40 - 80 µm Ra 0.36 – 0.48, Rz 1.6 – 3.2 mil
Volume rate with standard parameters (full density) [2]	3.0 mm³/s 0.65 in³/h

[1] Mechanical stability is dependent on geometry (wall height etc.) and application

[2] Volume rate is a measure of build speed during laser exposure. The total build speed depends on the average volume rate, the recoating time (related to the number of layers) and other factors such as DMLS-Start settings.

Physical and chemical properties of parts

Material composition	Al (5.5 – 6.5 %) V (3.5 – 4.5 %) O < 2000 ppm N < 500 ppm C < 800 ppm H < 120 ppm Fe < 2500 ppm Ti Balance
Relative density with standard parameters	approx. 100 %
Density with standard parameters	4.43 g/cm³ 0.160 lb/in³

EOS GmbH - Electro Optical Systems
Robert-Stirling-Ring 1
D-82152 Krailling / München

Material data sheet

Mechanical properties of parts

Ultimate tensile strength [3]	1150 ± 60 MPa 166 ± 9 ksi
Yield strength (Rp 0.2 %) [3]	1030 ± 70 MPa 150 ± 10 ksi
Elongation at break [3]	11 % ± 2 %
Young's modulus [3]	110 ± 7 GPa 16 ± 1 msi
Hardness [4]	approx. 400 - 430 HV (41 - 44 HRC)

[3] According to ISO 6892:1998.

[4] Vickers hardness measurement (HV) according to DIN EN ISO 6507-1. Values in parentheses are converted in accordance with DIN 50150, which is applicable to cast steels and therefore only gives an indication for laser-sintered materials. Note that depending on the measurement method used, the measured hardness value can be dependent on the surface roughness and can be lower than the real hardness. To avoid inaccurate results, hardness should be measured on a polished surface.

Thermal properties of parts

Maximum long-term operating temperature	350 °C 660 °F

The quoted values refer to the use of these materials with EOSINT M 270 systems according to current specifications (including the latest released process software PSW and any hardware specified for the relevant material) and operating instructions. All values are approximate. Unless otherwise stated, the quoted mechanical and physical properties refer to standard building parameters and test samples built in horizontal orientation. They depend on the building parameters and strategies used, which can be varied by the user according to the application. The data are based on our latest knowledge and are subject to changes without notice. They are provided as an indication and not as a guarantee of suitability for any specific application. EOS®, EOSINT®, DMLS®, DirectTool® and DirectPart® are registered trademarks of EOS GmbH.

EOS GmbH – Electro Optical Systems
Robert-Stirling-Ring 1
D-82152 Krailling / München

Figure 28 Datasheet of the material

7.3.4.2 Post-Production

To remove residual particles from the manufacturing process, the sample was sonicated for 5 minutes in distilled water at 25°C, immersed in sodium hydroxide (20 g$L−1) and hydrogen peroxide (20 g$L−1) at 80°C for 30 minutes, and then further sonicated for 5minutes in distilled water. Acid etching was carried out by immersion of the samples in a mixture of 50% oxalic acid and 50% maleic acid at 80°C for 45 minutes, followed by washing for 5 minutes in distilled water in a sonic bath. The surface topography of the SLS implants had no clear orientation. The direct laser preparation provided an implant surface with a roughness surface with the mean 6 SD of the absolute values of all profile points, the root-mean-square of the values of all points, and the average value of the absolute heights of the 5 highest peaks, and the depths of the 5 deepest valleys of 66.8 6 6.6 mm, 77.6 6 11.1 mm, and 358.3 6 101.9 mm, respectively.[50]

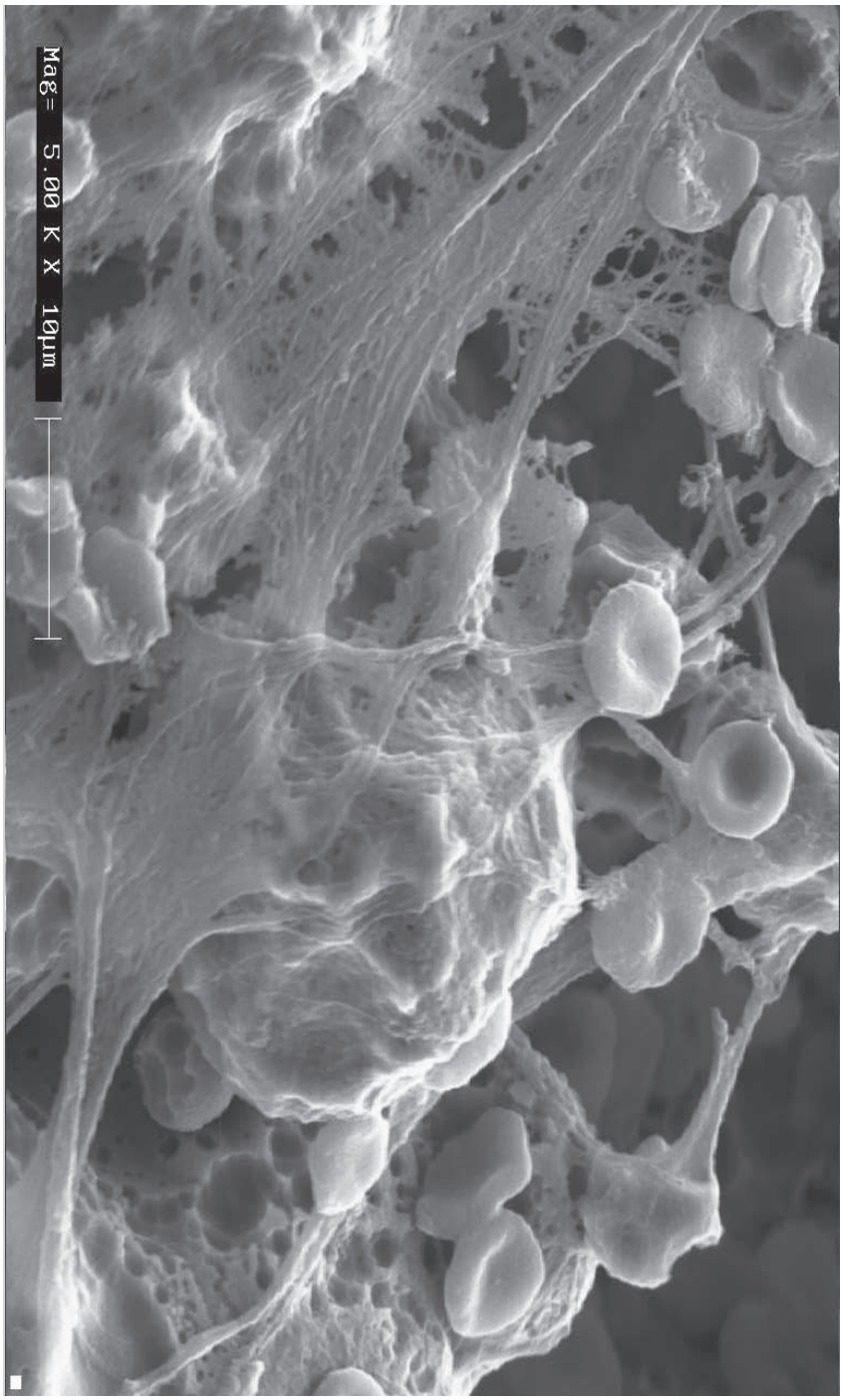

Figure 29 biocompatibility tests with erythrocytes

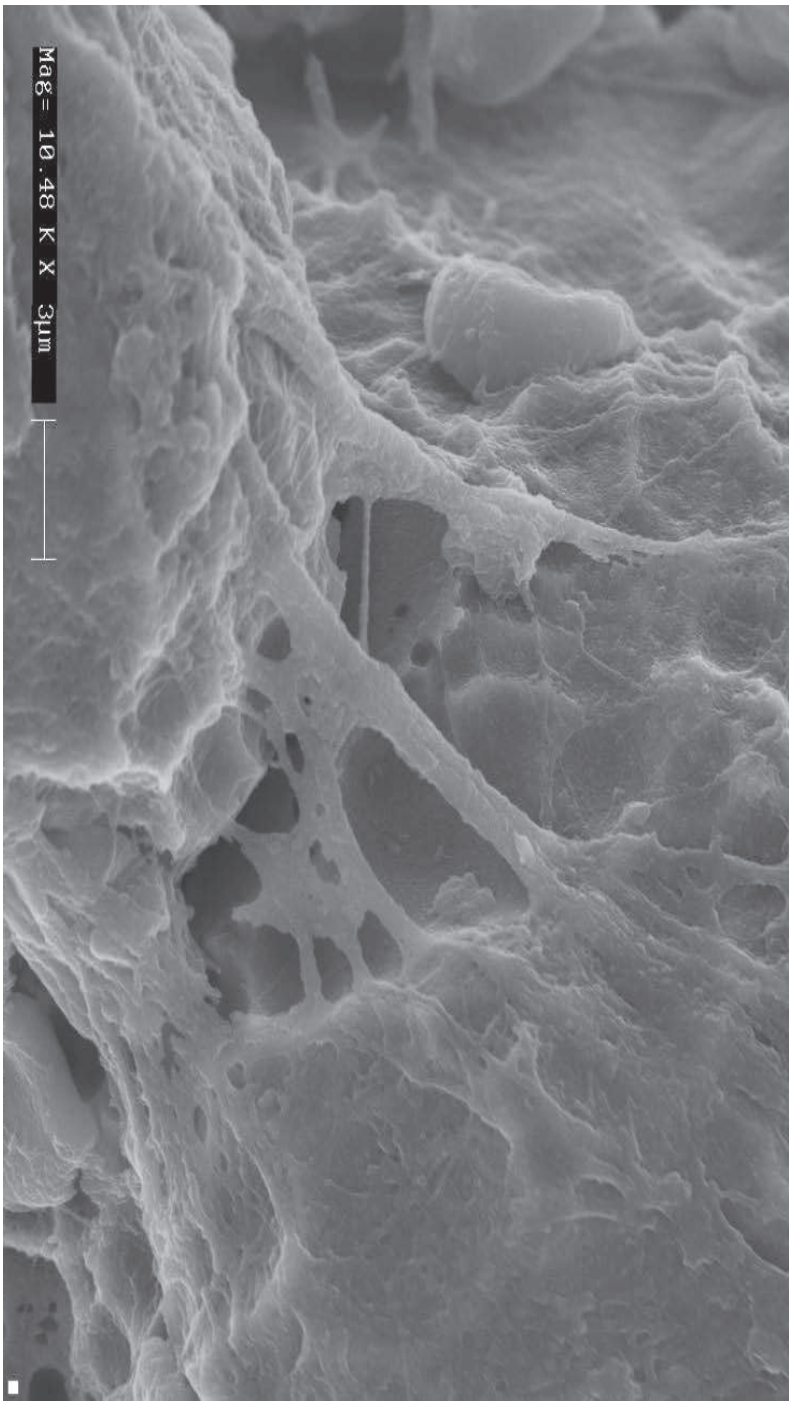

Figure 30 biocompatibility tests with erythrocytes. Notice fibrils

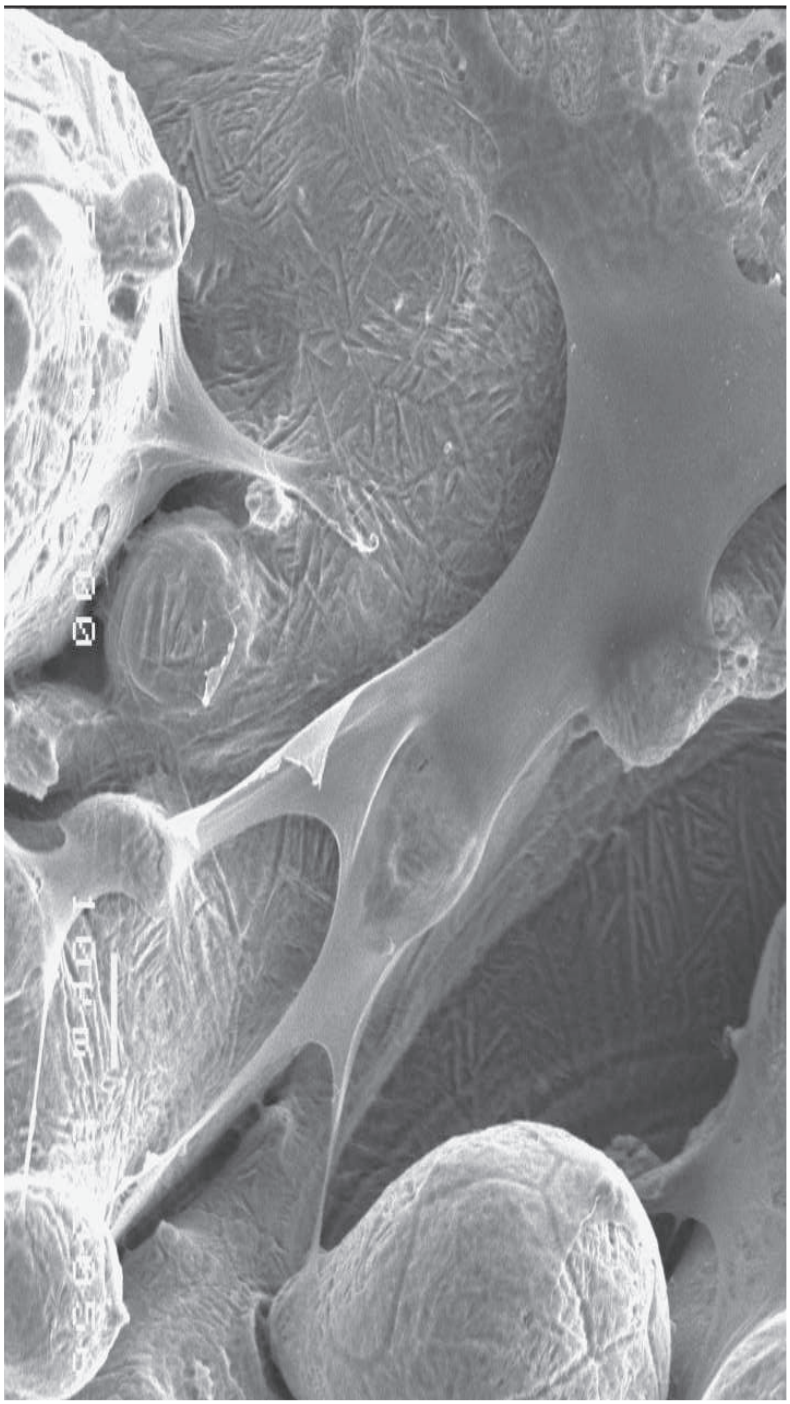

Figure 31 biocompatibility tests with erythrocytes. Polygonal cells in the cavities

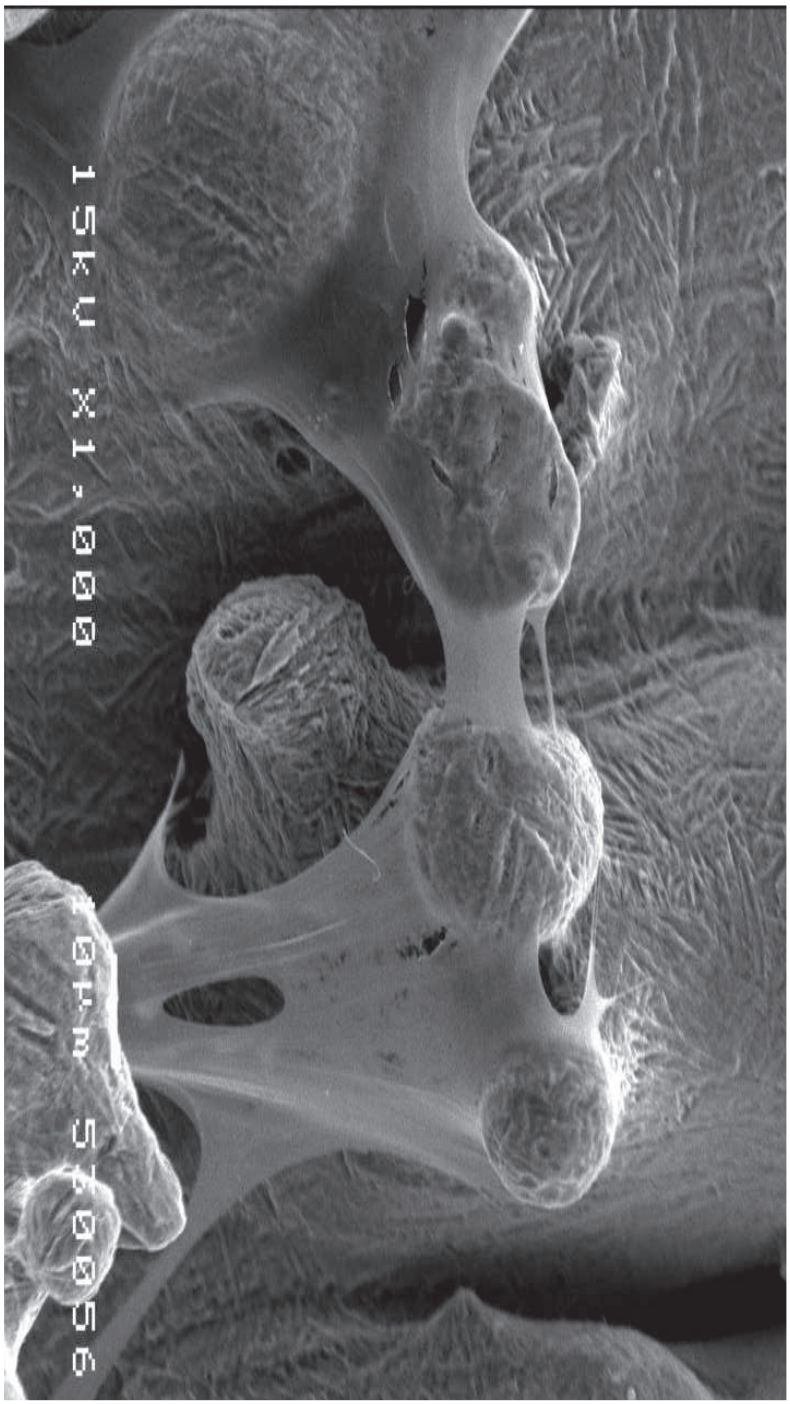

Figure 32 biocompatibility tests with erythrocytes. Note the tight fibrils

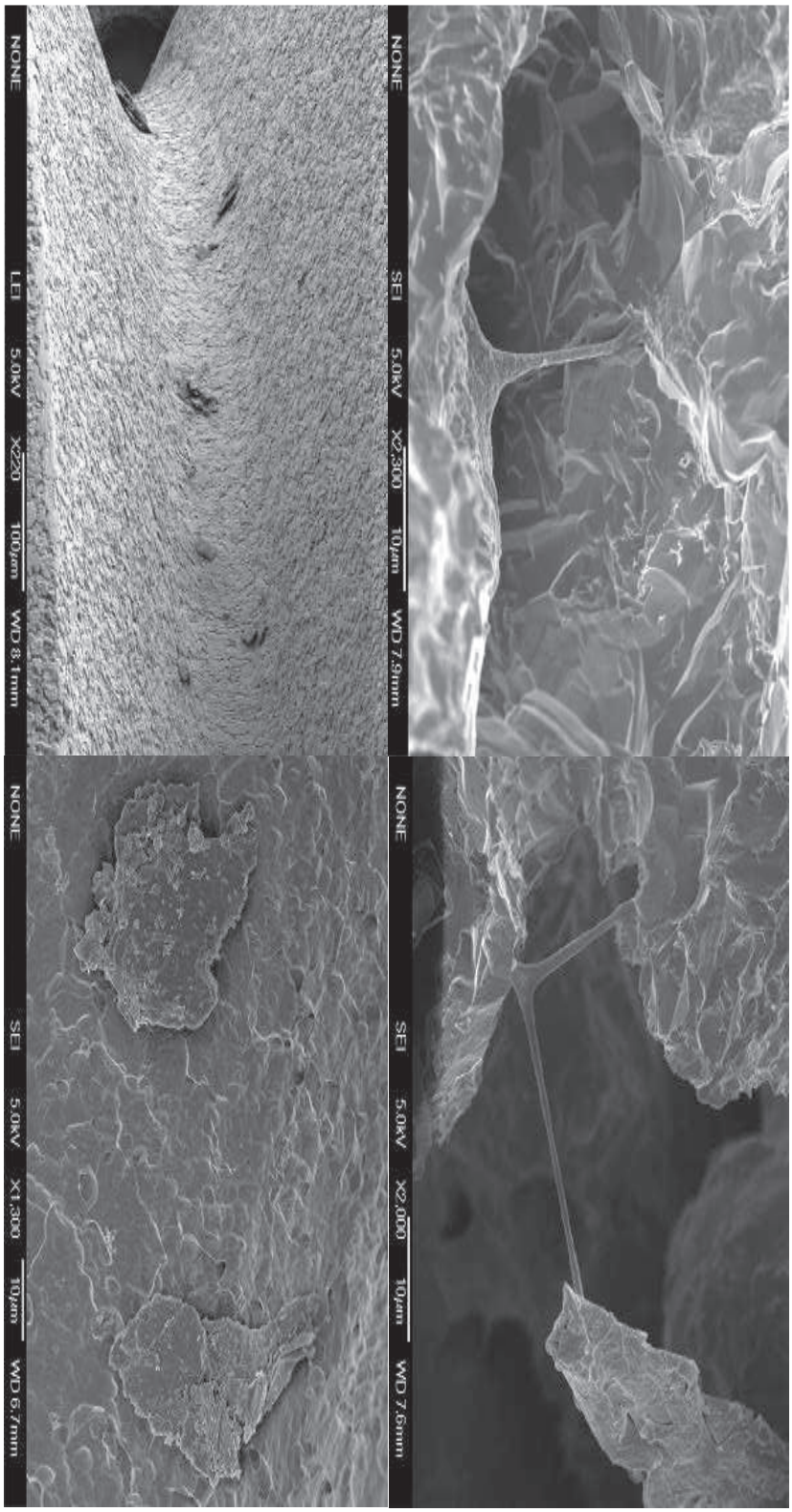

Figure 33By contacting pulp stem cells with sintered titanium and titanium machined, after four hours, while the cells on the new surface begin to initiate proliferative processes, those on the machined surface have not yet begun.Upper machined and lower sintered

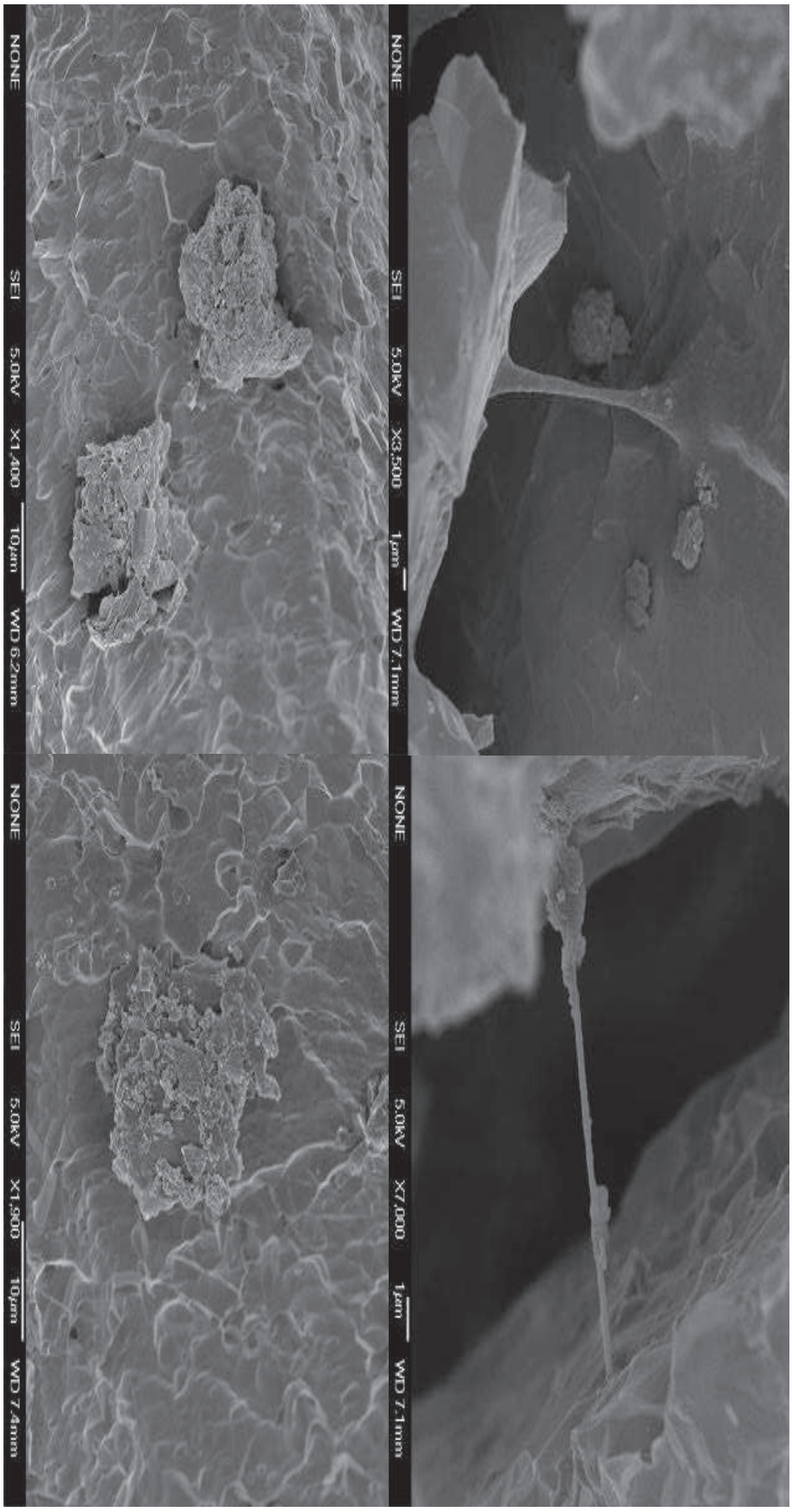

Figure 34 We find the same situation after 8 hours. Upper machined lower sintered.

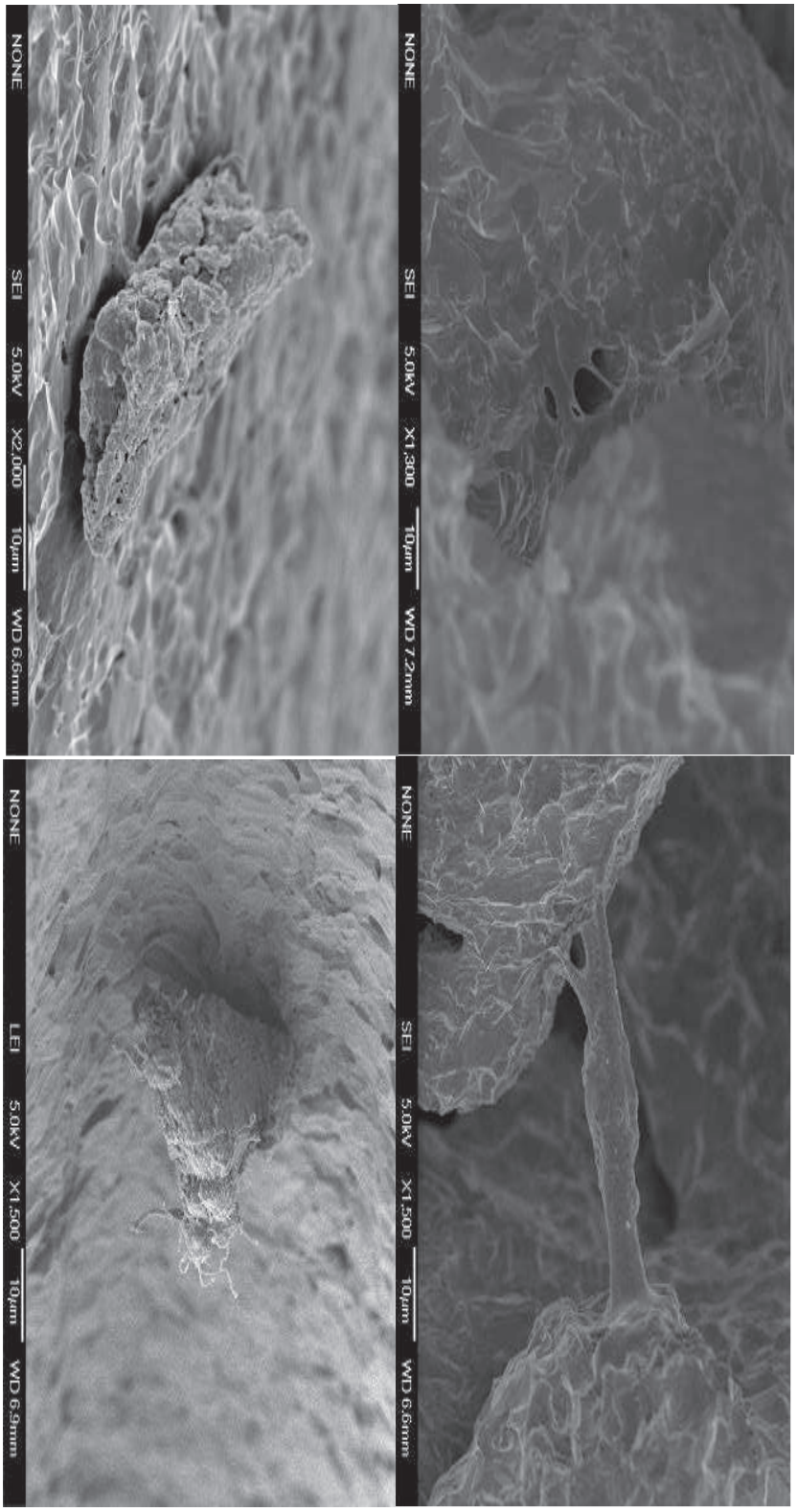

Figure 35 And even at 24 o'clock. Upper machined lower sintered.

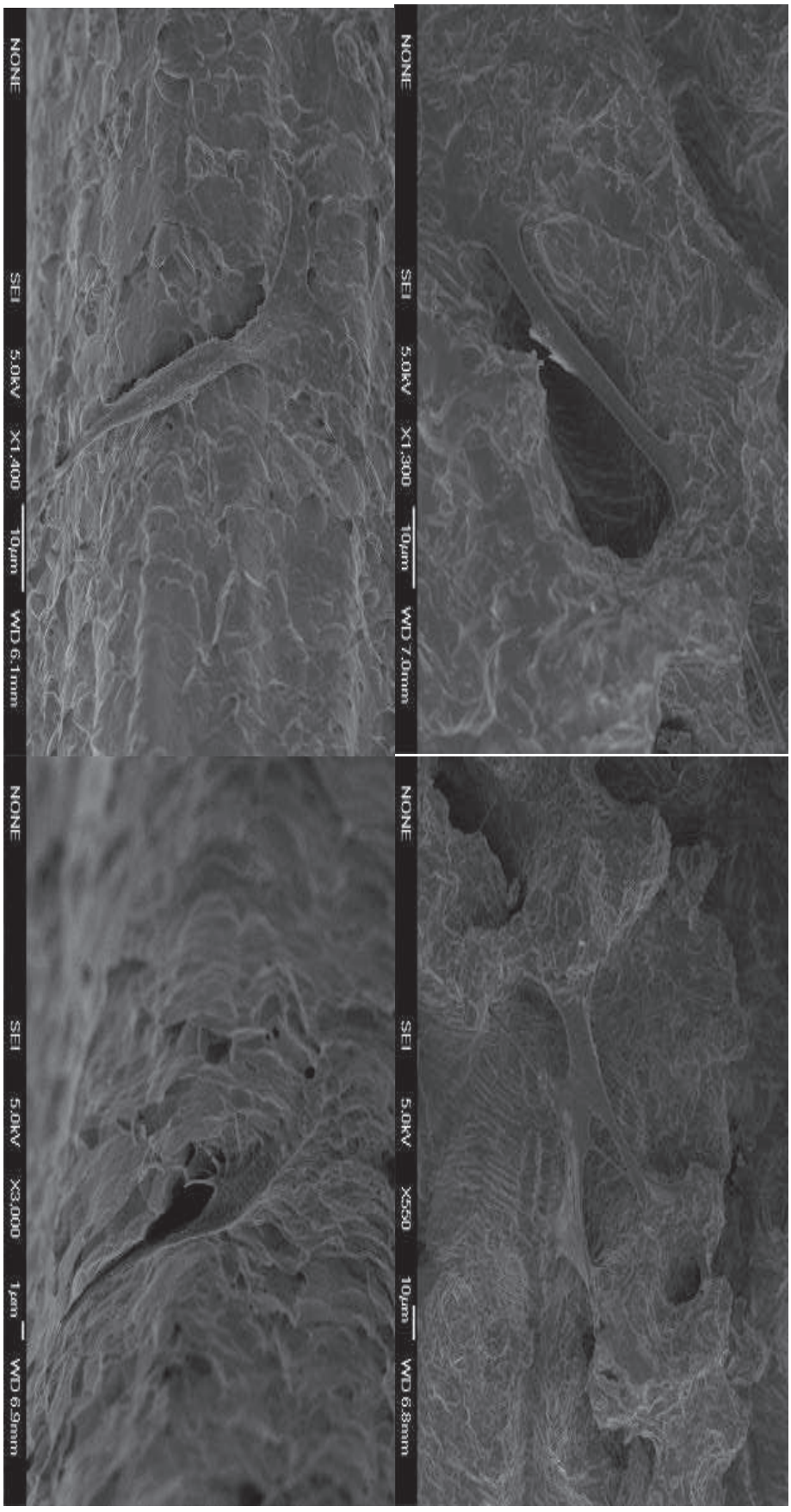

Figure 36 Only after 48 hours the cells on the machined surface begin proliferating processes.

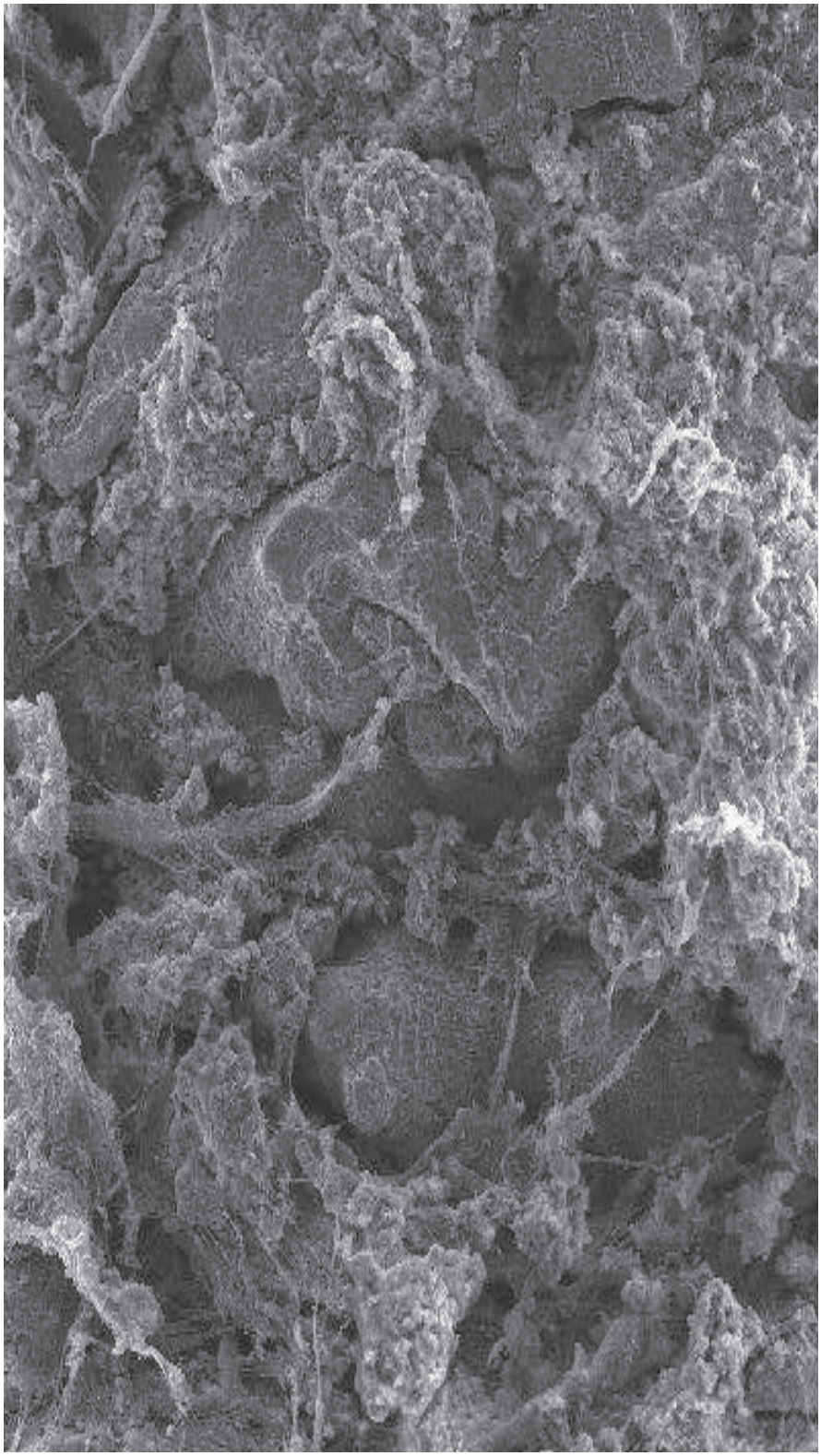

Figure 37analysis of a sintered plant removed at 2 months. In green the bone, blue titanium

7.4 PROCEDURE

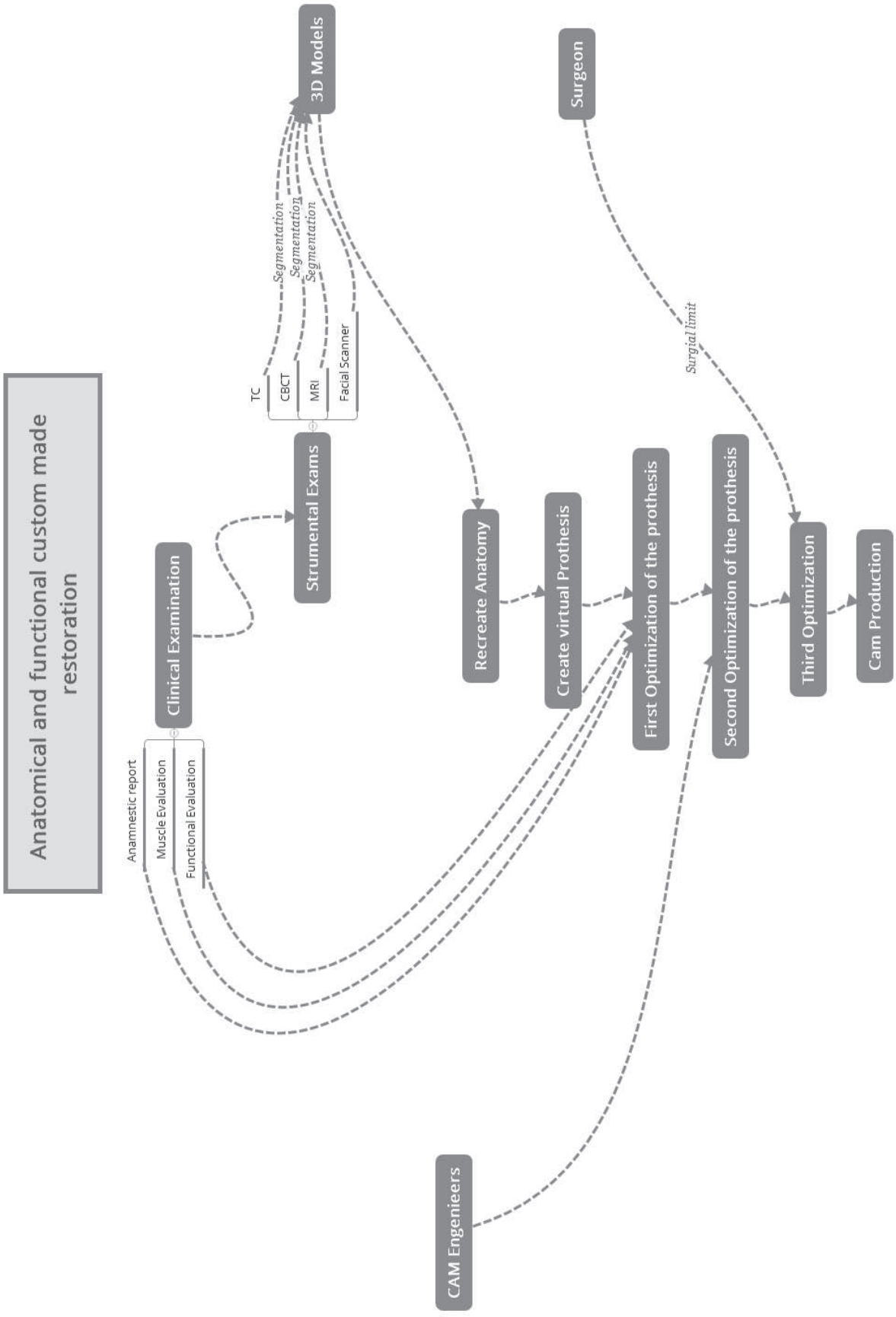

Figure 38 workflow for anatomical and functional custom made prothesys

The image above describes the process of making the maxillo-facial prosthesis. In every medical decision, you need first to collect the anamnestic investigation and all clinical evaluations and secondly, youc a passes to an instrumental evaluation with the acquisition of three-dimensional images coming from all image diagnostics and the evaluation of the soft tissue with a facial scanner and MRI images. Through a segmentation process, is realized the patient's virtual anatomical model.

7.5 CODIFICATION

Any procedure must be standardized and codified. Standardization is the process of establishing a series of steps for any procedure which are proven to be effective. A standardized protocol is easy to understand by both workers and supervisors, and aids in training workers. Standardization has begun to be accepted in medicine and surgery, as evidenced by the protocol for optimal timing of antibiotics before surgery. However, this is yet to be applied about surgical procedures and even the same procedure performed by two different surgeons can have several variations. Similarly, work that is codified helps to eliminate errors and can aid in implementing corrective action when required.[51]

File codification was done using software versioning, which involved assigning each state of computer software a unique version name or number. The number assigned reflects the new developments and revisions of the software. Generally, a four-sequence identifier is used. The first number in the sequence may be changed only when the code is completely rewritten, while the fourth number would change only for minor revisions. The third number sometimes reflects the grade of testing; production grade testing rather than real world testing would reflect changes in this number. However, the major number is usually increased only when the functionality improves significantly; which could cause incompatibility with interfaces owing to changes in the framework.

7.6 SUBJECT

In this study 14 patients with different cranio-facial bone defects were enrolled: 8 were men and 7 were women (mean age 53 yr and SD 21 yr). They were on a waiting list to have new bone reconstruction on different university settings.

7.7 VARIABLES

The aim of the present study was to test the reliability of the proposed workflow for the construction of grafts for craniofacial rehabilitation. Two evaluation methods were associated to test the results of the workflow. First surveys were given to patients undergone surgery and their surgeons to have a subjective analysis of the workflow. Then an objective evaluation was performed by the superimposition between the virtual prediction of the graft position and shape with the post-treatment CBCT/TC to evaluate the correspondence of the virtual setup with the final surgery results.

7.7.1 Subjective Evaluation: Surveys for patient and surgeon

A different questionare was used for patients and surgeons. For the patients, demographic data such as age, sex and income was collected. For the surgeons, educational information was collected. Both groups were asked to use a visual analog scale of 100mm (VAS) which was drawn below the questions. The scale had values marked from 0 to 100, and the responders were asked to mark a point on this scale corresponding to their answer. This was evaluated by measuring the distance from the left external point of the line using digital calipers (Ultra-CalMark III, Fred V. Fowler, Newton, MA, USA). Every patient after 7 days of surgery was given the following questionnaire.

Survey for the Patient

GENDER

☐ MALE

☐ FEMALE

AGE .....

EDUCATION LEVEL .....

For the following questions draw a cross on the correspondent level of the line:

LEVEL OF PAIN/DISCOMFORT 2 DAYS AFTER SURGERY

1 5 10

LEVEL OF PAIN/DISCOMFORT 2 WEEKS AFTER SURGERY

1 5 10

LEVEL OF PAIN/DISCOMFORT 4 WEEKS AFTER SUGERY

1 5 10

AESTHETIC IMPROVEMENT 4 WEEKS AFTER SURGERY

1 5 10

AESTHETIC IMPROVEMENT 8 WEEKS AFTER SURGERY

1 5 10

AESTHETIC IMPROVEMENT 12 WEEKS AFTER SURGERY

1 5 10

AESTHETIC IMPROVEMENT 1 YEAR AFTER SURGERY

1 5 10

AESTHETIC IMPROVEMENT ACCORDING TO EXPECTATIONS

1 5 10

Figure 39 patients survey

And every surgeon after the surgery was given the following questionnaire.

Survey for the Surgeon

GENDER

☐ MALE

☐ FEMALE

AGE .....

YEARS OF PRACTISING .....

LEVEL OF DIFFICULTY OF SURGERY COMPARED WITH SAME SURGERY USING TRADITIONAL BONE GRAFT

1 5 10

LEVEL OF CORRESPONDANCE WITH THE VIRTUAL PLANNING

1 5 10

AESTHETIC IMPROVEMENT 4 WEEKS AFTER SURGERY

1 5 10

AESTHETIC IMPROVEMENT 8 WEEKS AFTER SURGERY

1 5 10

AESTHETIC IMPROVEMENT 12 WEEKS AFTER SURGERY

1 5 10

AESTHETIC IMPROVEMENT 1 YEAR AFTER SURGERY

1 5 10

AESTHETIC IMPROVEMENT ACCORDING TO EXPECTATIONS

1 5 10

Figure 40 surgeon survey

7.7.2 Objective Evaluation

The prosthesis produced was evaluated by digital scanning using Einscan-pro. For each patient, a threshold segmentation was selected and applied to generate a 3D virtual surface model. This prosthesis was then superimposed on the original prosthesis design and the two were compared using Cloudcompare (version 2.6.2). The displacement between the original file and produced file was evaluated.

7.8 ANALYSES OF THE DATA

To estimate the effect size selecting as main outcome the mean error according to previous study (Chang et al. 2003), a sample of 6 subjects was required. The alpha was set at 0.05 and the power was 0.8. For a significant effect, an effect size of 0.8 was determined. Considering the prospecting design of the study and the 20% possibility of dropouts a greatest sample of 14 patients was enrolled to fully satisfy power analysis.

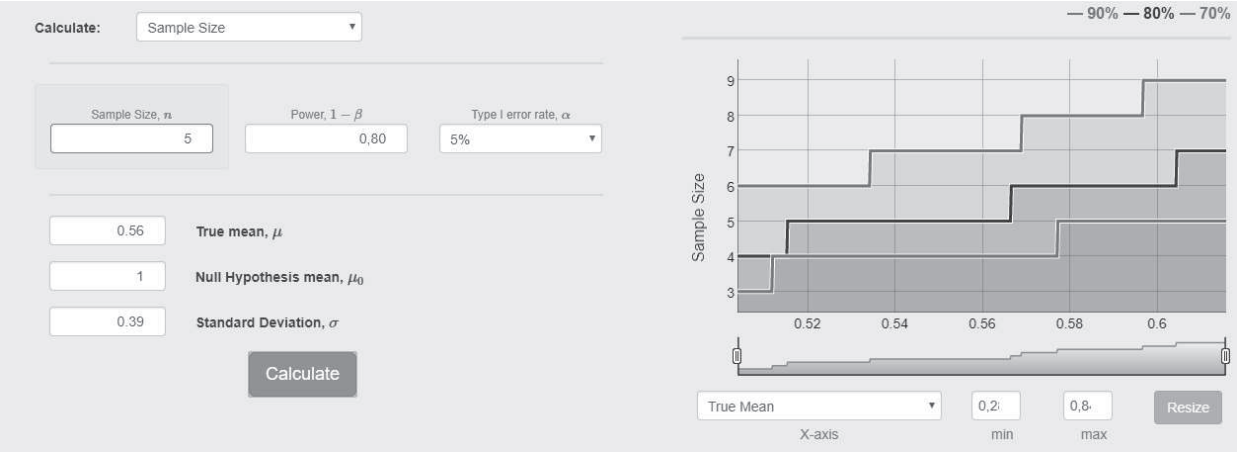

Figure 41 power analisys

The Statistical Package for Social Sciences Software release 22.0 (SPSS Inc., Chicago, IL, USA) was used for data analysis. After testing the normality of the data with the Shapiro-Wilk test and Q-Q normality plots and the equality of variance among the datasets using a Levene test, parametric methods were used for data analysis.

7.8.1 Subjective evaluation

First an intragroup analysis was performed for patients and surgeons. For patients means of VAS scores were compared for the following variables: 1) Pain /Discomfort (2 days, 2 weeks and 4 weeks after surgery); 2) Aesthetic improvement (4 weeks, 8 weeks, 12 weeks and 1 year after surgery). A one-way analysis of variance (ANOVA) was used to assess the significance of the differences in VAS scores among the timepoints for each variable.

When significant interactions were seen, an independent sample t-test was employed for pairwise comparisons among all the possible combinations of the variables. Each of the retrieved p values was multiplied for three and six, respectively. Moreover, Pearson correlation coefficient was employed to investigate the correlation between the aesthetic improvement 1 year after surgery and aesthetic improvement according to expectations in both groups of respondents. Level of significance was set at $p<0.05$.

Then Student-t Test was employed to compare answers from the two groups of respondents, patients and surgeons, regarding the aesthetic improvement at every timepoint and according to expectations. Level of significance was set at $p<0.05$.

7.8.2 Objective evaluation

Data were analyzed using descriptive statistics, and comparisons were made with the Student t-test, after having confirmed the normality of the sample through Sapiro-Wilk test. Linear difference was measured on the wider length of the object. Differences between digital model and sintered model was calculated as the absolute difference (mm). Relative differences (%) were calculated as the absolute difference divided by the original files X100, in accordance with studies conducted by Choi et al. (2002) and Chang et al. (2003)., also was measured the 3D surface differences.

7.9 ARTICLE APPENDIX

In this section, there're the full articles used and written by the author in this section

7.9.1 Extracted from: Correlation Assessment between Three-Dimensional Facial Soft Tissue Scan and Lateral Cephalometric Radiography in Orthodontic Diagnosis. Piero Antonio Zecca, Rosamaria Fastuca, Matteo Beretta, Alberto Caprioglio, and Aldo Macchi. International Journal of Dentistry, Volume 2016, Article ID 1473918, 8 pages.

Introduction

Skeletal and dental components are of great importance in craniofacial diagnosis and orthodontic treatment planning[52]. Hard tissue is routinely evaluated by means of lateral cephalometric radiography collected by clinicians prior to orthodontic therapy. Besides skeletal evaluation, facial soft tissue analysis is assuming a relevant role in orthodontic diagnosis and treatment planning, since clinicians need to carefully assess the effects of dental and skeletal changes on the soft tissue profile when managing orthodontic treatment in order to estimate facial changes along with occlusal improvement[53]. Therefore, soft tissue analysis might represent an important source of treatment outcome evaluation and additional information for diagnosis. Although cephalometric analysis of lateral radiography is spreading among orthodontists, its role in diagnosis and treatment planning is still debated[54]. Moreover, the fundamental principles of justification, optimization, and dose limitation should always be considered when radiographic examinations are performed at the beginning of the orthodontic treatment. The growing interest in noninvasive diagnosis has allowed the development of new imaging tools which could enhance the role of soft tissue in diagnosis. Nevertheless, the difficulty of performing facial examinations reliably is probably responsible for the secondary role of soft tissue analysis in supporting diagnosis compared with skeletal analysis[55, 56]. Several analyses have been proposed for the evaluation of facial soft tissue. Most of them include photographic images in lateral position [57-60]. Some authors [55, 56] have also proposed soft tissue evaluation with frontal pictures and underlined the importance of reproducible head position during image acquisition. Among the recently introduced noninvasive imaging techniques, stereophotogrammetry and laser scanning allow accurate acquisition of three-dimensional (3D) facial soft tissue with the possibility of locating landmarks and measuring angles, distances, surfaces, and volumes [61-64]. Even though normative values of 3D facial soft tissue are not available for the general population, some proposals have been made for specific sagittal and vertical measurements [65, 66] but further studies are needed to improve their reliability. The difficulties related to the use of the appropriate equipment and software and the absence of reliable normative values for 3D facial soft tissue measurements might prevent their adoption by clinicians, who are still using lateral cephalometric radiography to perform their diagnosis. The relationships between facial soft tissue and underlying hard tissue should be considered and investigated for any correspondences that might improve noninvasive orthodontic diagnosis and thus reduce patients' exposure to ionizing radiation. The soft tissue profile may reflect the underlying skeletal and hard tissue, and it

would be possible to estimate the skeletal configuration by visual inspection of the soft tissue profile alone, as suggested by previous studies [67]. Validation of the anatomy of facial soft tissue is fundamental for an objective analysis of craniofacial morphologies. The aim of the present study was therefore to investigate correlations between facial soft tissue scans and lateral cephalometric radiography measurements.

Materials and Methods

Signed informed consent to the release of diagnostic records for scientific purposes was obtained from patients prior to enrolment in the present prospective study. The protocol was reviewed and approved by the Ethical Committee (Approval number 6154) and procedures followed adhered to the Declaration of Helsinki. The final study sample comprised 312 subjects: 155 males (mean age of 24.3) and 157 females (mean age of 25.8). Inclusion criteria were Caucasian ethnic origin, age between 20 and 30 years to avoid errors arising from soft tissue laxity which might increase with age, and normal body mass index (BMI) [68]. Subjects were selected from those patients seeking orthodontic treatment for whom a diagnostic lateral cephalometric radiograph had been recorded within the previous six months. Exclusion criteria were craniofacial syndromes or anomalies, noticeable asymmetries, and previous or current orthodontic treatment that might affect the homogeneity of the sample. Lateral cephalometric radiographs were then collected for all subjects and cephalometric measurements were performed with Deltadent software (Outside Format, Milan, Italy) (Figure 6).

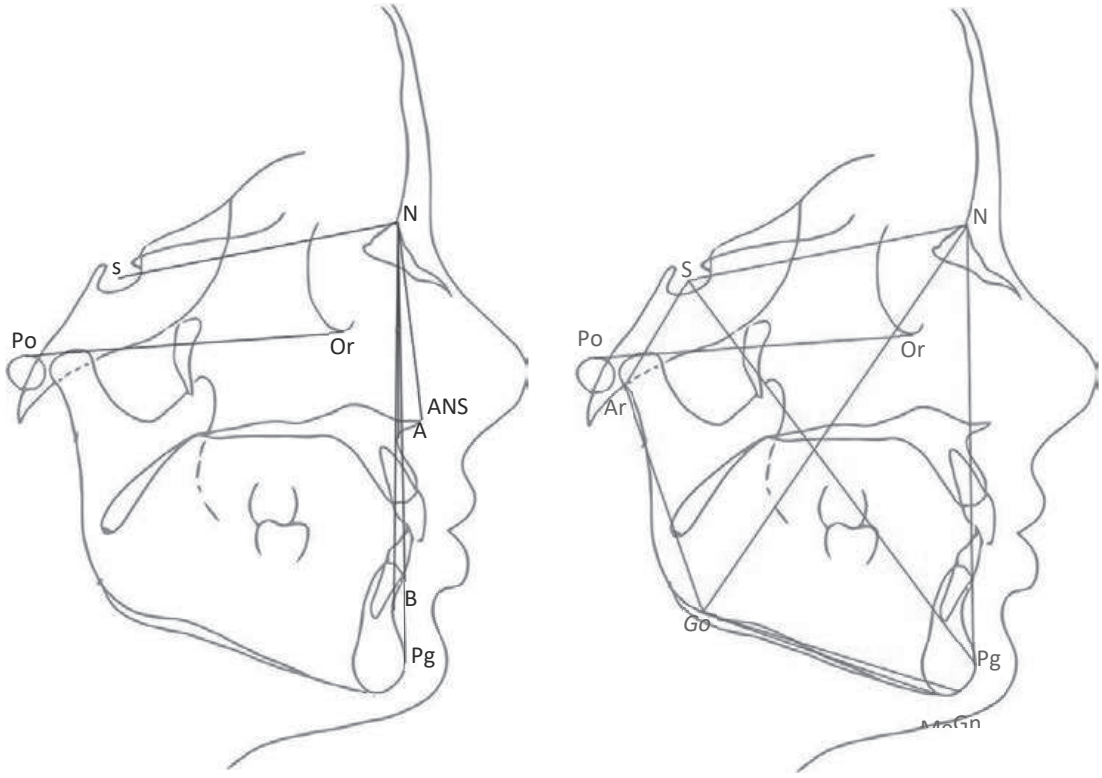

Figure 42 2D tracings and cephalometric analysis performed with lateral cephalometric radiography. (a) Sagittal measurements and (b) vertical measurements.

A facial scanner (Primesense Carmine 1.09, Subsidiary of Apple Inc., Israel, 2005) was employed for acquisition of the facial soft tissue of the subjects. The subject-to-scanner distance was set at 80 cm and scan time was 30 s on average. The scanner depth sensor data were 640 × 480 pixels. Data were recorded on a desktop workstation with a 2.6GHz i7 Intel processor (Dell, Wicklow, Ireland). Light conditions were set for reliable data capture. The subjects were seated with the lips relaxed and with the head in natural head position (NHP) (self-balance “mirror” position) as described by previous authors [69-71]. If a subject moved between scans, the procedure was repeated and the data of the first scan were eliminated from the study. The data were acquired by dedicated Skanect software (developed by the ManCTL Company, 2011, Madrid) (Figure 7).

Figura 1: Facial soft tissue scan. Frontal, prospective, and right lateral 3D views of facial soft tissue scan of female patient.

Mimics software (version 10.11, Materialise Medical Co., Leuven, Belgium) was used to import the surface model and to perform 3D cephalometric analysis. All the lateral cephalometric radiographs underwent reposition of the head on the basis of the orientation of the soft tissue scan position by superimposition on the right lateral view of the 3D facial scan using Deltadent software. A set of reproducible landmarks was developed to compute the soft tissue cephalometric analysis (Figure 8).


N'
Obs
Or
Tr
Sp
Go'
Si
Pg'
Gn'
Me'

Figura 2: Facial soft tissue scan. Frontal, prospective, and right lateral 3D views of facial soft tissue scan of female patient.

Fourteen sagittal (Figures 4, 5, and 6) and 14 vertical (Figures 7, 8, and 9) angular measurements were selected and performed for good anatomical correspondence between hard tissue and soft tissue structures and reference landmarks. The average of the angles was computed for symmetric structures. Then, every skeletal measurement was coupled and assigned to one or more soft tissue measurement (Table 1) for the correlation analysis.

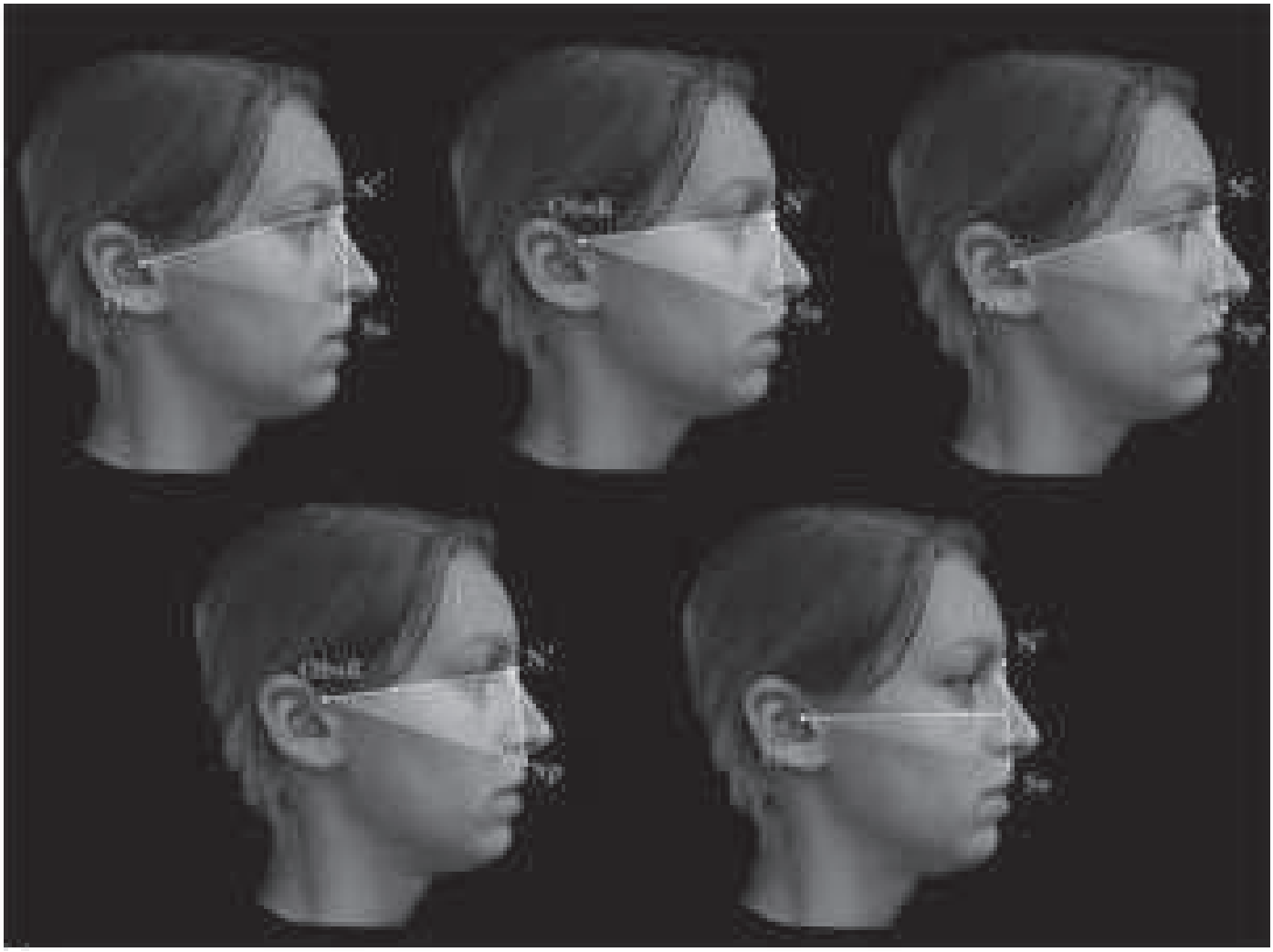

Figura 3: Sagittal angular measurements for 3D facial soft tissue. Part I

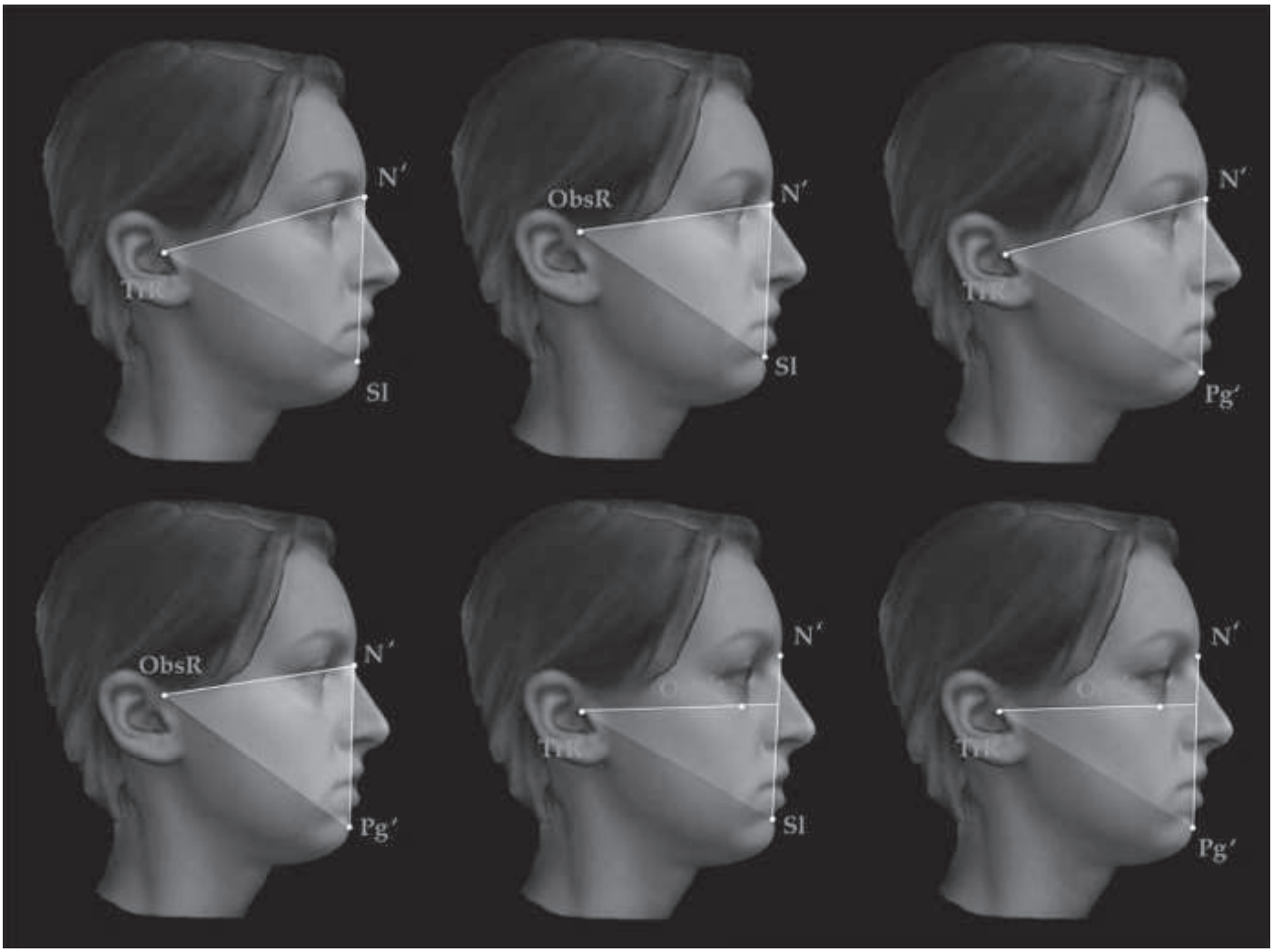

Figura 4: Sagittal angular measurements for 3D facial soft tissue. Part II

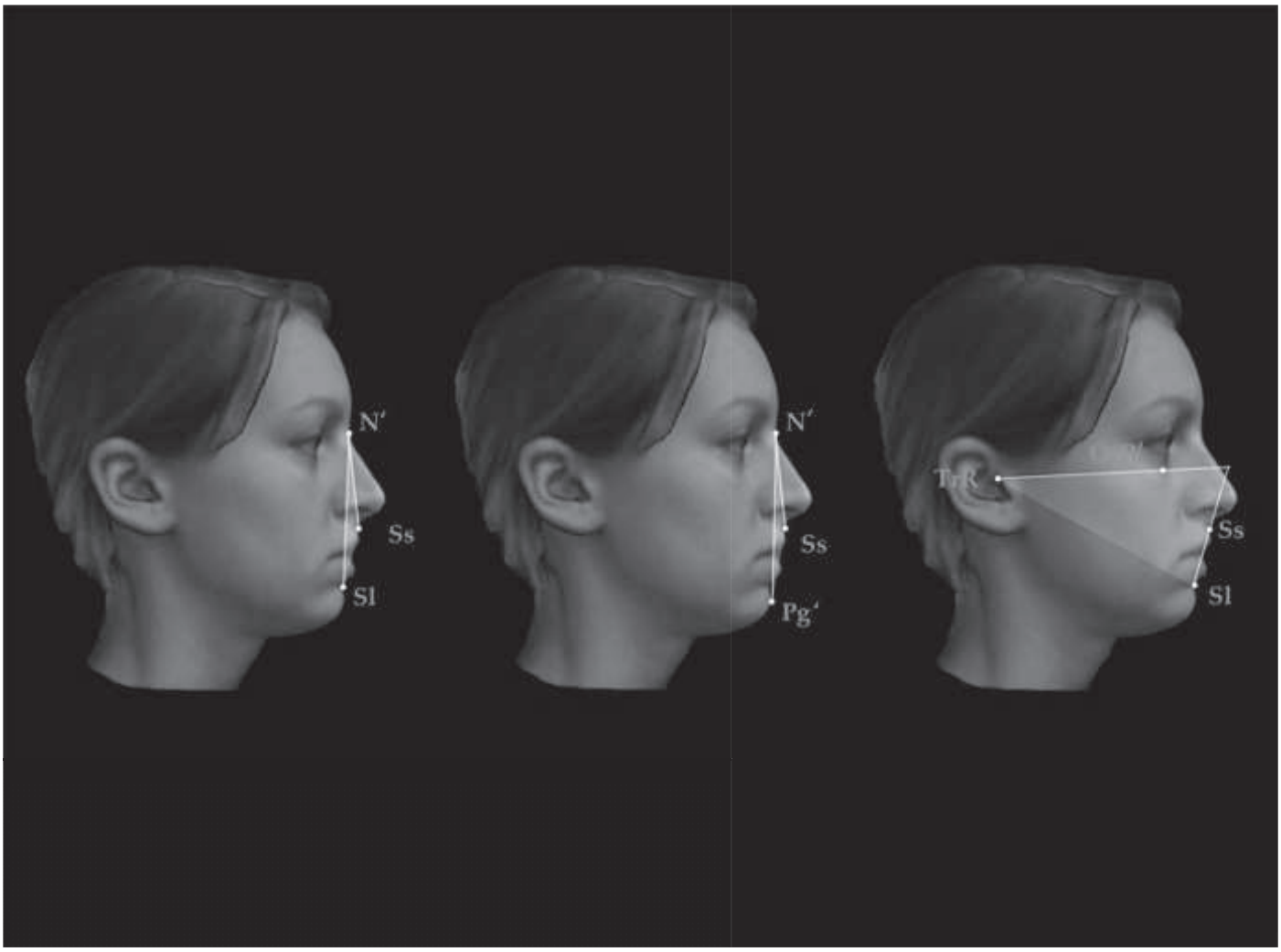
N'
Ss
Sl
N'
Ss
Pg'
Ss
Sl

Figura 6: Sagittal angular measurements for 3D facial soft tissue. Part III

Figura 5:Vertical angular measurements for 3D facial soft tissue.

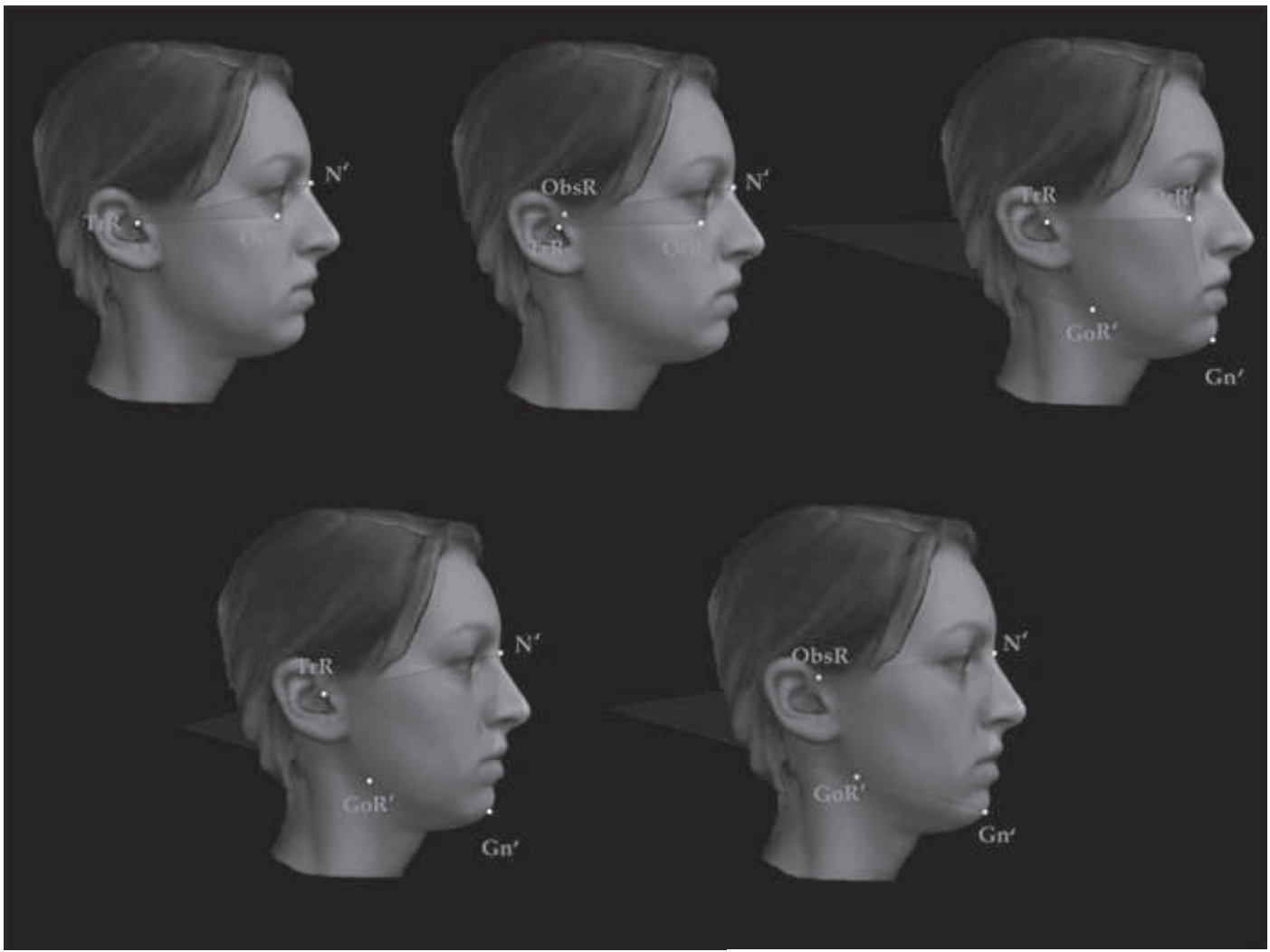

Figura 7: Vertical angularmeasurements for 3D facial soft tissue.

Figura 8: Vertical angularmeasurements for 3D facial soft tissue.

Statistical Analysis. A pilot study was executed on 20 patients (12 males and 8 females) for the power analysis. One sagittal and three vertical measurements were employed as main outcome for the power analysis as follows: SsN'Sl, TrOr'∧Go'Gn', TrN'∧Go'Gn', and ObsN'∧Go'Gn'. No differences in gender were included in the power analysis. According to the power analysis, 300 subjects were required in order to obtain power of 0.80 for the present study. SPSS software, version 22.0 (SPSS® Inc., Chicago, Illinois, USA), was used to run statistical analyses. The Shapiro-Wilk test revealed a normal distribution of tested variables. The mean and standard deviation (SD) of each of the variables were then calculated. Independent t-test was used to compare the mean differences between females and males and $P < 0.05$ was set as the level of significance. All the variables were then further analyzed for any correlations with corresponding lateral cephalometric radiography measurements with the Pearson correlation coefficient (r) with the level of significance set at $P < 0.05$.

Method Error. All the measurements were performed by the same trained operator. Thirty of the 3D facial scans were repeated two weeks after the first recording and measurements were performed. The Dahlberg coefficient[72] was used to test the reproducibility of all the soft tissue landmarks employed. All the parameters displayed a method error < 1◦, which is considered clinically irrelevant.

Results. Mean and standard deviations were calculated for each lateral cephalometric radiograph and soft tissue measurement. The tested variables such as mean and SD did not show significant differences in terms of gender-specific differences (Table 2), and the following statistical analyses were performed for the total sample. Medium, low, and high correlations were found for sagittal parameters and vertical parameters in assessment of correlation with the corresponding lateral cephalometric radiography measurements previously assigned (Tables 3 and 4). ANB, ANPg, and FHΛAB were the only sagittal variables which showed high correlation coefficients compared with the respective soft tissue variables. Conversely, FHΛNA and SNans showed low correlation coefficients (Table 3). No high correlations coefficients were found for the vertical parameters which showed medium correlation coefficients except for SNΛFH that exhibited low correlation compared with the respective soft tissue variables (Table 4).

Tabella 2: 2D and 3D cephalometric analyses. Cephalometric sagittal and vertical analyses and corresponding 3D soft tissue measurements.

Cephalometrics	3D soft tissue
Sagittal	
SNA	TrN′Ss
	ObsN′Ss
SNans	TrN′Sp
	ObsN′Sp
FH^NA	TrOr′^N′Ss
SNB	TrN′Sl
	ObsN′Sl
SNPg	TrN′Pg′
	ObsN′Pg′
FH^NB	TrOr′^N′Sl
FH^NPg	TrOr′^N′Pg′
ANB	SsN′Sl
ANPg	SsN′Pg′
FH^AB	TrOr′^SsSl
Vertical	
SN^FH	TrN′^TrOr′
	ObsN′^TrOr′
FMA	TrOr′^Go′Gn′
SN^GoGn	TrN′^Go′Gn′
	ObsN′^Go′Gn′
Gonial s ArGoN	ObsGo′N′
Gonial i NGoMe	N′Go′Me′
Articulare SArGo	N′ObsGo′
NPg-GoMe	N′Pg′^Go′Me′
SN^ArGo	TrN′^ObsGo′
	ObsN′^ObsGo′
FH^ArGo	TrOr′^ObsGo′
FH^SPg	TrOr′^TrPg′
	TrOr′^ObsPg′

Tabella 3:Sex differences. Data are shown as mean (in bold) and stan- dard deviation (SD) (in italic) for the whole sample for females and for males.

3D soft tissue	Mean female	SD female	Mean male	SD male	*P* value
		Sagittal			
TrN′Ss	**79.75**	*2.53*	**81.46**	*3.41*	0.08
ObsN′Ss	**82.03**	*2.73*	**84.02**	*3.74*	0.06
TrN′Sp	**82.66**	*2.59*	**84.08**	*3.39*	0.12
ObsN′Sp	**84.94**	*2.43*	**86.63**	*3.83*	0.08
TrOr′^N′Ss	**86.67**	*1.82*	**85.83**	*2.47*	0.17
TrN′Sl	**71.63**	*3.39*	**71.74**	*3.93*	0.47
ObsN′Sl	**73.91**	*3.48*	**74.30**	*4.29*	0.41
TrN′Pg′	**71.16**	*3.69*	**71.86**	*3.79*	0.33
ObsN′Pg′	**73.44**	*3.81*	**74.42**	*4.21*	0.28
TrOr′^N′Sl	**84.24**	*3.63*	**83.92**	*3.53*	0.42
TrOr′^N′Pg′	**83.71**	*3.97*	**84.02**	*3.38*	0.43
SsN′Sl	**8.11**	*1.99*	**9.72**	*2.43*	0.06
SsN′Pg′	**8.59**	*2.45*	**9.60**	*2.14*	0.17
TrOr′^SsSl	**70.10**	*5.77*	**65.74**	*7.82*	0.06
		Vertical			
TrN′^TrOr′	**12.65**	*2.29*	**12.43**	*1.09*	0.41
ObsN′^TrOr′	**10.41**	*3.06*	**9.68**	*1.47*	0.28
TrOr′^Go′Gn′	**30.52**	*6.10*	**28.22**	*4.12*	0.18
TrN′^Go′Gn′	**43.17**	*6.19*	**40.65**	*4.02*	0.16
ObsN′^Go′Gn′	**40.92**	*6.41*	**37.91**	*3.72*	0.13
ObsGo′N′	**64.09**	*6.03*	**65.40**	*2.63*	0.29
N′Go′Me′	**70.19**	*5.84*	**70.36**	*5.51*	0.47
N′ObsGo′	**84.09**	*3.94*	**82.15**	*4.66*	0.14
N′Pg′^Go′Me′	**65.72**	*4.63*	**67.76**	*6.46*	0.18
TrN′^ObsGo′	**85.56**	*3.70*	**84.58**	*3.79*	0.27
ObsN′^ObsGo′	**84.09**	*3.94*	**82.15**	*4.66*	0.14
TrOr′^ObsGo′	**76.24**	*5.23*	**72.47**	*4.52*	0.05
TrOr′^TrPg′	**38.31**	*2.85*	**36.62**	*1.86*	0.08
TrOr′^ObsPg′	**44.47**	*3.01*	**43.99**	*1.80*	0.35

Tabella 4 Sagittal measurement c∗orrelations. Pearson correlation coefficients (r) are shown for sagittal measurements as low (in italic), medium (lightface), and high (in bold). ∗P < 0.05.

Cephalometrics			3D soft tissue			r
Variable	Mean	SD	Variable	Mean	SD	
SNA	81.43	3.35	TrN′Ss	80.08	2.81	0.36*
			ObsN′Ss	82.41	3.05	0.34
SNans	85.55	3.84	TrN′Sp	82.94	2.82	0.31*
			ObsN′Sp	85.27	2.84	*0.27*
FH^NA	87.13	1.93	TrOr′^N′Ss	86.51	1.99	*0.16**
SNB	76.79	3.02	TrN′Sl	71.66	3.50	0.59*
			ObsN′Sl	73.99	3.66	0.62*
SNPg	77.47	3.02	TrN′Pg′	71.30	3.72	0.54*
			ObsN′Pg′	73.63	3.91	0.56*
FH^NB	86.46	2.63	TrOr′^N′Sl	84.17	3.61	0.67*
FH^NPg	86.70	2.20	TrOr′^N′Pg′	83.77	3.87	0.66*
ANB	4.65	2.36	SsN′Sl	8.42	2.18	**0.74***
ANPg	4.03	2.61	SsN′Pg′	8.79	2.43	**0.74***
FH^AB	79.92	6.12	TrOr′^SsSl	69.26	6.46	**0.81***

Tabella 5: Vertical measurement correlations. Pearson correlation coefficients (r) are shown for vertical measurements as low (in italic) and medium (lightface). ∗P < 0.05.

Cephalometrics			3D soft tissue			r
Variable	Mean	SD	Variable	Mean	SD	
SN^FH	10.38	2.76	TrN′^TrOr′	12.60	2.11	*0.25**
			ObsN′^TrOr′	10.26	2.84	*0.15**
FMA	25.00	4.42	TrOr′^Go′Gn′	30.07	5.84	0.59*
SN^GoGn	35.38	5.06	TrN′^Go′Gn′	42.68	5.92	0.54*
			ObsN′^Go′Gn′	40.34	6.10	0.53*
Gonial s ArGoN	53.46	4.06	ObsGo′N′	64.35	5.56	0.42*
Gonial i NGoMe	75.66	4.56	N′Go′Me′	70.22	5.78	0.45*
Articular SArGo	142.06	6.62	N′ObsGo′	83.72	4.16	0.45*
NPg-GoMe	67.15	4.28	N′Pg′^Go′Me′	66.12	5.10	0.61*
SN^ArGo	84.69	3.97	TrN′^ObsGo′	85.37	3.74	0.33
			ObsN′^ObsGo′	83.72	4.16	0.43
FH^ArGo	75.87	5.38	TrOr′^ObsGo′	75.51	5.32	0.45
FH^SPg	57.16	3.13	TrOr′^TrPg′	37.98	2.77	0.57
			TrOr′^ObsPg′	44.38	2.82	0.59

Discussion. The purpose of this study was to compare facial soft tissue analysis, obtained from facial scans, with lateral cephalometric radiography, in order to highlight possible correspondences between hard tissue and soft tissue diagnoses. The growing role of noninvasive imaging tools could be of great importance in orthodontic diagnosis since 3D facial soft tissue might be employed as the first screening examination for guiding clinicians through skeletal diagnosis and performance of further radiological exams only when needed. The tested infrared scanner showed good reliability and reproducibility in facial morphology acquisition. Moreover, the facial scans proved appropriate for

landmark location and the method error for soft tissue cephalometric analysis was acceptable. The possibility of evaluating soft tissue components in 3D allowed us to relocate the head and did not present the limitation of bidimensional (2D) photographic pictures where head position errors can be of great importance in landmark identification. The sample was first tested for any gender-specific differences. Kochel et al. [66] employed stereophotogrammetry for the evaluation of facial soft tissue focusing on sagittal measurements and found significant differences between males and females with the mean age (25.4 years) similarly to the sample in the present study. According to the present results, no significant differences in facial soft tissue sagittal and vertical dimensions were found between the genders, even though a tendency toward statistical significance (P <0.08) was reported for TrN'Ss and ObsN'Ss measurements (Table 2). These measurements indicated maxillary protrusion and were reported to be smaller in females. Although similar samples were tested, the results of the present study were not in agreement with those of Kochel et al. [66]. Indeed, the methods of facial scanning and the soft tissue analysis employed should be considered as possible reasons for the different results in the variability of sagittal dimensions between genders. Moreover, in the present sample, gender differences seemed to have no influence on vertical dimensions in agreement with previous investigations [65]. Since no differences were assessed between genders, the sample was considered as a whole and Pearson correlation coefficients were computed for each variable in order to check for any correlations between sagittal and vertical soft tissue measurements and corresponding skeletal measurements in lateral cephalometric radiography. Little previous evidence has been presented for correspondences between soft tissue and skeletal measurements with 3D and 2D image acquisition tools [73, 74] but they showed high correlations between the tested variables. The present results were analyzed for sagittal and vertical measurements, separately. Most of the sagittal parameters showed medium correlation coefficients (between 0.31 and 0.67) (Table 3). ANB, ANPg, and FH∧AB showed high correlation coefficients (r > 0.7) when compared with the respective soft tissue variables. These angles are usually applied in the evaluation of sagittal relationships between maxilla and mandible and account for the diagnosis of skeletal malocclusion. According to the present results, the diagnosis performed on soft tissue seemed to be reliable in predicting skeletal cephalometric outcomes since the coefficients showed high values and reached the level of significance. Kochel et al. [66] evaluated sagittal soft tissue measurements and their correspondences with lateral cephalometric radiography, describing a set of variables defined on the basis of common skeletal cephalometric measurements. Their findings are in agreement with the present investigation. The selection of the corresponding landmarks between skeletal and soft tissue seemed very important in the outcomes of correlation coefficients. Previous studies [75] found no correlation between soft tissue measurements of facial profile and cephalometric ANB angle, employing the landmarks subnasal and skin pogonion as correspondent of skeletal

landmarks A and B, respectively. The present investigation used the landmarks subspinal (Ss) and sublabial (Sl) and high correlation between soft tissue andANB skeletal angle was found, showing that different outcomes might be owing to the selection of different landmarks. The measurements of maxillary sagittal position (SNA, SNans, and FH∧NA) showed the lowest r values (ranging from 0.16 to 0.36) in relation to soft tissue corresponding measurements. On the other hand, the converse was the case for measurements of mandible sagittal position such as SNB, SNPg, FH∧NPg, and FH∧NB with r values ranging from0.54 to 0.81. This result suggested that stronger sagittal relations between soft tissue and underlying hard tissue involved the lower third of the face compared with the middle third of the face. Medium correlation coefficients were found for the vertical parameters (Table 4) in agreement with other studies[65]. Only SN∧FH exhibited low correlation with the respective soft tissue variables (r = 0.15 and r = 0.25). This may be because of the difficulty of locating corresponding soft tissue landmarks for the middle cranial base and the Go' landmark that might have a small correspondence with the external soft tissues. All the facial scans in the present study were performed with relaxed lips and this position was considered accurate in terms of diagnosis and treatment planning [55, 56] and allowed comparison with lateral cephalometric radiographs that are routinely performed with relaxed lips. Unfortunately, the collected lateral cephalometric radiographs were not all performed with the same X-ray machine and this could be seen as a limitation of the present study. Moreover, only selected cephalometric landmarks were employed and only one operator analysed the data. Also, the inclusion of Caucasian patients only could be considered a limitation of the present investigation. Even though encouraging results were obtained from the present study, they are still limited to our sample and methods. Also, the selected sample showed normal BMI, possibly the ideal condition for the present investigations since excessive BMI was reported to have significant effects on the ratio between skeleton and overlying soft tissue, so the results should not be extended to altered BMI conditions where the correspondences between hard and soft tissues may be less precise. Further studies are needed in order to clarify the complex relationships between soft and hard tissues and help clinicians and researchers with diagnosis and treatment planning with noninvasive tools.

Conclusions. From the results of the present study, the following facts can be stated:

(i) No statistically significant differences were found for sagittal and vertical soft tissue measurements between females and males in the tested sample.
(ii) Sagittal measurements seemed to be more reliable in terms of providing a soft tissue diagnosis than lateral cephalometric radiography measurements (ANB and ANPg), especially for the lower third of the face (SNB, SNPg, FH∧NPg, and FH∧NB).

(iii) Vertical soft tissue measurements showed weaker correlation with the corresponding lateral cephalometric radiography variables.

The present soft tissue analysis proposal based on 3D facial scans showed good reliability and reproducibility even though further studies are needed in order to confirm the findings of the research.

7.9.2 Extracted from: Immediate Restoration of Fixed Partial Prostheses Supported by One-Piece Narrow-Diameter Selective Laser Sintering Implants: A 2-Year Prospective Study in the Posterior Jaws of 16 Patients. Francesco Mangano, Samuele Pozzi-Taubert, Piero A. Zecca, DDS, Giuseppe Luongo, Rachel L. Sammons, and Carlo Mangan. Implant Dentistry 2013 Aug;22(4):388-93.

Introduction: Prosthetic rehabilitation of partially and totally edentulous patients with osseointegrated oral implants has been extensively documented, and predictable results can be achieved in most indications.1–3 In the severely resorbed posterior mandible/maxilla, however, the use of standard diameter implants may present a challenge. Some residual ridges, in fact, are very thin and cannot accept a standard diameter (3.75–4.1 mm) implant within the confines of the available bone with 1 to 2 mm circumferential thickness of bone.4 Reconstructive surgery represents the treatment of choice to recreate the correct bone volume and morphology. 5 In some cases, however, reconstructive procedures are not accepted by the patients, for economic reasons or due to higher morbidity. The use of narrow-diameter implants would enable the dentist to rehabilitate the patient without grafting.6 “Narrow diameter implants,” “small-diameter implants,” or “mini dental implants” are terms used to describe implants with diameters less than 4 mm.7 Narrow-diameter implants have been used for retention of complete removable maxillary and mandibular overdentures, 3,8 but there are also reports for their use in fixed prosthetics. In fact, several articles reporting data on the use of narrow implants not only in the frontal areas9,10 but also in posterior partially edentulous jaws and in totally edentulous patients11–16 have been published in recent years. The results from clinical studies on narrow-diameter implants have shown high survival rates, irrespective of the surgical approach that was used, ranging between 96.0% and 98.7% at 5 years using a 2-stage surgical approach.17,18 A 1-stage surgical approach saw a success rate of 96.4%19 and 99.4% was found with the immediate function approach.14 However, caution in the use of narrow-diameter implants has been advocated because of the concern regarding the negative impact of loading in these implants.5,20 As demonstrated by a number of publications, the risk of “fatigue” and increased probability of fracture of the implants exists in these cases.4,18,21,22 A nonlinear finite element analysis has shown that the neck of the narrow diameter implant represents a potential

zone of fracture when subjected to high bending forces,23 making it mandatory to increase the implant support to improve the biomechanical outcome of the treatment.24 In recent years, considerable progress has been made in the development of solid freeform fabrication methods, including selective laser sintering (SLS).25 SLS is a time-saving procedure in which a high power laser beam is directed on a metal powder bed and programmed to fuse particles according to a computer-assisted design (CAD) file, generating a thin metal layer. Apposition of subsequent layers gives shape to a desired 3-dimensional form with minimal postprocessing requirements.25 With SLS, it is possible to fabricate dental implants of different size and shape, directly from CAD models.3 This layered manufacturing method enables the fabrication of functionally graded titanium implants, with a gradient of porosity perpendicular to the long axis.25 Moreover, with SLS, a porous surface structure for bone ingrowth is provided.3 The aim of this study was to evaluate the survival and success rate of immediately restored, 1-piece, narrow-diameter, SLS implants, after 2 years of functional loading.

Materials and Methods: Patient Selection: Between January 2009 and January 2010, all patients referred to the Dental Clinic, University of Varese, for treatment with oral implants, were considered for inclusion in this study. Only patients presenting with partial edentulism associated with horizontal defects of the lateral-posterior alveolar ridges of the maxilla or mandible (from first premolar to second molar), which render the placement of standard-diameter implant (4 mm) difficult or impossible, were selected for this study; additional inclusion criteria were adequate bone height and width to place an implant of at least 2.7 mm diameter and 10.0 mm length. Exclusion criteria consisted of poor oral hygiene, active periodontal infections, uncontrolled diabetes, bruxism, and heavy smoking

habit (more than 10 cigarettes per day). The study protocol was explained to each subject, and signed informed consent was obtained. The study was performed according to the principles outlined in the World Medical Association Declaration of Helsinki on experimentation involving human subjects, as revised in 2008, and it was approved by the Local Ethics Committee for Human Studies at the University of Varese, Italy.

Preoperative Workup: A complete examination of the oral hard and soft tissues was carried out for each patient. Preoperative workups included an assessment of the partially edentulous posterior ridge using casts and diagnostic wax-up. Panoramic radiographs and CT scans were taken. CT data sets were acquired using a cone beam scanner and then transferred in the digital imaging and communication in medicine format to specific implant navigation software (Mimics; Materialise, Leuven, Belgium) to perform a 3-dimensional reconstruction of the jaw. Through this navigation software, it was possible to correctly assess the width of each implant site, the thickness and the density of the cortical plates and the cancellous bone, and the ridge angulation. Bone density was also assessed to obtain a reliable and valid description of preoperative

jawbone condition. On the basis of all this information, surgical templates were manufactured. SLS Implants Screw-type, 1-piece, narrow diameter implants (Fig. 1) were manufactured with an SLS technique (TixOs Nano; Leader-Novaxa, Milan, Italy).3,25 The SLS implants were made of master alloy powder (Ti-6Al-4V), with a particle size of 25 to 45 mm, as the basic material. Processing was carried out in an argon atmosphere using a powerful Yb (Ytterbium) fiber laser system with the capacity to build a volume up to 250 3250 3215 mm using a wavelength of 1054nm with a continuous power of 200 W, at a scanning rate of 7 m$s−1. The size of the laser spot was 0.1 mm. To remove residual particles from the manufacturing process, the sample was sonicated for 5 minutes in distilled water at 25°C, immersed in sodium hydroxide (20 g$L−1) and hydrogen peroxide (20 g$L−1) at 80°C for 30 minutes, and then further sonicated for 5minutes in distilled water. Acid etching was carried out by immersion of the samples in a mixture of 50% oxalic acid and 50% maleic acid at 80°C for 45 minutes, followed by washing for 5 minutes in distilled water in a sonic bath. The surface topography of the SLS implants had no clear orientation. The direct laser preparation provided an implant surface with a roughness surface with the mean 6 SD of the absolute values of all profile points, the root-mean-square of the values of all points, and the average value of the absolute heights of the 5 highest peaks, and the depths of the 5 deepest valleys of 66.8 6 6.6 mm, 77.6 6 11.1 mm, and 358.3 6 101.9 mm, respectively.3,25

Implant Placement: Local anesthesia was obtained by infiltrating articaine 4% containing 1:100.000 adrenaline (Ubistesin; 3M Espe, St. Paul, MN). A midcrestal incision was made at the sites of implant placement. The mesial and the distal aspects of the crestal incision were connected to 2 releasing incisions. Full-thickness flaps were reflected exposing the alveolar ridge, and preparation of implant sites was carried out with spiral drills of increasing diameter (2.0 and 2.3 mm, to place an implant with 2.7 mm diameter; 2.0, 2.3 and 2.6 mm, to place an implant with 3.2 mm diameter) under constant irrigation. The 1-piece, narrow-diameter, SLS implants were positioned at the bone crest level. The flaps were then repositioned and were secured around the emerging abutment by interrupted sutures (Supramid; Novaxa, Milan, Italy). Immediately after implant placement, provisional restorations, fabricated in the dental laboratory before surgery, using either a technique where a diagnostic waxing was duplicated to create a gypsum cast or by using cast-based guided surgery with prefabricated provisional restorations, were placed in position, relined intraorally (Unifast LC; GC Corp, Tokyo, Japan), and cemented with temporary cement (Temp-Bond; Kerr, Orange, CA). Care was taken to prevent cement from penetrating subgingivally or to remove it thoroughly, if this occurred. The occlusion was carefully checked. The provisional restorations were placed in light maximum intercuspation contact without working and nonworking contacts. Finally, the patients received postoperative instructions. All patients received oral antibiotics, 2 g each day for 6 days (Augmentin; GlaxoSmithKline, Brentford, United Kingdom). Postoperative pain was controlled by administering 100 mg nimesulide (Aulin; Roche Pharmaceutical, Basel,

Switzerland) every 12 hours for 2 days, and detailed instructions about oral hygiene were given, with mouth rinses with 0.12% chlorhexidine (Chlorhexidine; Oral-B, Boston, MA) administered for 7 days. Suture removal was performed at 8 to 10 days.

Prosthodontic Procedure: Provisional restorations were used to monitor implant stability under a progressive load and to obtain good soft tissue healing around the implant before fabrication of the definitive restorations. The placement of the definitive prosthetic restorations was performed on an individual basis, after soft tissue maturation, at least 3 months after implant placement. All definitive restorations were ceramic-metallic, cemented with temporary cement (Temp-Bond; Kerr). These restorations were carefully evaluated for proper occlusion, and protrusion and laterotrusion were assessed on the articulator and intraorally.

Clinical, Radiographic, and Prosthetic Evaluation: The following clinical parameters were investigated after 2 years of functional loading for each implant: presence/ absence of pain, suppuration, or exudation and presence/absence of implant mobility, tested manually using the handles of 2 dental mirrors. Intraoral periapical radiographs were taken of each implant, using an alignment system with a rigid film-object x-ray source coupled to a beam-aiming device to achieve reproducible exposure geometry. 26 Customized positioners, made of polyvinyl siloxane, combined with an alignment system with a rigid film object x-ray source coupled to a beamaiming device, were used for precise repositioning and stabilization of the radiographic template. Radiographs were taken at the baseline (immediately after implant insertion) and at the 2-year follow-up session, and 2 different radiographic parameters were evaluated: presence/absence of continuous periimplant radiolucencies and distance between the implant shoulder and the first visible bone contact (DIB) in millimeters, measured with the aim of an ocular grid.3,26 With the latter value, crestal bone level changes at 2 years were registered as modifications in the distance from the implant shoulder to the bone level on the mesial and distal implant side. To correct dimensional distortion, the apparent dimension of each implant was measured on the radiograph and then compared with the real implant length.26 Finally, at the 2-year follow-up session, prosthesis function was tested. Static and dynamic occlusion was evaluated, using standard occluding papers. Careful attention was dedicated to the analysis of any potential prosthetic complications.

Implant Survival and Implant: Success Criteria: The evaluation of implant survival and implant success was performed according to the following clinical and radiographic parameters. Implants were divided into 2 categories: survived and failed implants. A survived implant was classified as such when it was still functional at the end of the study, after 2 years of functional loading. Implant losses were categorized as failures. Implants presenting pain on function, suppuration, or clinical mobility were removed and categorized as failures. The conditions for which implant removal could be indicated included failure of osseointegration or infection, recurrent periimplantitis, or implant loss

caused by mechanical overload. To achieve implant success, the following clinical and radiographic success criteria had to be fulfilled: absence of pain on function, absence of suppuration or exudation, absence of clinically detectable implant mobility, absence of continuous periimplant radiolucency, DIB ,2.0 mm from initial surgery, and absence of prosthetic complications.27

Patient Population and Implant-Supported Restorations: A total of 18 patients (10 males and 8 females, aged between 48 and 69 years, mean age 58.5 years) were considered to take part in this prospective clinical study. Two patients, however, could not be included in the study (1 for bruxism and 1 for heavy smoking habit). Sixteen patients (9 males and 7 females, aged between 48 and 69 years) fulfilled the inclusion criteria, presenting none of the conditions listed in the exclusion criteria, and were enrolled in this study. In total, 37 implants were positioned by an experienced surgeon. Fourteen implants (37.8%) were inserted in the posterior maxilla, whereas 23 implants (62.2%) were inserted in the posterior mandible. The distribution of implants by length and diameter was in accordance with Table 1. The prosthetic restorations comprised 16 fixed partial prostheses (FPPs) supported, respectively, by 2 (8 FPPs) or 3 (7 FPPs) implants.

Implant Survival and Success: At the end of the study, all implants were still in function giving an overall survival rate of 100%. Among these implants, 35 (94.6%) were classified in the implant success group (Figs. 2–5). None of these implants caused pain or clinical mobility, suppuration, or exudation, with a DIB ,2.0 mm from initial surgery, and none had any prosthetic complication. Two implants (5.4%), on the contrary, could not fulfill the success criteria. These 2 implants, in fact, revealed a DIB .2.0 mm after 2 years of function. All these implants were in the maxilla and were the distal elements of an FPP supported by 2 implants. At the end of the study, the radiographic evaluation of the implants revealed a mean 6 SD distance from the implant shoulder to the first crestal bone to implant contact (DIB) of 0.4 6 0.3 mm (95% confidence interval, 0.3–0.5). No implant fractures or prosthetic complications related to the suprastructure (FPPs) were observed.

DISCUSSION: Posterior regions of the jaws with reduced bone quantity and quality make it challenging to rehabilitate with standard diameter implants, without the use of complex reconstruction techniques. The use of small-diameter implants may represent a solution to this problem. 5 Narrow-diameter implants have been used primarily in multiples, to retain complete removable overdentures3,8 or to support fixed restorations in the atrophic frontal areas of the jaws, as they can fit into many of these atrophic sites with adequate interimplant and interocclusal spacing.9,10 More recently, some studies proposed the use of these implants also in the posterior areas of the jaws, as an alternative treatment option to horizontal bone reconstruction/regeneration, reporting good implant survival rates.11–16 As shown in a recent review of literature, the survival rate of small-diameter implants seems to be similar to that of regular diameter implants,

with the majority of studies reporting survival rates at 95% to 100% and no study reporting survival rates below 89%.7 However, caution has been suggested in the interpretation of these results. In cases of high occlusal loading, such as fixed partial rehabilitations of the posterior sectors of the jaws, the risk of fatigue fracture of narrow-diameter implants has been reported.4,18,21,22 Narrow implants, in fact, can be fractured by occlusal forces.4,22 To reduce this risk, new alloys that might present higher resistance to mechanical stress compared with pure titanium have been introduced together with technological breakthroughs, such as solid freeform fabrication techniques, including SLS. SLS is a laser-based solid freeform fabrication technique that allows the precise fabrication of complex 3-dimensional objects like dental implants created by computer-generated image-based design techniques, using a layer-by-layer manufacturing approach.25 With SLS, dental implants are built layer by- layer using powdered materials, radiant heaters, and a computer-controlled laser. The digital representation of an implant is mathematically sliced into a number of thin layers; the implant is then created by scanning a laser beam and selectively fusing (melting or sintering) patterns into sequentially deposited layers of titanium alloy micro powders. Each patterned layer is also fused to its underlying layer and corresponds to a cross-section of the object as determined from the mathematical slicing operation. In the present study, 1-piece narrow-diameter SLS implants, available in a range from 2.7 to 3.2 mm, placed in the posterior jaws and immediately restored with FPPs, showed high 2-year survival (100%) and success (94.6%) rates. These results seem to be consistent with those reported in the literature for standard-diameter implants placed in nondeficient edentulous ridges.1,2 Fewer surgical interventions, with the ability to place the implants in thin residual ridges without the need of complex reconstruction techniques, and shorter treatment time are advantages of this protocol.8,28 No implant fracture or prosthetic complications were reported, showing that narrow-diameter implants fabricated with SLS technique may predictably bear the mechanical stresses generated by occlusal loading and masticatory function in the lateral-posterior areas of the jaws. The implants used in the present study, in fact, were fabricated of a titanium alloy, which is stronger than conventional grade 1 titanium.25 Moreover, in terms of material strength, 1-piece implants are stronger than 2-piece implants. The 1-piece design, which incorporates the transmucosal abutment as an integral part of the implant, eliminates the structural weakness built into a 2-piece implant system. The abutment screw is eliminated, so there is no empty space in the implant, providing sufficient strength of the 1-piece implant despite its small diameter. 6 Recently, there has been some discussion about the gap at the implant abutment interface of conventional 2-piece implants, the so-called “microgap” that may become a bacterial reservoir that may provoke bone resorption to the first thread. It has been shown that a crestal bone loss of about 1 to 1.5 mm can occur with conventional 2-piece implants, placed at or below the alveolar crest, depending on the location of the microgap between the implant and the abutment.29,30

With 1-piece implants, this loss of alveolar bone around the implant could be minimized.6 This design benefit of the implant may be one reason for the favorable mean marginal bone level (DIB ¼ 0.4 6 0.3 mm) demonstrated in our present study, after 2 years of loading. Moreover, the 1-piece implant design enables undisturbed healing of the periimplant soft tissue, avoiding manipulation of the periimplant soft tissue after initial healing. 6 The reduced prosthetic versatility, resulting from the lack of options for abutment angulation, is a disadvantage of single-piece implants. However, the fabrication of dental implants with the SLS technique may offer some potential advantages that could be helpful in immediate restoration protocols. SLS enables fabrication of implants with a graded elasticity, incorporating a gradient of porosity, from the inner core to the outer surface. The outer surface, in fact, has an elastic modulus (77Gpa) closer to that of the surrounding cortical bone (10–26 Gpa) for a potentially more natural transfer of loading stress.3 In addition, the SLS technique allows the fabrication of a porous structure with controlled porosity, pore interconnection, size, shape, and distribution, which are requirements for rapid bone ingrowth.3 At present, excellent success rates have been documented with implants placed in a 1-stage procedure, including numerous cases in which the single-stage placement has been accompanied by attachment of a fixed provisional prosthesis placed in function, at least to some extent.31 Case selection, however, remains critical for the use of narrow diameter implants supporting fixed partial dentures.4,5 A patient may be a candidate for these implants if there are milder jaw forces, sites with denser bone, and adequate attached gingiva. Narrow-diameter implants should be used only with weak occlusal forces.4,6 The smaller surface area and volume of these implants places more force per square millimeter against the encasing bone than larger diameter implants, so that occlusal force control is needed. Bone density of type I, II, or III and bone available at a height of at least 10 mm and at least 1 mm of attached or augmentable gingiva are desirable.4 Finally, it is important to also consider patient selection with regard to gingival biotype profile. Because of the highly adherent nature of the soft tissue to the extended implant porous surface, there may be a greater tendency for eventual gingival discoloration in patients with thin overlying keratinized epithelium.4,6

CONCLUSIONS: Within its limits, such as the small patient (16) and implant (37) sample size, and the short follow-up (2 years), this study supports the hypothesis that single-piece narrow-diameter implants can be used in fixed prosthetic rehabilitations in the posterior regions of both jaws with a predictable positive outcome. Results, in terms of implant survival (100%) and success (94.6%) rates, are consistent with those reported in the literature for standard-diameter implants placed in nondeficient edentulous ridges. No implant fracture or prosthetic complications were reported. Further studies will be needed to investigate the clinical performance of 1-piece SLS implant. The results of the present study seem to demonstrate that narrow diameter implants fabricated with an SLS technique can predictably bear the mechanical stresses generated by occlusal loading

and masticatory function in the lateral-posterior areas of the jaws, in the case of fixed partial restorations. Careful patient selection in combination with good primary implant stability should be considered a prerequisite for successful immediate provisional restoration of single-piece implants used for supporting fixed partial restorations in the upper and lower jaw.

7.9.3 Extracted from: Mangano FG, Zecca PA, van Noort R, Apresyan S, Iezzi G, Piattelli A, Macchi A, Mangano C. Custom-Made Computer-Aided-Design/Computer-Aided-Manufacturing Biphasic Calcium-Phosphate Scaffold for Augmentation of an Atrophic Mandibular Anterior Ridge. Case Rep Dent. 2015;2015:941265. doi: 10.1155/2015/941265. Epub 2015 May 10. PubMed PMID: 26064701; PubMed Central PMCID: PMC4442008.

Hindawi Publishing Corporation
Case Reports in Dentistry
Volume 2015, Article ID 941265, 11 pages
http://dx.doi.org/10.1155/2015/941265

Hindawi

Case Report

Custom-Made Computer-Aided-Design/Computer-Aided-Manufacturing Biphasic Calcium-Phosphate Scaffold for Augmentation of an Atrophic Mandibular Anterior Ridge

Francesco Guido Mangano,[1,2] Piero Antonio Zecca,[1,2] Ric van Noort,[3] Samvel Apresyan,[4] Giovanna Iezzi,[5] Adriano Piattelli,[5] Aldo Macchi,[1,2] and Carlo Mangano[1,2]

[1] *Department of Surgical and Morphological Science, Dental School, University of Insubria, Via Ginseppe Piatti 10, 21100 Varese, Italy*
[2] *ITEB Research Centre, University of Insubria, Via Giuseppe Piatti 10, 21100 Varese, Italy*
[3] *Academic Unit of Restorative Dentistry, School of Clinical Dentistry, University of Sheffield, 19 Claremont Crescent, Sheffield S10 2TA, UK*
[4] *Academic Unit of Prosthodontics, Moscow State University of Medicine and Dentistry, 20 Delegatskaya Street, Moscow 127473, Russia*
[5] *Department of Medical, Oral and Biotechnological Sciences, Dental School, G. d'Annunzio University, Via dei Vestini 31, 66100 Chieti, Italy*

Correspondence should be addressed to Francesco Guido Mangano; francescomanganol@mclink.net

Received 6 February 2015; Accepted 21 April 2015

Academic Editor: Miguel Peñarrocha

This report documents the clinical, radiographic, and histologic outcome of a custom-made computer-aided-design/computer-aided-manufactured (CAD/CAM) scaffold used for the alveolar ridge augmentation of a severely atrophic anterior mandible. Computed tomographic (CT) images of an atrophic anterior mandible were acquired and modified into a 3-dimensional (3D) reconstruction model; this was transferred to a CAD program, where a custom-made scaffold was designed. CAM software generated a set of tool-paths for the manufacture of the scaffold on a computer-numerical-control milling machine into the exact shape of the 3D design. A custom-made scaffold was milled from a synthetic micromacroporous biphasic calcium phosphate (BCP) block. The scaffold closely matched the shape of the defect: this helped to reduce the time for the surgery and contributed to good healing. One year later, newly formed and well-integrated bone was clinically available, and two implants (AnyRidge, MegaGen, Gyeongbuk, South Korea) were placed. The histologic samples retrieved from the implant sites revealed compact mature bone undergoing remodelling, marrow spaces, and newly formed trabecular bone surrounded by residual BCP particles. This study demonstrates that custom-made scaffolds can be fabricated by combining CT scans and CAD/CAM techniques. Further studies on a larger sample of patients are needed to confirm these results.

1. Introduction

Dental implants are a valid and predictable modality to restore function and aesthetics in completely and partially edentulous patients, with satisfactory high long-term survival rates, particularly in the mandible [1, 2].

Sufficient alveolar bone volume is required to ensure the correct placement of implants and to achieve an aesthetically pleasing outcome [2–4]. However, a variety of processes, including absorption of alveolar bone after tooth loss, periodontal diseases, traumatic injuries, cysts, and tumors, may result in severe alveolar bone defects, with insufficient bone volume to place the implants correctly [5]. In this situation, alveolar ridge augmentation is indicated, either before or in conjunction with implant placement, in order to attain long-term function and an aesthetic outcome [3–5].

Different surgical techniques have been used to overcome alveolar ridge atrophy, including onlay/inlay bone grafting

[6–8], guided bone regeneration (GBR) [9, 10], ridge split technique/ridge expansion [11], and distraction osteogenesis [7, 12].

Autogenous bone has always been considered the "gold standard" for alveolar ridge augmentation because of its inherent osteogenic, osteoinductive, and osteoconductive properties [5, 13]. Accordingly, bone reconstructions often involve onlay bone grafts, harvested from either intraoral or extraoral sites [5–7, 13]. However, the use of autografts as onlays has drawbacks, such as additional surgery for harvesting, limited availability, donor site morbidity (which includes risk of infection, bleeding, pain, swelling, and damage to nerves and blood vessels), and high resorption rate of the graft [5, 13]. To overcome these limitations, bone substitute materials such as allografts [8], xenografts [14], and synthetic bone grafts [3, 10, 15] have been introduced.

Whereas all the aforementioned surgical techniques and materials can be successful to augment bone vertically and horizontally, the number of complications and failures of these procedures is still high [4, 5, 13]. Alveolar ridge augmentation remains a major challenge due to anatomical limitations and technical problems, such as the difficulty to shape the bone graft into an appropriate three-dimensional (3D) configuration [5, 13, 16].

Until recently, it was common practice for surgeons to estimate the size and shape of a bone graft on plain radiographs, decide the final shape, and manually cut the scaffold into the desired shape during the operation [16–19]. Unfortunately, this approach is complex and time-consuming and the size and shape of bone graft can be highly inaccurate, as it depends heavily upon the clinicians' ability to contour delicate 3D shapes manually. This may finally result in an unstable clinical outcome [19, 20].

Ideally, bone grafts should be customised to meet individual patient needs, since there are individual variations among patients and differences in damaged parts. The use of grafts that are made to fit precisely according to the 3D shape of the patient's bone defects may improve the vascularization and the biocompatibility of the scaffold following implantation [15–18].

At present, the combination of digital techniques such as model reconstruction based on medical images and computer-aided design/computer-aided manufacturing (CAD/CAM) offers new solutions for planning bone reconstructive surgery in relation to the aesthetic outcomes and the final prosthetic and functional rehabilitation [19–22]. In particular, owing to recent improvements in computer technology combined with advanced computer numerically controlled (CNC) milling units, it is now possible to fabricate 3D custom-made scaffolds in a biocompatible material. A block of bone substitute can be milled into the most appropriate shape that has been preoperatively calculated using 3D simulation [3, 19–24]. This new approach may provide a valuable alternative to conventional procedures that are based on manual intraoperatory modelling of the graft [3, 19, 23, 24].

Until now, however, only a few studies have dealt with custom-made scaffolds for alveolar ridge augmentation [3, 23, 24] and none of these has focused on bone regeneration of the anterior mandible.

The aim of the present report is therefore to document the clinical, radiographic, and histologic outcome of a custom-made, anatomically shaped CAD/CAM scaffold used for the alveolar ridge augmentation of a severely atrophic anterior mandible.

2. Case Presentation

An 18-year-old, nonsmoker female patient, with no history of systemic disease, was referred to the Oral Surgery Unit of the Department of Surgical and Morphological Science, University of Varese, Italy, for a fixed implant-supported prosthetic rehabilitation of the anterior mandible. One year earlier the patient had been involved in a car accident and had fractured her anterior symphysis, losing her lower incisors; in that context, internal fixation of the fracture was obtained by means of two rigid plates placed along the upper and lower border of the symphysis.

During the first visit, a complete clinical and radiographic examination was carried out. The patient was wearing a removable partial denture (RPD) as an interim prosthesis to replace the missing mandibular incisors and improve her aesthetic appearance. After removal of the RPD, the first clinical assessment revealed significant contraction of the soft tissues, probably associated with a vertical and horizontal bone defect in the edentulous area, as confirmed by dental casts analysis. Clinical examination revealed unsatisfactory oral hygiene and, consequently, the patient was provided with professional oral hygiene instruction, involving reinforcement in her oral hygiene efforts, followed by a scaling and root planning of the entire dentition. Probing pocket depth (PPD) was measured using a light probing force (of approximately 25 g) with a conventional periodontal probe (PCP-UNC 15, Hu-Friedy Manufacturing, Chicago, IL, USA) at 4 sites per tooth (mesial, midbuccal, distal, and midlingual). The patient was periodontally healthy with PPD values ranging from 3 to 5 mm. Finally, for a better assessment of the bony anatomy, computed tomography (CT) datasets of the mandible were acquired in the Digital Imaging and Communication in Medicine (DICOM) format and immediately transferred to specific segmentation software (Mimics, Materialise, Leuven, Belgium). In this software, the hard tissue threshold was carefully selected so that only bone would be reconstructed from the slices. Accordingly, it was possible to perform an accurate and complete 3D reconstruction of the mandible. Although CT evaluation and 3D reconstruction showed healing of the fracture, they also showed severe posttraumatic atrophy of the mandibular anterior ridge. In detail, a huge vertical bone defect was present in the symphyseal area (9.3, 10.0, 8.6, and 7.8 mm of alveolar bone were lost from the right lateral incisor to the left lateral incisor area, resp.) combined with a marked reduction in the horizontal alveolar ridge width (Figures 1(a)-1(b)).

Given this problematic anatomical situation, the placement of dental implants for supporting a fixed prosthetic rehabilitation was not possible without considering some form of preprosthetic bone reconstructive surgery. Based on the detailed clinical and radiographic examinations, a bone reconstructive procedure with a custom-made synthetic

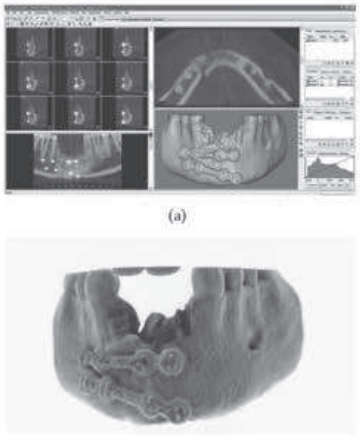

(a)

(b)

FIGURE 1: Preoperative situation. (a) 3D reconstruction of the atrophic anterior mandible by means of specific software: a huge vertical bone defect is present in the symphyseal area, combined with a marked reduction in the horizontal alveolar ridge width. (b) Photorealistic rendering of the mandible. The severe posttraumatic atrophy of the mandibular anterior ridge is evidenced.

scaffold, followed by delayed implant placement, was proposed to the patient. The patient was fully informed and received a thorough explanation about the planned treatment along with its potential risks and complications. She was also advised about the alternative treatment options of a fixed partial denture on natural teeth or a removable partial denture. After careful consideration, she accepted the proposed treatment and signed a written informed consent form. The study was approved by the Local Ethical Committee at the University of Varese, Italy, and was performed according to the principles outlined in the World Medical Association's Declaration of Helsinki on experimentation involving human subjects, as revised in 2008.

One week after the signing of the informed consent form, the process for the fabrication of the anatomically shaped, custom-made hydroxyapatite scaffold started, as previously reported [23, 24]. In brief, the 3D reconstruction of the mandible was transferred as a stereolithographic (STL) file to a 3D CAD program (Rhinoceros, Robert McNeel & Associates, Seattle, WA, USA). With this software, it was possible to reconstruct the alveolar ridge defect virtually and design an anatomically shaped, custom-made scaffold. The anatomically shaped, custom-made scaffold included a hole in its centre to allow the placement of a fixation screw (Figure 2). The 3D geometry of the scaffold was then imported into proprietary CAM software that is used to generate a set of tool-paths for fabrication on a CNC milling machine. A commercially available, synthetic micromacroporous biphasic calcium-phosphate (BCP) block, consisting of 70% beta-tricalcium phosphate and 30% hydroxyapatite (Biocer, Biocer Entwicklungs GmbH, Bayreuth, Germany), was then placed in the CNC milling machine and milled into the exact shape of the 3D project. In this way, an anatomically shaped, custom-made BCP scaffold was manufactured. In addition, a scaffold replica in polytetrafluoroethylene (PTFE) was fabricated; this PTFE replica was intended as a guide for the correct positioning of the hole for the fixation screw (using the BCP scaffold as a guide for drilling the hole could have led to fracture of the fragile scaffold). It took two weeks for the design and fabrication of the BCP scaffold with its replica. The BCP scaffold and its PTFE replica were sterilized before surgery.

Two weeks before surgery, the patient underwent periodontal treatment, involving instruction and reinforcement in her oral hygiene efforts, followed by a scaling and root planing of the entire dentition. On the day of surgery the interim removable prosthesis was removed (Figure 3(a)) and local anesthesia was obtained by infiltrating articaine 4% containing 1 : 100.000 adrenaline. Following a crestal incision with two deep lateral incisions, a mucoperiosteal flap was elevated with wide exposure of the mandibular symphysis. The mental neurovascular bundles were identified and protected with a retractor. The fixation plates were unscrewed and removed. Then, the PTFE replica was placed in position and used for precise positioning of the hole for the fixation screw of the scaffold (Figure 3(b)). Once the hole for the fixation screw was precisely drilled (Figure 3(c)), the PTFE replica was removed. Prior to implantation of the BCP scaffold into the alveolar bone defect area, multiple small holes were drilled through the remaining alveolar bone into the marrow cavity, with a 1 mm round bur under copious saline irrigation. This was done to enhance bleeding of the mandibular cortex (Figure 3(d)). A preparation rich in growth factor (PRGF) was prepared, in order to promote healing and tissue regeneration. The preparation was conducted such as to obtain a platelet-rich plasma preparation, a platelet-poor plasma preparation, and a fibrin scaffold. This protocol differed from the original one described by Anitua and colleagues [25] for the lack of sodium citrate and calcium chloride used as anticoagulant and activator, respectively. The platelet-rich plasma preparation was applied to the surgical site (Figure 3(e)). Once the site had been prepared the custom-made BCP scaffold was removed from its sterile packaging (Figure 3(f)) and placed in position, strictly overlapping the underlying alveolar crest and creating a biological rigid fixation (Figure 3(g)). Fixation of the scaffold was obtained by means of a small titanium screw (Figure 3(h)). The BCP scaffold rapidly acted as a sponge, absorbing a large amount of blood from the surgical site (Figure 3(i)). The surgical site was finally covered and protected with a fibrin membrane (Figure 3(j)). During wound closure great care was taken to obtain a tension-free suture above the scaffold, so as to avoid ischemic damage to the mucosa and suture dehiscence (Figure 3(k)). The patient was instructed to avoid hard food and received oral antibiotics, amoxicillin + clavulanic acid 2 g/d for 6 days (Augmentin, GlaxoSmithKline Beecham, Brentford, UK). Postoperative pain was controlled by administering 100 mg of nimesulide (Aulin, Roche Pharmaceutical, Basel, Switzerland) every 12 hours for 2 days, and detailed instruction about

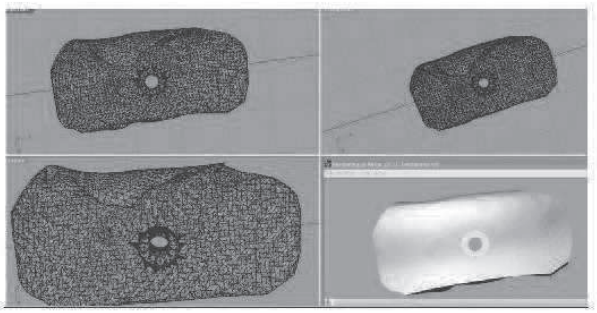

Figure 2: The anatomically shaped, custom-made scaffold is designed. The scaffold includes a hole in its centre to allow the placement of a fixation screw.

oral hygiene was given, along with mouth rinses with 0.12% chlorhexidine (Chlorhexidine, Oral-B, Boston, MA, USA) to be administered daily for 7 days. The patient was seen on a weekly basis during the first 4 weeks. At the first control visit, 7 days after the surgery, a clinically healthy marginal area was present, and no postoperative pain or swelling was reported. There was no bleeding or wound infection. At the second control visit, 14 days after the surgery, sutures were removed (Figure 3(l)). Monthly professional plaque control supplemented this healing phase for 6 months.

No clinical complications were observed during the 1-year healing period. In this period, the patient wore her RPD as interim prosthesis, primarily for aesthetic reasons. One year after surgery the patient underwent a postoperative CT scan. The new CT datasets were immediately transferred to the 3D reconstruction software (Mimics, Materialise, Leuven, Belgium) for the segmentation of the mandible (Figures 4(a)-4(b)). After that, the vertical and horizontal bone gain was radiographically evaluated by comparing the 3D reconstruction of the preoperative CT scan with that obtained 1 year later, using a method previously described [10, 26]. In brief, data from the preoperative and the postoperative CT scans were segmented using the aforementioned 3D reconstruction software. Based on the result of these segmentations, a surface mesh model was generated according to conventional matching cube algorithms, followed by automated surface mesh model generation. The postoperative mesh model was superimposed on the preoperative mesh model and rigidly aligned by anatomical landmarks with the help of software for the overlapping of digital images (Geomagic Studio, Geomagic, Morrisville, NC, USA). The distance between the 2 surface meshes was presented as color-coded graded figures to identify zones of facial bone resorption. By overlapping digital images the hard tissue gain could be confirmed (Figure 5).

Since the 3D radiographic examination showed sufficient bone increase and density for implant insertion in the treated anterior mandible, the placement of two implants was digitally planned with the aid of implant navigation software (Invivo Dental 5, Anatomage, San Jose, CA, USA) (Figure 6(a)). Two weeks later, two conical implants with internal connections (AnyRidge, MegaGen Implants Co., Ltd., Gyeongbuk, South Korea) were inserted under local anesthesia by the same surgeon who had performed the grafting procedure. Local anaesthesia was obtained by infiltrating articaine 4% containing 1 : 100.000 adrenaline. A full-thickness crestal incision was made and the soft tissue overlying the reconstructed alveolar process was elevated. The patient showed significant bone augmentation, confirming the possibility of placing two dental implants in the preplanned positions. Accordingly, two implants (3.75 × 11.5 mm) were placed in locations numbers 32 and 42 (Figures 6(b), 6(c), and 6(d)). The threads of the implants used in this study were designed to provide high insertion torque, by increasing their dimensions toward the coronal end of the implant. This specific macrotopographical feature may allow for axial and radial bone compression during implant insertion, and it may be particularly useful in regenerated areas, providing the increased primary stability. An insertion torque of 55 Ncm was registered. Implant stability was determined clinically as the absolute absence of axial or rotational movement by the removal of the implant driver without use of the stabilizing wrench.

During implant surgery, two bone core biopsies (approximately 2 × 6 mm, one for each site of implant placement) were retrieved with a 2 × 10 mm trephine bur, via a transcrestal path, with the aim of performing a histologic evaluation of the augmented bone. The biopsies were immediately stored in 10% buffered formalin and were subsequently processed (Precise 1 Automated System, Assing, Rome, Italy) to obtain thin ground sections. The specimens were dehydrated in an ascending series of alcohol rinses and embedded in glycolmethacrylate resin (Technovit 7200 VLC, Heraeus Kulzer GmbH & Co., Wehrheim, Germany). After polymerization, the specimens were sectioned lengthwise along the longer axis to about 150 μm using a high-precision diamond disk saw and subsequently ground down to about 30 μm. Two sections were obtained from each specimen. The sections were stained with basic fuchsin and toluidine blue and the histologic evaluation was performed. Histological evaluation revealed compact mature bone undergoing remodelling, marrow spaces

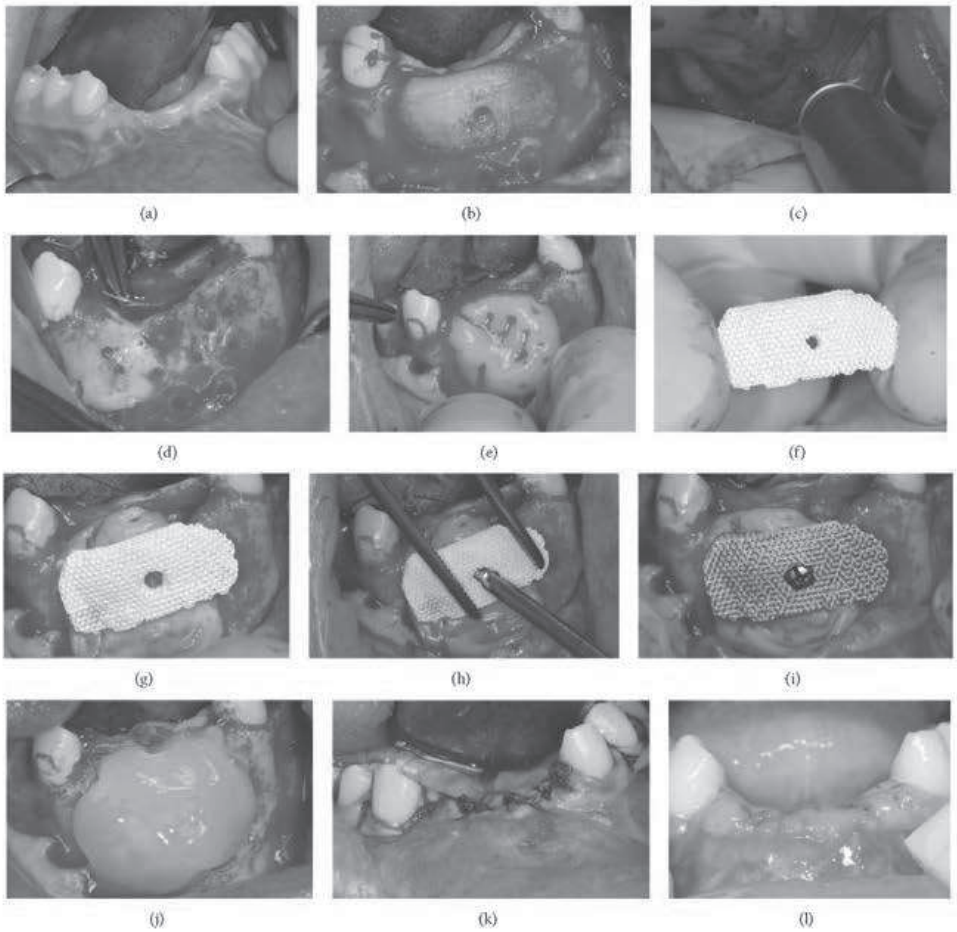

FIGURE 3: Surgery on patient. (a) Preoperative situation; (b) a PTFE replica is placed in position; (c) the PTFE replica is used for precise positioning of the hole for the fixation screw of the scaffold; (d) multiple small holes are drilled through the remaining alveolar bone into the marrow cavity, with a 1 mm round bur, under copious saline irrigation, to enhance bleeding of the mandibular cortex; (e) a preparation rich in growth factor (PRGF) is prepared and applied to the surgical site; (f) the custom-made BCP scaffold is removed from its sterile packaging; (g) the scaffold is placed in position strictly overlapping the underlying alveolar crest; (h) fixation of the scaffold is obtained by means of a small titanium screw; (i) the BCP scaffold rapidly acts as a sponge, absorbing a large amount of blood from the surgical site; (j) the surgical site is protected with a fibrin membrane; (k) care is taken to obtain a tension-free suture above the scaffold, so as to avoid ischemic damage to the mucosa and suture dehiscence; (l) 2 weeks after surgery sutures are removed.

and newly formed trabecular bone surrounded by residual BCP particles. The newly formed bone appeared well organized. Close to the porous BCP particles, new bone formation was observed, with newly formed osteoid matrix undergoing mineralization. In detail, the left specimen was made of compact mature bone undergoing remodelling, with a few marrow spaces; no residual biomaterial particles were found, as only traces of BCP mixed with mineralized bone matrix were evidenced (Figures 7(a)-7(b)). The right specimen was made of residual particles of BCP surrounded by compact bone. In some areas, traces of residual particles surrounded by mineralized bone matrix were found; multinucleated cells were in close contact with the BCP particles. In the marrow spaces, new blood vessels were evident (Figures 7(c)-7(d)).

The implants were left undisturbed for a period of 3 months after which a provisional acrylic resin fixed partial denture (FPD) was provided (Figures 8(a)-8(b)) which was left *in situ* for a further 3 months. This was replaced with

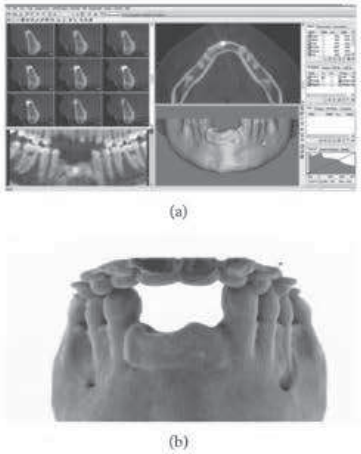

(a)

(b)

FIGURE 4: One year after surgery. (a) 3D reconstruction of the mandible by means of specific software: the vertical and horizontal bone gains are clearly evidenced. (b) Photorealistic rendering of the mandible.

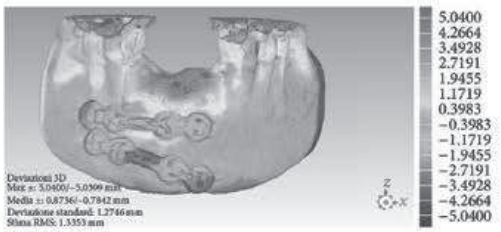

FIGURE 5: Overlapping of digital images. The DICOM (Digital Imaging and Communication in Medicine) files of the obtained CT datasets, before and 1 year after grafting, are converted into a surface mesh model with digital imaging software (Mimics, Materialise, Leuven, Belgium). The two surface mesh models are then superimposed and rigidly aligned with anatomical landmarks, with the aid of software for the overlapping of digital images (Geomagic Studio, Morrisville, NC, USA). The distance between the 2 surface meshes is presented as color-coded graded figures (blue: tissue loss; yellow/orange/red: tissue apposition; green: little or no modifications) to identify zones of apposition/resorption.

the definitive metal-ceramic restoration (Figures 8(c)-8(d)), which was cemented with a zinc oxide-eugenol cement (Temp-Bond, Kerr, Orange, CA, USA). Occlusion was thoroughly checked. The implant-supported FPD showed good functional and an acceptable aesthetic result.

3. Discussion

To perform aesthetic and prosthetic rehabilitation with dental implants, alveolar ridge augmentation is often needed for patients with extensive horizontal and vertical ridge resorption [3–5].

Strategies used to overcome mandibular atrophy include various techniques developed to increase bone volume, such as onlay/inlay bone grafting [6–8], GBR [9, 10], ridge expansion [11], and distraction osteogenesis [7, 12]. Although it has been shown that it is possible to augment bone with all these different techniques, each of these options poses a risk of complications or potential for dimensional graft loss [4, 5, 13, 16]. Moreover, all the aforementioned techniques are based on manual, intraoperative modelling of the graft. This procedure is challenging and time-consuming and may result in an unsatisfactory adaptation of the scaffold to the bony defect [4, 5, 13, 16, 17, 23, 24]. A poor adaptation of the graft material to the recipient site is a major problem during alveolar ridge augmentation, since the lack of mechanical stability of the scaffold may jeopardize the biological response and consequently the treatment outcome [4, 5, 13, 16, 17, 23, 24].

Nowadays, the combination of recent 3D computer simulation techniques, manufacturing technology, and novel bone substitutes with excellent bone tissue conductivity promises to open new interesting horizons for alveolar ridge augmentation. It is now possible to produce an accurate 3D shape of the graft calculated by computer simulation and create a synthetic bone substitute cut exactly into the required shape in a 3D milling machine [23, 24].

In the present report, we describe an onlay technique in the anterior atrophic mandible using a synthetic calcium-phosphate bone graft, shaped with a CAD-CAM system. This approach has the benefits that it avoids the need to harvest autologous bone block and assures a perfect fit of the implant above the alveolar crest. A clinically healthy, young female patient was referred to the Oral Surgical Unit of the University of Varese for treatment with dental implants. The patient presented a severe posttraumatic atrophy of the mandibular anterior ridge, with a huge vertical bone defect in the symphyseal area combined with a marked reduction of the horizontal alveolar ridge width. For this patient ridge augmentation was considered appropriate in order to improve soft and hard tissue volume. In particular, in this clinical situation, a strong rigid graft exceeding 3 mm in height and width was required to allow fixation to the recipient site and 3D stability to withstand muscular force. For these reasons, an onlay technique was selected.

Although autologous bone, harvested from either intraoral or extraoral sites, is currently the most reliable material for alveolar ridge augmentation, with the highest success rate, the use of autografts as onlays has many drawbacks, such as the need for multiple interventions, limited bone availability, the risk of morbidity at the donor site, and high resorption rate of the graft [3, 5–7, 13]. Not to be underestimated, patients prefer a bone substitute block over an autograft block, harvested from an intraoral/extraoral site [3].

Currently, a variety of bone substitute materials, such as allogenic [8], xenogenic [14], or synthetic materials [3, 10, 15], are available for ridge augmentation. An ideal bone substitute should be able to regenerate complex 3D anatomical defects [3, 5, 13, 16, 17, 20, 21]. It should be biocompatible, osteoconductive, and osteoinductive, encouraging appropriate cell

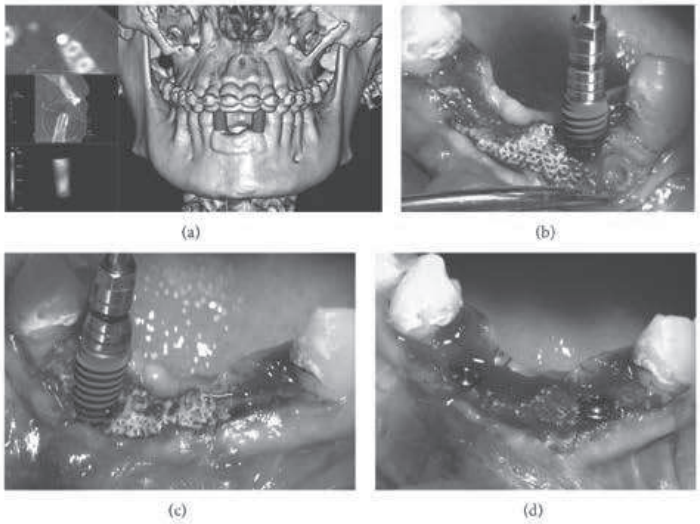

FIGURE 6: Placement of dental implants in the regenerated area. (a) The placement of two implants is planned with the aim of implant navigation software (Invivo Dental 5, Anatomage, San Jose, CA, USA). (b, c, and d) Two AnyRidge dental implants (AnyRidge, MegaGen Implants Co., Ltd., Gyeongbuk, South Korea), 3.75 mm diameter × 11.5 mm length, are placed in locations numbers 32 and 42.

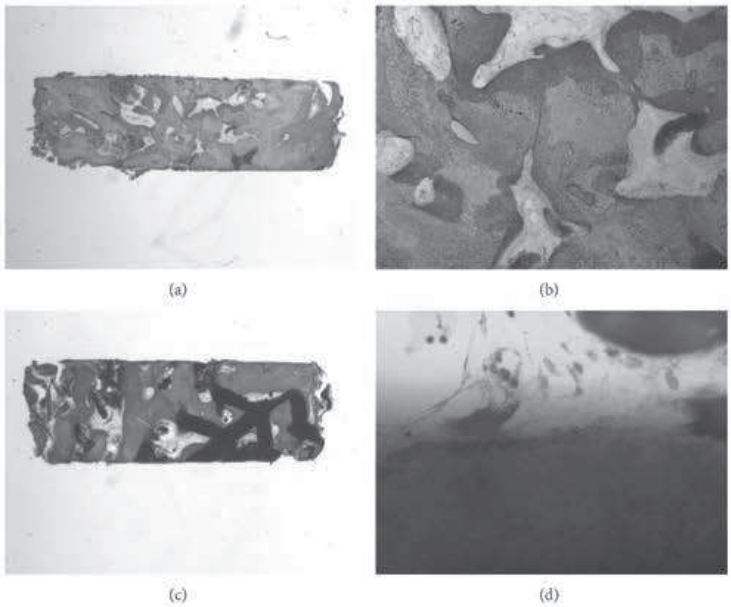

FIGURE 7: Histological evaluation. (a, b) The left specimen is made of compact mature bone undergoing remodelling, with a few marrow spaces; no residual biomaterial particles are found, as only traces of BCP mixed with mineralized bone matrix are present. (c, d) The right specimen is made of residual particles of BCP surrounded by compact bone. In some areas, traces of residual particles surrounded by mineralized bone matrix are evidenced; multinucleated cells are in close contact with the BCP particles. In the marrow spaces, new blood vessels are evident.

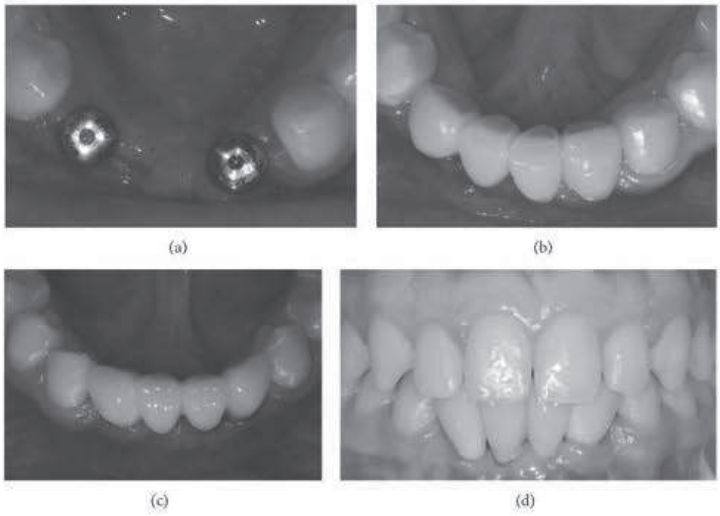

FIGURE 8: Prosthetic restoration. (a) The implants are left submerged for a period of 3 months, after which they are uncovered and healing abutments are placed. (b) A provisional acrylic resin fixed partial denture is provided. (c, d) Three months later, the definitive ceramometallic restoration is delivered.

differentiation through either soluble or insoluble factor signalling and allowing for delivery of pluripotent cell types [3, 10, 15, 23, 24, 27–29]. It should be structurally similar to bone, possessing mechanical properties similar to the native structures and allowing for function and load bearing [3, 10, 23, 24, 27–29]. It should be synthetic and should not be derived from human cadavers or animals [30, 31]. Finally, it should be easy to shape into various forms and bioresorbable. For these purposes, 3D porous materials are currently used as bone substitutes [3, 10, 15, 23, 24, 27–29]. The 3D porous structure provides space for new bone formation, supports the proliferation of cells, and maintains their differential function, thus mimicking many roles of the extracellular matrix, and its architecture defines the ultimate shape of the new bone [3, 10, 15, 23, 24, 27–29].

Among bone substitutes, synthetic calcium-phosphates materials has been suggested as being able to meet all these criteria [3, 10, 15, 23, 24]. In the present study, a synthetic micromacroporous biphasic calcium-phosphate (BCP) block, consisting of 70% beta-tricalcium phosphate and 30% hydroxyapatite, was selected as the scaffold material. Biphasic calcium-phosphates have been widely used for hard tissue repair and augmentation in different preclinical [32, 33] and clinical settings [10, 34, 35]. The structure and chemical composition of BCP is very similar to that of the mineral phase of bone [10, 32–35]; it is biocompatible, osteoconductive and possesses osteoinductive properties [32–35]; it possesses appropriate porosity for the diffusion of nutrients and the invasion of vascularity from the surrounding tissue and surface chemistry to allow cells to adhere and express the osteogenic phenotype [32–35]. It is characterised by appropriate mechanical properties; it is synthetic and cost-effective, is able to form a suitable shape easily, and ultimately replaces the bone within a short period [10, 32–35].

In the present study, a new protocol for computer-assisted surgery is introduced. This protocol can be divided into four phases: (1) the data acquisition phase, which includes CT scan of the patient; (2) the planning phase, which includes the importing of CT data into a software program for virtual planning and design of the anatomically shaped, custom-made scaffold; (3) the manufacture of the custom-made scaffold using CAD/CAM technology and proprietary CNC milling machine; and (4) the surgical phase, which includes utilizing CAD/CAM-derived scaffold for alveolar ridge augmentation of the anterior mandible. This combination of digital technologies has led to the fabrication of a customized scaffold of greater quality than what could be achieved with manual systems; the scaffold perfectly fitted the recipient site without any amendment required during surgery.

The present protocol offers several benefits. Most significantly it simplifies the surgery, considerably as well as reducing the treatment time [4, 23, 24]. The anatomically shaped, custom-made scaffolds arrive in the operating environment in sterile packaging and only need to be positioned and fixed to the recipient point in the final step of the surgery. The CNC milling process is highly precise, as it offers an extremely accurate, anatomically fitting scaffold, with the benefit of increased stability and excellent reproduction of the patient's bony contour [4, 19, 23, 24]. Improving the precision in adapting the graft is critical to its integration with the surrounding bone: a valid interface between graft and the osteogenic cell lines, and the mechanical stability of the scaffold is needed

for new bone formation [4, 16–19, 21, 23, 24]. In the present report, we had the opportunity to use an anatomically shaped, custom-made CAD/CAM scaffold that perfectly fitted the recipient site, without any amendment required during surgery. This precision may have supported the biological integration of the scaffold, resulting in excellent clinical and histological outcomes. The treatment time is considerably reduced, with clear benefits for the patient: in fact, intraoperative time is not consumed by repeatedly modelling the scaffold to the native bone (as in conventional procedures) [4, 23, 24]. The procedure allows a more rapid closure of the surgical wound, avoiding possible sources of contamination of the graft and reducing postoperative discomforts such as swelling and pain, which derive from long and difficult surgical procedures [4]. A consequence of this is that the entire procedure is simplified and more accessible even to less experienced surgeons [4, 23, 24].

Nevertheless, the protocol introduced in this study has some limitations. The first limitation is dimensional and is related to the maximum size of the customized scaffold (12 mm height × 10 mm width). The development of custom-made scaffolds of large dimensions remains challenging because of the requirements for appropriate oxygen and nutrient diffusion throughout the entire construct [4, 23, 24, 36]. To obtain favorable reconstructive results, the bone grafting procedure needs suitable vascular support [36, 37]. Because the osteoblasts require high oxygen tension for bone matrix production, the higher the permeability of the graft to the vascular network, the more effective the new bone formation [36, 37]. An adequate vascular invasion of the scaffold has to be considered an important prerequisite for successful bone regeneration [37]. Without complete vascular invasion and angiogenesis new bone formation is not possible and cells, nutrients, and soluble signals (growth factors), that are mandatory for new bone formation, would be missing [4, 23, 24, 36, 37]. If the scaffold is too big, vascular invasion can be poor, and this could finally jeopardize the healing process [4, 23, 24, 36].

In our present study, PRGF was added to the surgical site. The rationale for the use of PRGF stands in the delivery of a cocktail of proteins and growth factors that may promote wound healing and tissue regeneration to the surgical site [25, 38]. As reported in previous studies, PRGF may be effective in delivering many growth factors such as platelet-derived growth factor, transforming growth factor beta, endothelial growth factor, vascular endothelial growth factor, insulin-like growth factor-1, and fibroblast growth factor. All these soluble factors are capable of promoting healing and tissue regeneration [25, 38]. Other potential limitations of the present CAD/CAM technique include movement artifacts during CT scans and artifacts from filled teeth or metallic restorations close to the edentulous area [4, 23, 24]. In fact, if the patient moves during the radiologic exam, CT datasets can be rather inaccurate and the presence of metallic artifacts may complicate the CAD process and the custom-made scaffold design.

Finally, time is another limitation of this technique. In fact, the entire procedure (from CT scan to surgery on patient) should be carried out in a few weeks, in order to avoid that bone remodelling processes may alter the patient's anatomy; in fact, alteration of the residual anatomy may result in inaccuracy of the custom-made scaffold during surgery. In addition, the amount of time saved by using the CAD/CAM approach is still controversial since whereas the surgical time is considerably reduced, more time has to be spent during the virtual planning and design of the custom-made scaffold [18].

4. Conclusions

Digital technology is advancing rapidly in dentistry. Computers are making previously manual tasks easier, faster, cheaper, and more predictable. Personalized therapy is an emerging practice offering tailored solutions to each individual. This approach is envisioned to revolutionize healthcare, through greater cost-effectiveness, efficiency, and improved patient outcomes. In this paper, the authors have described a new digital approach for alveolar ridge augmentation, represented by the use of a CAD/CAM custom-made, anatomically shaped scaffold of BCP, a biomimetic and biocompatible material with the same chemical composition as the bone mineral phase and characterised by high porosity. Despite its limitations, the proposed protocol for alveolar ridge augmentation using CAD/CAM to fabricate custom-made scaffolds plates may represent a viable method of reproducing the patient's anatomical contour, giving the surgeon better procedural control and reducing theatre time. In fact, this technique allowed the successful development of a patient-specific scaffold from a CAD model of an alveolar bone defect obtained from CT images. The benefit is to shorten operating time, improve recovery, and achieve lower morbidity rate. Further clinical studies with longer dental implant follow-up are needed to verify these findings. In the future, the emergence of new rapid prototyping technologies for producing 3D constructs may help to modify the design of the synthetic onlays by adding geometrical features that would facilitate and enhance blood perfusion within the graft; this should improve the bone growth in these onlays *in vivo*. In addition, custom-made scaffolds may be preseeded with cells prior to implantation. The availability of personalized bone grafts engineered from the patient's own stem cells would probably revolutionize the way we currently treat these defects.

Conflict of Interests

The authors declare that they have no financial relationship with any commercial firm that may pose a conflict of interests regarding the publication of this study. No grants, equipment, or other sources of support were provided.

Acknowledgments

The authors are grateful to Marco Colombo for his help with writing this paper. Francesco Guido Mangano is a student of the Ph.D. Program in Biotechnology, Biosciences and Surgical Technologies School in Biological and Medical Sciences, University of Insubria, Varese, Italy.

References

[1] F. Mangano, A. Macchi, A. Caprioglio, R. L. Sammons, A. Piattelli, and C. Mangano, "Survival and complication rates of fixed restorations supported by locking-taper implants: a prospective study with 1 to 10 years of follow-up," *Journal of Prosthodontics*, vol. 23, no. 6, pp. 434–444, 2014.

[2] F. Mangano, J. A. Shibli, R. L. Sammons, G. Veronesi, A. Piattelli, and C. Mangano, "Clinical outcome of narrow-diameter (3.3-mm) locking-taper implants: a prospective study with 1 to 10 years of follow-up," *The International Journal of Oral and Maxillofacial Implants*, vol. 29, no. 2, pp. 448–455, 2014.

[3] F. Tamimi, J. Torres, K. Al-Abedalla et al., "Osseointegration of dental implants in 3D-printed synthetic onlay grafts customized according to bone metabolic activity in recipient site," *Biomaterials*, vol. 35, no. 21, pp. 5436–5445, 2014.

[4] M. Jacotti, C. Barausse, and P. Felice, "Posterior atrophic mandible rehabilitation with onlay allograft created with cad-cam procedure: a case report," *Implant Dentistry*, vol. 23, no. 1, pp. 22–28, 2014.

[5] M. Esposito, M. G. Grusovin, P. Felice, G. Karatzopoulos, H. V. Worthington, and P. Coulthard, "The efficacy of horizontal and vertical bone augmentation procedures for dental implants—a Cochrane systematic review," *European Journal of Oral Implantology*, vol. 2, no. 3, pp. 167–184, 2009.

[6] S. Arora, A. K. Lamba, F. Faraz, S. Tandon, and A. Ahad, "Role of cone beam computed tomography in rehabilitation of a traumatised deficient maxillary alveolar ridge using symphyseal block graft placement," *Case Reports in Dentistry*, vol. 2013, Article ID 748405, 6 pages, 2013.

[7] J.-W. Kim, M.-H. Cho, S.-J. Kim, and M.-R. Kim, "Alveolar distraction osteogenesis versus autogenous onlay bone graft for vertical augmentation of severely atrophied alveolar ridges after 12 years of long-term follow-up," *Oral Surgery, Oral Medicine, Oral Pathology and Oral Radiology*, vol. 116, no. 5, pp. 540–549, 2013.

[8] L. Laino, G. Iezzi, A. Piattelli, L. Lo Muzio, and M. Cicciù, "Vertical ridge augmentation of the atrophic posterior mandible with sandwich technique: bone block from the chin area versus corticocancellous bone block allograft—clinical and histological prospective randomized controlled study," *BioMed Research International*, vol. 2014, Article ID 982104, 7 pages, 2014.

[9] G. I. Benic and C. H. Hämmerle, "Horizontal bone augmentation by means of guided bone regeneration," *Periodontology 2000*, vol. 66, no. 1, pp. 13–40, 2014.

[10] F. G. Mangano, P. Zecca, F. Luongo, G. Iezzi, and C. Mangano, "Single-tooth morse taper connection implant placed in grafted site of the anterior maxilla: clinical and radiographic evaluation," *Case Reports in Dentistry*, vol. 2014, 11 pages, 2014.

[11] G. Sammartino, V. Cerone, R. Gasparro, F. Riccitiello, and O. Trosino, "The platform switching approach to optimize split crest technique," *Case Reports in Dentistry*, vol. 2014, Article ID 850470, 9 pages, 2014.

[12] M. J. Pfaff, P. Metzler, Y. Kim, and D. M. Steinbacher, "Mandibular volumetric increase following distraction osteogenesis," *Journal of Plastic, Reconstructive & Aesthetic Surgery*, vol. 67, no. 9, pp. 1209–1214, 2014.

[13] B. Al-Nawas and E. Schiegnitz, "Augmentation procedures using bone substitute materials or autogenous bone—a systematic review and meta-analysis," *European Journal of Oral Implantology*, vol. 7, supplement 2, pp. s219–s234, 2014.

[14] J. Li, F. Xuan, B.-H. Choi, and S.-M. Jeong, "Minimally invasive ridge augmentation using xenogenous bone blocks in an atrophied posterior mandible: a clinical and histological study," *Implant Dentistry*, vol. 22, no. 2, pp. 112–116, 2013.

[15] B. Ella, M. Laurentjoye, C. Sedarat, J.-C. Coutant, E. Masson, and A. Rouas, "Mandibular ridge expansion using a horizontal bone-splitting technique and synthetic bone substitute: an alternative to bone block grafting?" *The International Journal of Oral & Maxillofacial Implants*, vol. 29, no. 1, pp. 135–140, 2014.

[16] W. L. Grayson, M. Fröhlich, K. Yeager et al., "Engineering anatomically shaped human bone grafts," *Proceedings of the National Academy of Sciences of the United States of America*, vol. 107, no. 8, pp. 3299–3304, 2010.

[17] J. Li, L. Zhang, S. Lv, S. Li, N. Wang, and Z. Zhang, "Fabrication of individual scaffolds based on a patient-specific alveolar bone defect model," *Journal of Biotechnology*, vol. 151, no. 1, pp. 87–93, 2011.

[18] J. Rustemeyer, A. Busch, and A. Sari-Rieger, "Application of computer-aided designed/computer-aided manufactured techniques in reconstructing maxillofacial bony structures," *Oral and Maxillofacial Surgery*, vol. 18, no. 4, pp. 471–476, 2014.

[19] F. Mangano, P. Zecca, S. Pozzi-Taubert et al., "Maxillary sinus augmentation using computer-aided design/computer-aided manufacturing (CAD/CAM) technology," *The International Journal of Medical Robotics and Computer Assisted Surgery*, vol. 9, no. 3, pp. 331–338, 2013.

[20] R. Kontio, "Update on mandibular reconstruction: computer-aided design, imaging, stem cells and future applications," *Current Opinion in Otolaryngology & Head and Neck Surgery*, vol. 22, no. 4, pp. 307–315, 2014.

[21] A. Tarsitano, S. Mazzoni, R. Cipriani, R. Scotti, C. Marchetti, and L. Ciocca, "The CAD–CAM technique for mandibular reconstruction: an 18 patients oncological case-series," *Journal of Cranio-Maxillofacial Surgery*, vol. 42, no. 7, pp. 1460–1464, 2014.

[22] Y.-F. Liu, L.-W. Xu, H.-Y. Zhu, and S. S.-Y. Liu, "Technical procedures for template-guided surgery for mandibular reconstruction based on digital design and manufacturing," *Biomedical Engineering Online*, vol. 13, no. 63, pp. 1–15, 2014.

[23] F. Mangano, A. Macchi, J. A. Shibli et al., "Maxillary ridge augmentation with custom-made CAD/CAM scaffolds. A 1-year prospective study on 10 patients," *Journal of Oral Implantology*, vol. 40, no. 5, pp. 561–569, 2014.

[24] M. Figliuzzi, F. G. Mangano, L. Fortunato et al., "Vertical ridge augmentation of the atrophic posterior mandible with custom-made, computer-aided design/computer-aided manufacturing porous hydroxyapatite scaffolds," *Journal of Craniofacial Surgery*, vol. 24, no. 3, pp. 856–859, 2013.

[25] E. Anitua, R. Tejero, M. M. Zalduendo, and G. Orive, "Plasma rich in growth factors promotes bone tissue regeneration by stimulating proliferation, migration, and autocrine secretion in primary human osteoblasts," *Journal of Periodontology*, vol. 84, no. 8, pp. 1180–1190, 2013.

[26] V. Chappuis, O. Engel, M. Reyes, K. Shahim, L.-P. Nolte, and D. Buser, "Ridge alterations post-extraction in the esthetic zone: a 3D analysis with CBCT," *Journal of Dental Research*, vol. 92, no. 12, pp. 195s–201s, 2013.

[27] G. Staffa, A. Barbanera, A. Faiola et al., "Custom made bioceramic implants in complex and large cranial reconstruction: a two-year follow-up," *Journal of Cranio-Maxillofacial Surgery*, vol. 40, no. 3, pp. e65–e70, 2012.

[28] B.-J. Kwon, J. Kim, Y. H. Kim et al., "Biological advantages of porous hydroxyapatite scaffold made by solid freeform fabrication for bone tissue regeneration," *Artificial Organs*, vol. 37, no. 7, pp. 663–670, 2013.

[29] L. Ciocca, D. Donati, M. Fantini et al., "CAD-CAM-generated hydroxyapatite scaffold to replace the mandibular condyle in sheep: preliminary results," *Journal of Biomaterials Applications*, vol. 28, no. 2, pp. 207–218, 2013.

[30] J. A. Fishman, M. A. Greenwald, and P. A. Grossi, "Transmission of infection with human allografts: essential considerations in donor screening," *Clinical Infectious Diseases*, vol. 55, no. 5, pp. 720–727, 2012.

[31] Y. Kim, H. Nowzari, and S. K. Rich, "Risk of prion disease transmission through bovine-derived bone substitutes: a systematic review," *Clinical Implant Dentistry and Related Research*, vol. 15, no. 5, pp. 645–653, 2013.

[32] C. Ding, Z. Qiao, W. Jiang et al., "Regeneration of a goat femoral head using a tissue-specific, biphasic scaffold fabricated with CAD/CAM technology," *Biomaterials*, vol. 34, no. 28, pp. 6706–6716, 2013.

[33] M. Nevins, M. L. Nevins, P. Schupbach, S.-W. Kim, Z. Lin, and D. M. Kim, "A prospective, randomized controlled preclinical trial to evaluate different formulations of biphasic calcium phosphate in combination with a hydroxyapatite collagen membrane to reconstruct deficient alveolar ridges," *Journal of Oral Implantology*, vol. 39, no. 2, pp. 133–139, 2013.

[34] C. Mangano, V. Perrotti, J. A. Shibli et al., "Maxillary sinus grafting with biphasic calcium phosphate ceramics: clinical and histologic evaluation in man," *The International Journal of Oral & Maxillofacial Implants*, vol. 28, no. 1, pp. 51–56, 2013.

[35] C. Mangano, B. Sinjari, J. A. Shibli et al., "A Human clinical, histological, histomorphometrical, and radiographical study on biphasic ha-beta-tcp 30/70 in maxillary sinus augmentation," *Clinical Implant Dentistry and Related Research*, 2013.

[36] P. F. Costa, C. Vaquette, J. Baldwin et al., "Biofabrication of customized bone grafts by combination of additive manufacturing and bioreactor knowhow," *Biofabrication*, vol. 6, no. 3, Article ID 035006, 2014.

[37] G. H. Billström, A. W. Blom, S. Larsson, and A. D. Beswick, "Application of scaffolds for bone regeneration strategies: current trends and future directions," *Injury*, vol. 44, supplement 1, pp. S28–S33, 2013.

[38] E. Anitua, M. Sánchez, G. Orive, and I. Andía, "The potential impact of the preparation rich in growth factors (PRGF) in different medical fields," *Biomaterials*, vol. 28, no. 31, pp. 4551–4560, 2007.